00188.52-01f

Benefits Assessment Compilation for the En Route Descent Advisor (EDA) AATT Decision Support Tool

Tara J. Weidner

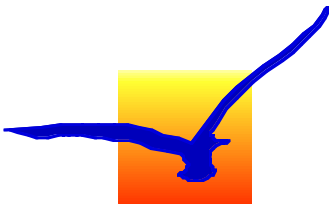

Seagull Technology, Inc.

Prepared for:
National Aeronautics and Space Administration
Ames Research Center, Moffett Field, CA 94035

Under:
SRC Subcontract No. 99-0249, Task Order No. RTO-52 1266-260
NASA Prime Contract No. NAS2-98005
Seagull Project No. C188.52

December 2000

Acknowledgment

This research was performed by Seagull Technology, Inc., as a subcontract to System Resources Corporation (SRC) for the National Aeronautics and Space Administration (NASA) Ames Research Center's Advanced Air Transportation Technologies (AATT) Program. The research was performed by under the program management of Tara Weidner with extensive report review and editing assistance from John Sorensen and technical support from Susan Dorsky, Darren Dow, and Tysen Mueller on the related RTO26, EDA and EDX ATM Interruptions benefits analysis.

This work represents the compilation and update of several previous EDA benefits efforts performed by Seagull technology, dating back to 1996. Previous efforts were performed for the FAA Terminal Area Traffic Control Automation (TATCA) program and the NASA En Route Systems and Operations Group.

The author appreciates the extensive discussions, technical direction, report editing, and program lead of Steve Green, manager of En Route Systems and Operations under the AATT program, at NASA Ames Research Center. Additional thanks is extended to Rich Coppenbarger and other key members of the NASA En Route Operations branch that provided guidance on various segments of this work.

Table Of Contents

List Of Tables

List Of Figures

Benefits Assessment Compilation for the En Route Descent Advisor (EDA) AATT Decision Support Tool

Summary

The National Aeronautics and Space Administration (NASA) is producing a suite of Decision Support software Tools (DSTs) under the Center-TRACON Automation System (CTAS) project, to support FAA Air Traffic Control (ATC), Airline Operations Control (AOC), and flight crew operations. CTAS, a human-centered design based around a core-set of software modules, is intended to enhance the capacity, efficiency, and flexibility of the National Airspace System (NAS) [1] and advance industry initiatives such as Free Flight [2]. En Route/Descent Advisor (EDA) is one such CTAS tool, designed to aid FAA En Route ATC provide more efficient management of air traffic within and between Air Route Traffic Control Centers (ARTCCs, also known as "Centers"). EDA will served aircraft at all phases of en route flight, including climb, cruise, and descent, with the goal of reducing deviations from the airspace users' preferred trajectory (due to separation assurance and conformance with dynamic flow restrictions). This document is the culmination of a series of past studies of individual benefit mechanisms expected from the functionality of the CTAS EDA tool. This study compiles and refines these previous and ongoing EDA benefits efforts, and is the first to present cross-comparable annual National Airspace System (NAS)-wide quantitative benefit estimates using common baselines and assumptions, where available. These estimates reflect new results based upon improved models and recent field tests of en route trajectory prediction. Additionally, where quantitative results are unavailable, an effort has been made to discuss qualitative benefits, in order to provide a more complete picture of expected EDA impacts. The EDA benefits, limited to those that occur from DSTs operating in en route (ARTCC) airspace, are categorized under AATT benefit metrics categories of capacity, predictability, flexibility, environment, and safety.

Study Cases

In this report, EDA benefits are computed by comparing air traffic management (ATM) operations of a proposed future EDA DST as an enhancement relative to a Baseline system. Both systems are defined below.

FFP1 Baseline

The assumed Baseline case reflects en route operations aided by FAA Free Flight Phase 1 (FFP1) arrival metering and conflict probe tools. FAA's Free Flight Phase 1 program is currently deploying a first generation of advanced ATM DSTs including the following tools assumed in the study Baseline:

- **Traffic Management Advisor (TMA)** [3], one of the first CTAS tools, schedules and meters arrival flights into high-density terminal areas. TMA sets an arrival aircraft metering fix-crossing schedule at the Center/TRACON boundary and displays flight-specific delay advisories to the controller. The controller cognitively creates a strategy to absorb the specified delay to meet the TMA schedule. Delay feedback, updated several times a minute, dynamically indicates the amount of delay remaining in order to meet the TMA schedule.

- **User Request Evaluation Tool (URET CCLD)** [4] is an initial implementation of conflict probe (CP) prediction and trial-planning tools. This tool independently probes all en route airspace predicted trajectories and alerts controllers of potential separation assurance conflicts with a trial planner to assist in the development of effective conflict resolution clearances. Because the metering conformance and conflict probe functions are not integrated in

FFP1 operations, the conflict probe's performance (i.e., its ability to determine potential conflicts accurately) suffers by being unaware of the controller metering conformance flight changes.

- **Passive Final Approach Spacing Tool (pFAST)** [5], another CTAS tool, assists TRACON merging operations by providing runway assignments and runway sequence advisories to the controllers soon after the aircraft passes the arrival metering fix. (Note: The pFAST tool is only employed in these analyses, when the analysis requires TRACON technology assumptions.)

EDA System

The future ATM system, for which EDA benefits analyses are directed herein, refers to the next generation of en route operations, where FFP1 operations are enhanced with the integrated capabilities of the CTAS En Route/Descent Advisor (EDA) tools. EDA addresses three key elements missing from the FFP1 Baseline operations and procedures [6].

First, en route DST capability is enhanced to improve the efficiency with which en route controllers direct traffic to conform to flow-rate restrictions. In general two types of flow-rate restrictions need to be considered: time-based arrival metering and en route miles-in-trail (MIT) spacing. Such restrictions are dynamically used when it is necessary to delay or schedule incoming flights to relieve capacity-constrained airspace or airports. Though flow restrictions impact only a small share of all flights, the resulting deviations are significant. EDA can enable controllers to strategically plan their flow-rate conformance actions, subject to arrival metering and MIT restrictions, resulting in a reduction in workload, flight deviations, and fuel consumption.

Secondly, EDA integrates DST flow-rate conformance capabilities with conflict detection and resolution (CD&R) tools. Integration reduces fuel consumption and workload by reducing the rate of conflict probe false alarms and missed alerts. The improved accuracy due to better knowledge of the controller's intended conformance actions also reduces the number of corrective clearances needed to achieve flow-rate conformance while avoiding conflicts. Under the FFP1 Baseline, controllers have no automated assistance to develop a conflict-free plan that conforms to flow-rate restrictions. That is, although FFP1 conflict probe trial-planning functions help identify conflict-free plans, these plans are independent of flow-rate conformance restrictions. Likewise, although FFP1 arrival metering provides the controller with delay feedback, explicit conflict-free flight maneuvers to meet the arrival metering schedule are not provided, and en route MIT spacing restrictions are not addressed.[1]

Third, the limitations of today's inter/intra-sector coordination procedures will curtail user-ATM collaboration and user flexibility beyond FFP1 within en route airspace. Current ATM procedures are predominantly oriented towards airspace or sector boundaries, to protect the internal airspace of a sector. However, user preferences are predominantly oriented towards trajectories that extend across several sectors and Centers. This paradox is a primary obstacle to fully realizing en route user-ATM collaborative operations benefits. Although automation of existing procedures provides some benefit, a fundamental change is required to achieve long-term industry objectives of user flexibility and distributed air-ground traffic management. A goal of EDA development is to enable a shift towards a trajectory orientation by enabling efficient controller actions that work cooperatively across sectors, in maintaining both separation and conformance to flow-rate restrictions [7].

In this study, EDA System functionality is assumed to include:

- **TMA** metered arrival scheduling and delay feedback, as in the Baseline case.

---

[1] FFP1 metering is done to a one-minute precision (approximately 5-6 nm). EDA precision is targetting an error of several seconds, as required to support EDA development of realistic conflict-free maneuver advisories.

- **EDA Arrival Metering** assists controllers in efficiently planning and executing a traffic delay strategy to conform to the TMA schedule by allowing the controller to quickly and accurately assess the impact of various delay methods. The resulting EDA maneuver advisories provide conflict-free, fuel-efficient aircraft clearance advisories to meet the TMA schedule. In order to generate maneuver advisories that result in conflict-free trajectories, the EDA tool includes a built-in conflict prediction/resolution capability, which also assists controllers in accommodating user-requested arrival preferences, such as direct routes.

- **Conflict Probe Tool** with both detection and trial planning capabilities. The integration of the resulting flow-rate conformance flight changes with the conflict probe tool improves conflict probe intent performance, reducing false and missed alert rates.

- **pFAST** TRACON sequencing and scheduling assistance, as in the Baseline case.

EDA System with Data Exchange

Additionally, the benefits summary includes a case where the EDA system is augmented with user-ATM data exchange. Although this case is not explicitly modeled in this report, some estimates of EDA data exchange benefit enhancements are included, based on reference [8]. CTAS is designed with the long-term goal of integrating ATM-flight deck automation systems, including the aircraft Flight Management System (FMS). Indeed, the usefulness of data exchange rests on advanced ATM DSTs, which can utilize higher accuracy input data and incorporate detailed user preferences within their complex algorithms where prior cognitive processes would be overloaded. Near-term benefits of data exchange include enhanced ATM surveillance and estimation of aircraft intent, augmenting and/or increasing the accuracy of currently available data. The integration provided by data exchanges will improve the accuracy of ATM and user trajectory prediction models, allow ATM to receive and accommodate user preferences, improve ATM and pilot workload, and allow more informed collaborative decision making among the airspace users and ATM [9]. For this effort, the following set of near-term data parameters are assumed to be exchanged in the "EDA with Data Exchange" case:

- **Wind/Temperature**–Airborne wind/temperature measurements are used to upgrade weather forecasts, while dissemination provides a common weather forecast for ATM-FMS and airline operations control (AOC) trajectory modeling.

- **Aircraft Weight and Thrust/Drag Coefficients**–Flight-specific information critical to DST modeling of climb/descent flight profiles.

- **Arrival/Departure Speed Intent**–Flight-specific intended Mach/CAS climb/descent speed profiles provides a user trajectory preference that improves DST trajectory prediction. When flights are interrupted, DSTs can attempt to accommodate this user speed preference.

- **Next Two Waypoints**–Waypoint intent (names, and/or locations) improves DST trajectory predictions when flight clearances off the filed flight plan are not recorded as flight plan amendments in the ARTCC computer.

It should be noted that this data set does not address future EDA data exchange enhancements that will facilitate advanced concepts, such as four-dimensional (4D) user-ATM trajectory negotiation.

Potential EDA Benefit Mechanisms

Previous and ongoing research has identified potential benefits expected under the CTAS En Route Descent Advisor (EDA) tools [10-29]. The identified range of EDA benefit mechanisms, limited to those occurring within the Center airspace environment, is summarized with references to relevant

research efforts. The mechanisms are first described in terms of the key underlying DST performance improvements, followed by the specific user and controller benefit mechanisms. Finally, benefits of augmenting EDA with data exchange are noted. The particular benefit mechanisms evaluated, at least in part, within this report are noted with a checkmark (√). Note that the included data exchange benefits, are summarized from a similar NASA AATT report compiling En Route Data Exchange (EDX) benefits [8]:

EDA DST Performance Benefits

√ **Improved Arrival Trajectory Prediction** – EDA-calculated maneuver advisories for arrival aircraft, given to pilots by controllers, reduces the adherence and actuation of TOD placement and descent speed adherence. With pilot and ATM targeting the common EDA descent profile, the trajectory prediction accuracy of descending aircraft will improve. As a result, improved arrival predictions of both time and position will be available to support all CTAS DST functions. These improvements will afford increased performance in CTAS sequencing and scheduling algorithms, more accuracy in the conflict probe tool, and improved clearance advisories to resolve schedule and traffic conflicts. Indeed, observations of flights during the 1997 CTAS TMA prototype field test identified a significant reduction in the arrival metering fix delivery error with TMA over Baseline operations [10]. Further reduction of the delivery error is expected with EDA trajectory prediction enhancement. [11-12]

√ **Improved Metered Arrival Flight Intent –** Integration of metering conformance flight changes with other DST functions will improve CTAS trajectory prediction accuracy. In EDA, ATM-cleared flight changes made to meet metering constraints will automatically enhance flight plan intent for other DST functions, such as conflict probe to ensure separation assurance. [11-12]

EDA User Benefits

√ **Increased Airport Throughput** – Reduced runway threshold separations (in excess of minimums) are expected from EDA as a result of improved arrival metering fix delivery accuracy. The reduced variance in arrival metering fix crossing times leads to reduced runway gaps with associated airport throughput increased and aircraft delay and delay propagation reduction, especially during rush periods. [13-14]

√ **Improved Center/TRACON Delay Distribution** – Reduced variance in EDA arrival metering fix delivery accuracy results in arrival flight efficiency benefits due to the ability to absorb delay more efficiently in Center airspace while still maintaining a given TRACON entry rate. The large TRACON delay, currently needed to absorb variability in arrival metering fix crossing time variability, can be reduced under EDA. [13, 15]

√ **Improved Metering Conformance Efficiency –** Metering conformance actions delay arrival aircraft to meet airport capacity constraints. Inefficient actions may result in both excess fuel and time costs. EDA is designed to improve the fuel efficiency of these clearances in absorbing the required delay to meet the CTAS arrival metering fix crossing schedule. EDA maneuver advisories assist controllers in formulating and executing a traffic delay strategy to meet arrival metering fix crossing schedule. EDA allows controllers to quickly and accurately assess the impact of various delay strategies, and more effectively use fuel-efficient strategies, such as speed control. [11-12,16]

√ **Improved Separation Assurance Interruptions** – CTAS relies on accurate predictions of flight trajectories within its conflict probe tool to accurately identify the location and nature of potential separation assurance violations. With more accurate EDA arrival intent (metering advisories and intent inputs) ATM would less frequently perceive aircraft to be incorrectly or out of conflict (missed and false alerts), resulting in fewer ATM flight interventions and

associated resolution fuel penalties. Additionally, improved traffic conflict prediction will include more accurate estimation of conflict geometry and speeds, leading to more efficient resolution maneuvers. [11-12,17]

√ **Arrival Trajectory Optimization** – CTAS EDA is designed to allow both horizontal and vertical trajectory optimization of arrival flight trajectories. All these trajectory optimization mechanisms provide more fuel-efficient arrival. [17-20]

TOD Optimization – EDA improves a flight's vertical descent profile by moving its top of descent (TOD) location further downstream, minimizing flight time at less efficient, lower altitudes. The bottom of descent (BOD) is constrained to coincides with the airport's existing arrival metering fixes.

User Preferred Routing – EDA facilitates flow-rate conformance, independent of path (i.e., ATM preferred routing, such as STARs). This allows user-preferred routing to be extended through the arrival metering fix (terminal area) within reasonable "arrival-path" corridors.

Relaxed Static Metering Fix Restrictions – Accurate EDA metering conformance allows ATM to relax current conservative, static, restrictions at the arrival metering fix (TRACON entry).

Vertical Anchor Point – EDA improves a flight's vertical descent profile by moving the bottom of descent (BOD) (i.e. the vertical anchor point) downstream of the current metering fix location. Using this vertical anchor point as the new BOD enables aircraft to spend more time at the more fuel-efficient higher altitudes.

Horizontal Anchor Point – EDA improves the horizontal arrival trajectory by moving the current metering fix, the aircraft point of entry into the TRACON, along the Center-TRACON boundary, enabling a more direct route to the runway. Aircraft-specific anchor points can be defined to accommodate various aircraft arrival paths and runways.

EDA Controller Benefits

- **Easier Controller Clearance Development** – EDA automation assists controllers in formulating and executing conflict-free flo-rate conformance plans. EDA generates clearance advisories to resolve problems via speed, altitude, or heading changes, subject to controller confirmation. EDA reduces controller workload by helping controllers identify resolution strategies as well as develop specific clearance instructions. [23-24]

√ **Reduced False/Missed Conflict Alert** – The improved EDA arrival trajectory prediction and integration of flow-rate conformance flight intent changes with conflict detection and resolution functions enables improved conflict probe performance. With more accurate EDA arrival trajectory predictions the conflict probe would less frequently perceive incorrect aircraft conflicts, reducing controller workload by providing conflict alerts at an earlier time (averting missed alerts) and avoiding unnecessary deviations (averting false alerts). [11-12]

- **Improved Controller Workload Distribution** – By enabling more path-independent routes and pushing ATM flow-restriction control points downstream, the EDA enables a more equitable distribution of controller workload across sectors and limits the pass-back of flow-restrictions to upstream facilities. This may also increase sector capacity in current bottleneck traffic sectors. [21-22]

- **Reduced Corrective Clearances** – EDA advisories, calculated from high-fidelity aircraft trajectory models, are expected to more accurately resolve traffic situations such as metering conformance, flow-rate conformance, and separation assurance than possible today using

controller cognitive processes. As a result, the EDA advisories reduce the need for additional corrective clearances, at a shorter time horizon, in order to resolve inaccuracies in meeting the crossing time or separation constraint with the initial clearance. [10]

EDA-Data Link Benefits

√ **Data Calibration of EDA Functions** - Augmenting EDA-based en route operations with en route calibration data will enhance CTAS trajectory prediction algorithms enhancing all of the EDA benefit mechanisms discussed previously. Calibration data, as discussed in reference [8], includes aircraft weight, wind/temperature, aircraft thrust/drag coefficients, runway threshold crossing speed intent, and climb/descent speed intent. User benefits of calibration include more accurate and efficient metering and reduced separation assurance deviations. Controller benefits include less workload with reduced false and missed conflict alerts and reduced need for corrective clearances.[8, 25]

√ **FMS-EDA Descents Profile Negotiation** – En route trajectory negotiation can benefit users through enhanced fuel-efficiency and user flexibility of aircraft descents, by replacing EDA descent advisories with user-preferred trajectories during metering conditions. This mechanism implies a required time of arrival (RTA)-capable FMS to downlink its preferred speed profile to meet an ATM uplinked arrival metering fix crossing time. Longer-term data-exchange concepts could enable the negotiation of user preferred trajectories. [8, 25-29]

- **Uplink of Trajectory Constraints** – As in en route trajectory negotiation, uplink of specific airspace constraints can allow accommodation of user-preferred descent advisors during metering conditions. However, rather than negotiating specific 4D trajectories, EDA would uplink to equipped aircraft, specific airspace constraints (e.g. at/above altitude, at/before or RTA time restrictions). Users would benefit from user flexibility and limiting deviations, while controller workload is reduced through more appropriate strategic clearances that can employ data link auto-load capabilities.[8, 25]

- **Improved Clearance Delivery with Datalink** – EDA and data link can provide controller benefits by facilitating clearance development and delivery. EDA alone provides advisories to facilitate the development of likely clearances. Data link enhances the clearance process by auto-loading the EDA advisory, once confirmed by the controller, into a CPDLC message that can be sent to the pilot with a single keystroke. [23-25]

- **Automatic Flight Intent Update -** Because the EDA-developed CPDLC clearance messages advising speed, altitude or heading changes are recorded and made available to all DST functions, the data link clearance procedure enhances DST knowledge of current aircraft trajectory intent, with associated benefits in controller workload and user separation deviations. [6, 25]

Analysis Process Overview

In general, the EDA benefit analyses methodology included in this and past studies employed the approach shown in Figure S.1. The process quantifies how improved DST calculations and ATM advisories leads to changes in ATM operations that are modeled over a typical day at one (or more) airport(s), to provide a basis for annual and NAS-wide benefit estimation. It employs four primary analysis steps:

1. **Technology Definitions** for each case are defined by associated parametric accuracy values and their improvements due to application of the technology. Statistical values for various parameters used to define the accuracy, or stochastic nature, of an aircraft trajectory are used. These values indicate, for each case, the estimated accuracy of DST trajectory predictions relative to the nominal trajectory followed.

2. **A Trajectory Prediction Accuracy Model,** based on Monte-Carlo simulation, uses these statistical parametric values to calculate DST expected timing and position errors for aircraft crossing key en route waypoints. These timing and position errors can be used in a conflict probe model and/or converted into excess spacing buffers, that would be used in ATM DSTs or imposed by air traffic controllers to protect against separation minima violations.
3. **An Air Traffic Operations Simulation**, typically over a day or rush period, combines the scenarios, parameters, and spacings defined for Baseline and EDA cases, with a traffic scenario and ATM operating procedures. The simulation computes measures of the DST improvements to scheduling/airport capacity, conflict probe flight interruptions, and overall flight fuel-efficiency.
4. **Economic models** are then used to convert the measured/simulated ATM performance improvements into user direct operating cost savings (time and fuel), which are extrapolated to annual and NAS-wide levels. It is important to note that not all benefits can be captured in direct operating cost metrics.

The specific methodology employed by each benefit mechanism assessed in this report is discussed in more detail in the following chapters.

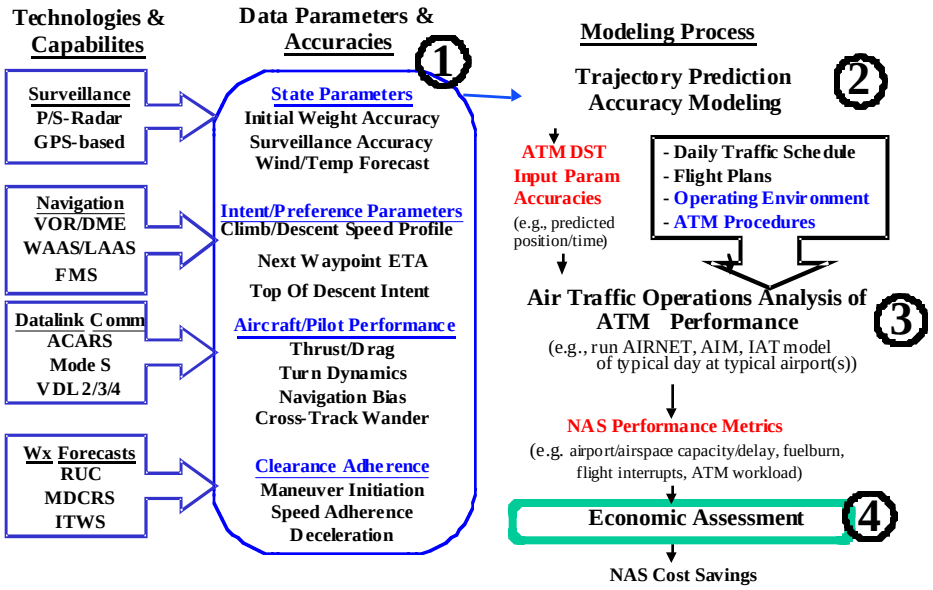

Figure S.1 EDA Study Analysis Process

Results Summary

Table S.1 summarizes the annual EDA benefits estimates found in this study for a cumulative set of 37 Airports.[2] This set was chosen to represent high-demand NAS airports, including FAA Free Flight Phase 1(FFP1) and Phase 2 deployment locations. Each row identifies the specific EDA benefit mechanisms, while each column identifies the estimates relevant to the five AATT benefit metric categories. The table identifies the benefits of EDA alone (EDA) as well as the additional benefits of EDA with en route data exchange (+EDX), as defined earlier. The data exchange benefits are summarized from Reference [8], while further details of the listed EDA benefit mechanisms can be found in later chapters of this report: Chapter 1 Airport Throughput Benefits,

[2] ATL, BDL, BNA, BOS, BWI, CLE, CLT, CVG, DCA, DEN, DFW, DTW, EWR, FLL, HOU, IAD, IAH, JFK, LAS, LAX, LGA, MCO, MDW, MEM, MIA, MSP, OAK, ORD, PDX, PHL, PHX, PIT, SAN, SEA, SFO, SLC, STL

Chapter 2 Center/TRACON Delay Distribution Benefits, Chapter 3 Metering Conformance Efficiency Benefits, Chapter 4 Separation Assurance Interruption Benefits, and Chapter 5 Trajectory Optimization Benefits. Qualitative information is provided in the table to note other EDA benefits too difficult to quantify or not assessed to date. Quantitative benefits are given for alternate metrics including time (minutes), fuel (lbs), and cost ($). Cost estimates assume aircraft and airline crew and maintenance time rates, shown in Appendix C, and a value of $0.10 per lb for fuel. Fuel conservation is important, since fuel is a non-renewable resource and prices are subject to significant political forces. Note that for the metering conformance and trajectory optimization mechanisms, EDA advisories imply optimal maneuvers, which may require data exchange in order to realize the full benefits. Shaded regions are assumed to encompass the key benefits of EDA, although many are not quantified to date.

Critical among these qualitatively described benefits is the impact on workload and safety. Safety is enhanced due to enhanced surveillance under improved EDA metered arrival trajectory prediction capabilities. Controller workload is lessened by EDA assistance in strategic planning to meet the dual objectives of separation assurance and compliance with flow-rate restrictions. EDA maneuver advisories embody an efficient inter-sector approach to these restrictions, enabling more efficient controller strategy and clearance development. By assisting controllers in the formulation of problem-resolution strategies and clearance details, EDA reduces controller workload. Indeed, in early testing of EDA integration with Controller-Pilot Data Link Clearances (CPDLC) where EDA maneuver advisories were auto-loaded into CPDLC messages for uplink, the EDA metering advisories identified the controller-preferred type of clearance (route, altitude, speed changes) two-thirds of the time, with the clearance details (e.g. speed values, chosen altitude) acceptable without modification three-fourths of the time (see Table S.1 footnote 3) [23-24].

Additionally, the EDA strategy is designed with a “trajectory” orientation that enables more path-independent routes. This will improve the workload distribution among sectors upstream of a flow-rate restriction. With path-independent routes, controllers no longer have to channel flights into a common merged path to orchestrate the desired flow-rate. The ability to provide a strategy independent of airspace boundaries, may provide more efficient flights and airspace capacity, as demonstrated by the EDA enabled anchor point concept, relaxing current metering fix restrictions. This trajectory orientation will facilitate user flexibility and distributed air-ground traffic management decision-making when EDA is augmented with data exchange.

Additionally, the use of a high-fidelity trajectory model within the DST to develop the EDA maneuver advisories improves their accuracy over cognitively-developed maneuvers, reducing the need for additional corrective interruptions closer to the restriction.

Finally, the improved metered arrival prediction and integration of flow-rate conformance flight changes with conflict probe functions, greatly reduces the probability of missed or nuisance (false) conflict alerts. Indeed, the separation assurance analysis identifies a 20-30 percent reduction in the number of missed (MA) and false (FA) conflict alerts under EDA, with an overall conflict alert reduction of 5 percent (see Table S.1 footnote 9).

Of the $290M NAS-wide annual quantified EDA benefits, the largest estimate results from the trajectory optimization mechanisms, saving $85M annually under existing restrictions (90% from TOD optimization) and $88M annually when restrictions are lifted (67% from vertical anchor point). EDA fine tuning of descent profiles under existing metering fix restrictions, especially the replacement of current early descents with optimal idle descent profiles, appear very beneficial despite the simplified analysis approach. Likewise under the future anchor point mechanism, EDA arrival metering accuracy enables large savings with the relaxation of conservative static restrictions on TRACON entry (position and altitude). The next largest EDA benefit estimates result from the related mechanisms of airport throughput and Center/TRACON delay distribution, saving over $40M each per year. Improved EDA arrival metering fix delivery accuracy enables improved

TRACON merging, with resulting airport throughput and delay savings. Additionally, the smoother downstream operations require less front-loading of the TRACON,[3] enabling delay to be absorbed more efficiently in the upstream ARTCC airspace. (It should be noted that despite a small average delay savings of less than one minute per rush arrival under EDA, the significant value of time, relative to fuel, resulted in large benefits for this mechanism. Airport throughput is the only EDA mechanism to include time savings, which represents two-thirds of the airport throughput benefit.) The next largest benefits estimate results from improved ATM clearance or flight interruptions for metering conformance, saving $25M annually. The more efficient metering operations stem from EDA high-fidelity calculation of delay absorption strategies. Finally, improved separation assurance interruptions saves $2M. Despite the significant reductions in false and missed alert rates with EDA integration of metering conformance flight changes with the conflict probe, the low average cost for these interruptions ($1-$3 resolution costs) leads to low user cost benefits. However, the un-quantified controller benefits of this mechanism are significant.

It should be noted that due to the many assumptions, varying levels of analysis fidelity, and lack of detailed technical and operational assessment of these study cases and benefit mechanisms, these benefits assessments should be used as engineering estimates. These estimates should be validated and improved through further study, ongoing experimental results, and maturation of the EDA concept capabilities. Specific recommendations to improve the analyses are included in the final chapter of the report.

[3] Current operations front-load the TRACON during rush periods, which entails pushing several minutes of the total flight delay into the TRACON (e.g. longer final approach flight segments) in order to address metering fix delivery and other flight uncertainties.

Table S.1 NAS Annual EDA Benefits

37-Airport Annual Benefits ($) Benefit Mechanism	Study Case	AATT Benefit Categories: Flight Efficiency	User Flexibility	Workload / Productivity	Throughput & Access	Environment	Safety
Airport Throughput	EDA			(5)	$42.9M 445.53 hrs	Reduced Emissions(4)	(5)
	+EDX			(5)	$0.7M 6.80 hrs	Reduced Emissions(4)	(5)
Center/TRACON Delay Distribution	EDA	$47.7M (11) 477 Mlbs				Reduced Emissions(4)	
	+EDX	$6.0M 60 Mlbs				Reduced Emissions(4)	
ATM Metering Conformance Interruptions	EDA	$25.1M (11) 251 Mlbs		Strategic Planning (3)	Future (1)	Reduced Emissions(4)	
	+EDX	$1.1M (10) Future	RTA Traj Negotiation (10)	Reduced Corrective Clearances	Future (1)	Reduced Emissions(4)	
ATM Separation Assurance Interruptions	EDA	$2.3M 23 Mlbs		-30%MA -21%FA -5% Overall (9)	Future (1)	Reduced Emissions(4)	-30%MA (9)
	+EDX	$3.6M 36 Mlbs	Trajectory Negotiation	-25%MA -7% FA -10% overall	Future (1)	Reduced Emissions(4)	-25% MA
Arrival Trajectory Optimization (6) - Existing MF Restrictions	EDA	$84.7M 847 Mlbs	Arrival Direct Routes	Strategic Planning	Future (1)	Reduced Emissions(4)	
	+EDX	Future	RTA Traj Negotiation	Reduced Corrective Clearances	Future (1)	Reduced Emissions(4)	
Arrival Trajectory Optimization (8) - Future Anchor Point Restrictions	EDA	$88.3M 883 Mlbs	Arrival Direct Routes	Strategic Planning	Future (1)	Reduced Emissions(4)	
	+EDX	Future (8)	RTA Traj Negotiation	Reduced Corrective Clearances	Future (1)	Reduced Emissions(4)	

Note: Data Exchange (EDX) benefits are pulled from a previous study [8].
ATM En Route Flow-Conformance Interruptions are preliminary estimates from a concurrent study [22].

(1) Potential en route throughput benefit with improved metering/flow-conformance strategy.
(2) Includes ARR-ARR benefits with metering conformance flight change intent integration with conflict probe
(3) Additionally, auto-loading EDA advisories into CPDLC messages for uplink will reduce workload and allow intent to be recorded without additional effort. Indeed, in an EDA-CPDLC integration study, 66% of EDA advisories included the preferred controller strategy (speed, altitude, heading), and of these, 75% required no manual modification [23-24].
(4) Reduced emissions from improved fuel efficiency and/or delay reduction.
(5) Improved EDA arrival fix delivery accuracy facilitates downstream TRACON merging operations.
(6) Combines two near-term trajectory optimization mechanisms, assumed to improve rush arrival operations only. TOD optimization and direct arrival comprise 45 % and 55% of the total benefit, respectively.
(7) Combines two far-term trajectory optimization mechanisms, assumed to improve ALL arrival operations. Vertical and horizontal anchor point concepts comprise 67% and 33% of the total benefit, respectively.
(8) Data link may be required to enable the future trajectory optimization anchor point concept.
(9) EDA integration improves number of conflict probe missed alerts (MA) by 30% and false alerts (FA) by 21%.
(10) EDX FMS Speed Profile negotiation. Additional benefits would be expected with more accurate EDA metering conformance maneuver advisories
(11) Represents benefits of EDA-STAR case, slightly more benefits available with EDA-Direct Arrivals case (see Chap. 3 and 4).

1. Airport Throughput Benefits

Air Traffic Management automation tools rely on accurate predictions of flight trajectories to derive terminal area arrival and departure sequences and schedules. In the en route environment, this scheduling process can be evaluated by the ability of ATM to consistently deliver flights to the arrival metering fixes as scheduled. EDA trajectory prediction enhancement results in increased DST schedule integrity, increased efficiency of controller clearances to meet the schedule and subsequent enhanced arrival metering fix delivery accuracy, and thus provides a smoother traffic stream for downstream operations.

A key scheduling benefit of improved trajectory prediction is the ability to increase airport throughput by tightening runway threshold in-trail spacing at the same level of safety. This occurs because more accurate metering fix schedule adherence at the Center/TRACON boundary, leads to improved TRACON scheduling integrity and flight efficiency, which allows less excess spacing (above the required separation minima) at the runway threshold. A related mechanism, addressed in the next chapter, allows a more fuel-efficient allocation of delay between the Center and TRACON because of the improved metering fix schedule adherence. Due to delay propagation during rush periods, small savings in individual aircraft pair separation at the runway threshold leads to large decreases in delay. Because user time costs per minute are significantly larger than fuelburn per minute, implementing spacing buffer reduction can reduce delay time leading to significant user benefits [13-14].

Specifically, this benefit mechanism concerns the reduction in spacing gaps between aircraft on final approach, thereby producing a higher airport runway system throughput. EDA is expected to enable this mechanism by improving arrival scheduling operations, which assist controllers in delivering aircraft to the Center/TRACON metering fixes in accordance with the CTAS crossing schedule. Reference [10] discusses EDA improvement of arrival trajectory prediction and the resulting metering fix schedule, based on prototype EDA operations at DFW. In references [13-14] the associated EDA benefits of reduced spacing buffers leading to improved runway throughput and airport capacity was estimated. Since then, additional field evaluations and analysis have lead to improved estimates of EDA trajectory prediction accuracy that were used here to update the results of the previous studies

Analysis Process

The benefits methodology process employed in previous research [13-14] and updated here, includes a sequence of analytical formulations and computer-based modelings which follows the Figure S-1 approach (and numbering) presented in the introduction summary section. Baseline and EDA-defined data parameter accuracies (1) are used in the Trajectory Prediction Accuracy Model (2) to calculate the expected statistical timing error in CTAS' prediction of when the aircraft will cross the meter fix (MF) and runway threshold waypoints. This MF timing error is then converted into excess spacing buffers, which would be imposed by air traffic controllers to limit separation minima violations. These aircraft spacings, defined for Baseline and EDA cases, are then combined with airport daily traffic schedule in a runway system demand and capacity model (3). The resulting delay savings from the EDA cases at 29 airports are then converted to user direct operating cost savings (time and fuel) and extrapolated to annual and NAS-wide levels (4). These model components are discussed in more depth with the analysis results in the next section. (It is again noted that a higher-fidelity Integrated Air Traffic (IAT) model has been developed to evaluate ATM scheduling DSTs. Use of this model to update the analysis would improve the confidence and accuracy of the resulting EDA airport throughput benefit estimates.)

Trajectory Parameter Accuracies

The Baseline and EDA operational cases are described in terms of values of statistical parameters that contribute to DST aircraft trajectory prediction accuracy. These parametric values, shown in

Table 1.1, represent stochastic distributions, which quantitatively describe the accuracy of each contributing parameter. The parameters used in the model have been calibrated and adjusted to reflect the findings of recent CTAS prototype field tests [10].

Trajectory Accuracy and Traffic Spacing Modeling

Air traffic controllers impose an intentional spacing buffer added to the minimum spacing between adjacent aircraft. This buffer serves in part to assure that separation minima are not violated because of trajectory uncertainties. Much of this excess spacing is generated because of uncertainty in the delivery of arrival aircraft at the inbound metering fixes. A schedule of aircraft crossing times at each fix is set by the CTAS-based ATM process according to a TRACON airspace and runway system utilization rate. However, deviations from the metering fix crossing schedule due to timing delivery inaccuracies require subsequent trajectory adjustments by the TRACON ATM operation to prevent violations of separation minima and, to the extent possible, eliminate extraneous gaps at downstream merge points and the runway threshold.

The reduction in trajectory uncertainty due to EDA, relative to the Baseline, would result in a reduction in the size of the excess spacing buffer needed to compensate for trajectory variances. The smaller buffer would reduce the spacing applied between successive aircraft as shown in Figure 1.1, thereby increasing the throughput of the runway system. The increased throughput would reduce delays experienced by aircraft when demand approaches or exceeds the capacity of the runway system. These reduced delays result in reduced fuel and time costs incurred by aircraft operators. Reduced delays also support the integrity of the airline schedule of connecting flights.

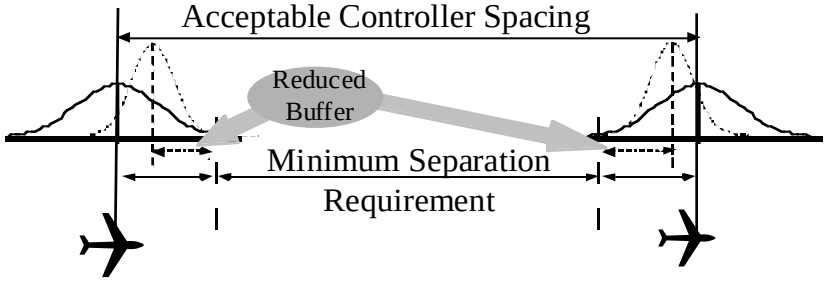

Figure 1.1 Reduced Excess Spacing with Improved Trajectory Prediction Accuracy

Table 1.1 Assumed Trajectory Accuracy Parameters

Parameter	Units	Mean	Standard Deviation FFP1 Baseline	EDA
Center				
Initial Weight	%	0	7.8	7.8
Aerodynamic Drag	%	0	5.9	5.9
TOD Placement	nm	0	20	0.25
Spd Adherence (CAS)	kt	0	15	4
X-Track Wander	nm	0	0.14	0.14
Aircraft Nav. Bias	deg.	0	0.15	0.15
Turn Dynamics	sec	0	2.3	2.3
Wind Forecast	kt	0	12	12
Temp. Forecast	°C	0	1	1
Surveillance	kt	0	13.1	13.1
TRACON (pFAST)				
Final Advisory	sec	0	9.75	9.75
Turn variation	sec	35	7.0	7.0
Deceleration	%	0.52	0.120	0.120
Descent rate	ft/min	1440	160	160
Speed adherence	kt	0	4.0	4.0
Wind forecast	kt	0	4.7	4.7
Tracker	kt	0	3.5	3.5
AFAST Optimal Rwy Balancing/Sequencin	sec	2.3	No	No
Final Approach (pFAST)				
Outer Marker Speed	kt	0	5.0	5.0
Threshold Speed	kt	0	9.0	9.0
Headwind	kt	0	4.7	4.7
Decel delay time	sec	0	12	12

The accuracy with which trajectories can be predicted is estimated using computer simulation, closed-form analytical solutions, and a combination of the two, as appropriate, for each phase of flight. The nominal simulated trajectories, from arrival metering fix to runway threshold, are shown in Figure 1.2; these represent a typical set of approach paths not specific to any one airport. A more extensive discussion of the assumed parameter uncertainties and the trajectory accuracy modeling are included in Chapter 4 and References [12-13]. (Note that simulating the specific STAR routes could generate more accurate results and approach paths nominally used at each of the subject airports.)

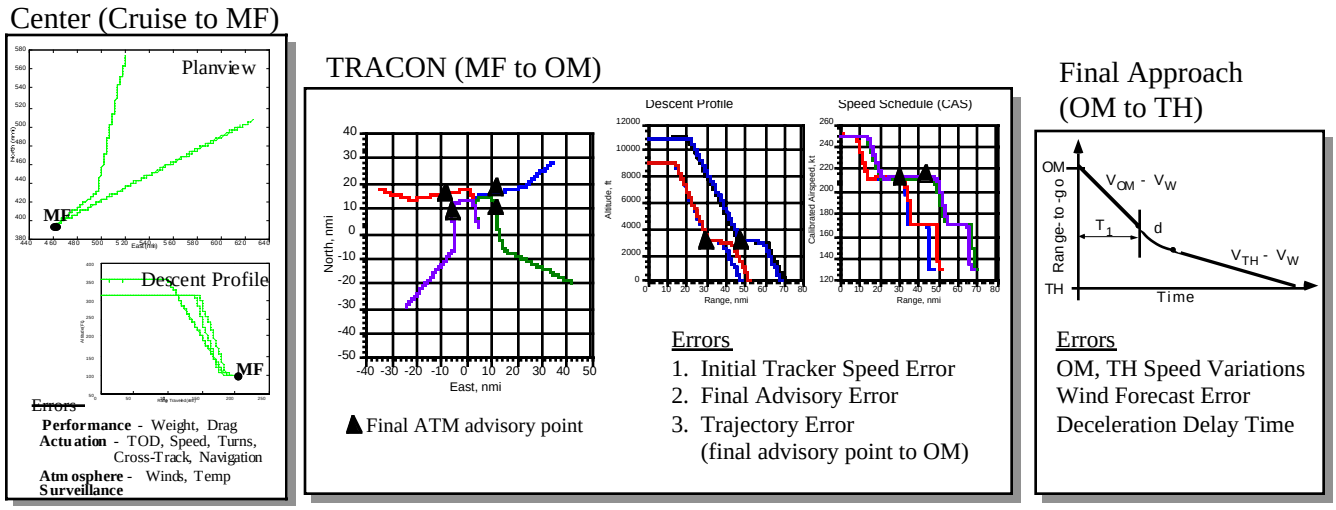

Figure 1.2 Arrival Trajectory Prediction Accuracy Simulation

The parameter accuracy distributions, defined for each operational case in Table 1.1, are inputs to the trajectory modeling process. The outputs, shown in Table 1.2, are the arrival metering fix uncertainty (see Appendix A) and the resulting runway threshold excess spacing buffer contribution. Although only the Center spacing contribution improves under EDA, the TRACON and Final Approach buffer contributions are also provided to gauge of the relative importance of the various contributions. The contributions are combined using Equation (1.1), with the Center contribution to the runway buffer (μ_{OM}) derived from the metering fix delivery accuracy per Reference [15]:

$$\textit{Runway Excess Spacing Buffer} = \mu_{MS} + \sqrt{\sigma_{OM}^2 + \sigma_{FA}^2} \qquad (1.1)$$

The runway spacing buffers, using Equation (1.1) with the Table 1.2 contributions are given in matrix form in Table 1.3, as a function of the various leading/trailing weight-dependent aircraft minimum spacing combinations. Note that the Center model metering fix delivery uncertainty values (assuming a 15-minute descent) were calibrated to match findings of TMA [30] and EDA [10] prototype operations at DFW, as discussed in Appendix A.

Table 1.2 Assumed Arrival Trajectory Prediction Accuracy

	Units	FFP1 Baseline	EDA
Center			
MF uncertainty (σ_{MF})	Sec	86.1 (1)	17.9 (2)
TH Excess Spacing Contribution	Sec	0.72	0.07
TRACON (pFAST)			
OM pairwise spacing	Sec	22.53	22.53
Final Approach (pFAST)			
Final Approach TH Equivalent Buffer Contribution (DFW)	Sec	11.31	11.31

(1) Calibrated to approximate 90 second (1-sigma) metering fix delivery error of TMA prototype field tests [30].
(2) Calibrated to approximate 15-20 second (1-sigma) metering fix delivery error of EDA prototype field tests [10].

Table 1.3 Arrival Runway Threshold Excess Spacing Buffer (sec)

	FFP1 Baseline			EDA		
	Trailing Aircraft			Trailing Aircraft		
Lead a/c:	Small	Large	Heavy	Small	Large	Heavy
Small	25.91	25.54	25.28	25.25	24.89	24.62
Large	27.27	25.49	25.04	26.62	24.84	24.38
Heavy	28.87	27.38	25.55	28.22	26.73	24.90

Table 1.4 gives the airport-specific fleet-weighted equivalent runway buffers estimated for each study case and each of the subject airports. The buffers of Table 1.4 are applied as additions to the FAA runway spacing minima of Table 1.5.

Table 1.4 Equivalent Threshold Excess Spacing Buffers

	Equivalent Threshold Excess Spacing Buffer (sec)	
Airport	FFP1 Baseline	EDA
Atlanta (ATL)	25.79	25.14
Nashville (BNA)	26.03	25.37
Boston (BOS)	26.11	25.46
Baltimore (BWI)	25.89	25.24
Charlotte (CLT)	25.96	25.31
Cincinnati (CVG)	25.73	25.08
Washington National (DCA)	25.93	25.28
Denver (DEN)	26.01	25.36
Dallas – Ft. Worth (DFW)	25.77	25.12
Detroit (DTW)	26.04	25.39
Newark (EWR)	25.85	25.20
Washington Dulles (IAD)	26.20	25.54
Houston – Intercontinental (IAH)	25.74	25.09
N.Y. Kennedy (JFK)	26.00	25.35
Las Vegas (LAS)	26.06	25.41
Los Angeles (LAX)	26.19	25.54
N.Y. LaGuardia (LGA)	25.86	25.20
Orlando (MCO)	26.07	25.42
Memphis (MEM)	26.07	25.42
Miami (MIA)	26.10	25.45
Minneapolis (MSP)	26.14	25.49
Chicago O'Hare (ORD)	25.80	25.15
Philadelphia (PHL)	25.99	25.34
Phoenix (PHX)	26.07	25.42
Pittsburgh (PIT)	26.01	25.35
Seattle (SEA)	26.03	25.37
San Francisco (SFO)	26.06	25.41
Salt Lake City (SLC)	26.03	25.38
St. Louis (STL)	25.86	25.21

Table 1.5 FAA Minimum Separation

	FAA Minima (nm/sec)		
	Trailing Aircraft		
Lead a/c:	Small	Large	Small
Small	2.5/75	2.5/72	2.5/67
Large	4.0/120	2.5/72	2.5/67
Heavy	6.0/180	5.0/144	4.0/107

Runway System Demand and Capacity Model

A computer simulation model is used to evaluate airport throughput and determine traffic delay using the excess spacing buffer data and minimum separation requirements as input. Twenty-nine study airports were individually modeled over a single typical daily traffic schedule. The model incorporates data describing time-varying daily schedules for various types of commercial, general aviation and military aircraft and detailed configurations of the major domestic airports for instrument flight rules (IFR) and visual flight rules (VFR). Runway spacing parameters describing separation procedures for the IFR and VFR runway configurations at each of the airports are adjusted to enable comparison of the Baseline and EDA scenarios. The DFW modeled runway configurations is shown in Figure 1.3, with other airport configurations described in Appendix C.

Although the daily traffic schedule used in this analysis differs from that employed in the other benefits evaluations, cross-comparable results are achieved by extrapolating the daily per operation savings results to annual airport activity levels consistent with the other studies.

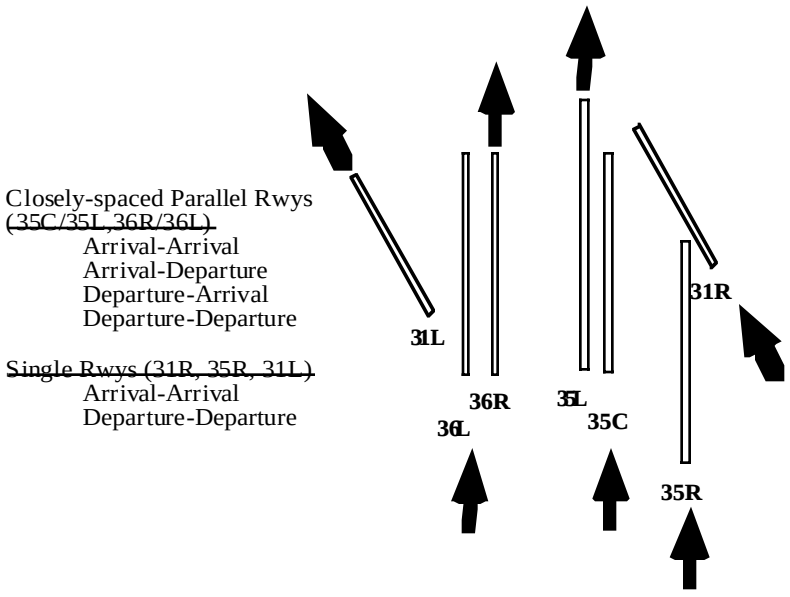

Figure 1.3 Average Airport Delay as a Function of Runway Excess Spacing

The modeling of each airport resulted in delays of four categories as a function of the input runway spacing buffer, as shown in Figure 1.4. The four delay categories include:

- Instrument Flight Rules (IFR) Arrival Delay
- Visual Flight Rules (VFR) Arrival Delay
- IFR Departure Delay
- VFR Departure Delay

IFR delays were averaged over a morning IFR period from 7-10 am, weighted by the historical persistence of IMC at each airport. VFR delays reflect the average delay over the remaining VFR period. Figure 1.4 shows how delays (y-axis) decline at each airport with a reduction in the runway threshold excess spacing buffer (x-axis). Using the Figure 1.4 simulation results and the equivalent spacing buffers of Table 1.3, delay estimates in each category were identified for the Baseline and EDA systems. Assuming an even split of arrivals and departures and historical share of instrument meteorological conditions (IMC) (see Appendix C), the four delay categories are combined and summarized, as shown in Table 1.6.

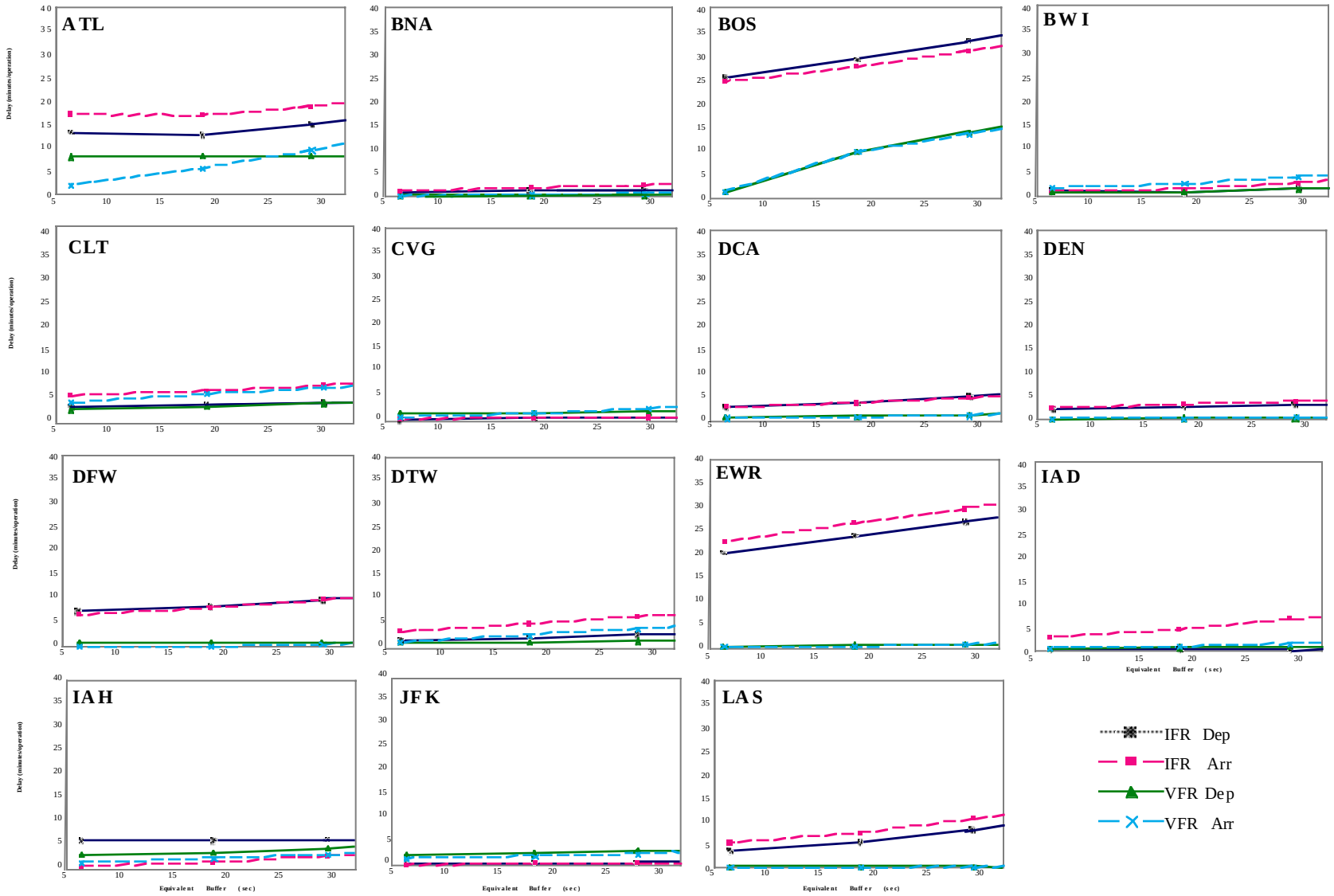

Figure 1.4a Airport Delay as a function of Runway Excess Spacing Buffer

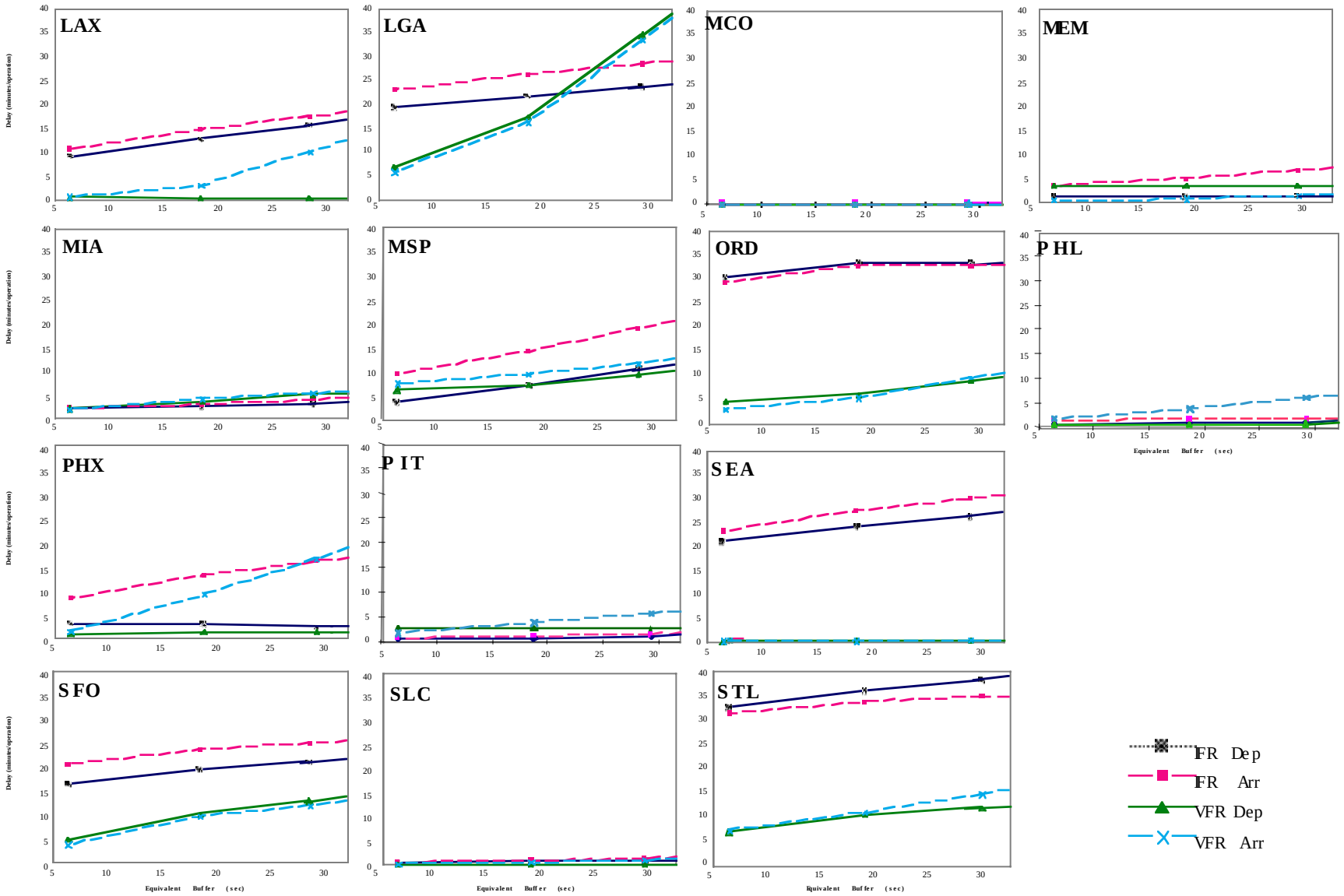

Figure 1.4b Airport Delay as a function of Runway Excess Spacing Buffer (cont'd)

Table 1.6 EDA Delay Savings

	EDA Average Delay Savings (minutes/operation)				
	IMC		VMC		Airport
Airport	Dep	Arr	Dep	Arr	Average
Atlanta (ATL)	0.14	0.13	0.00	0.23	0.12
Nashville (BNA)	0.01	0.03	0.00	0.01	0.01
Boston (BOS)	0.25	0.20	0.26	0.24	0.24
Baltimore (BWI)	0.07	0.09	0.03	0.10	0.07
Charlotte (CLT)	0.02	0.07	0.04	0.08	0.06
Cincinnati (CVG)	0.00	0.00	0.00	0.05	0.03
Washington National (DCA)	0.08	0.07	0.02	0.02	0.03
Denver (DEN)	0.02	0.04	0.00	0.01	0.01
Dallas – Ft. Worth (DFW)	0.08	0.10	0.00	0.02	0.02
Detroit (DTW)	0.03	0.09	0.01	0.09	0.05
Newark (EWR)	0.17	0.19	0.01	0.01	0.04
Washington Dulles (IAD)	0.00	0.14	0.01	0.03	0.03
Houston – Intercontinental (IAH)	0.01	0.09	0.04	0.05	0.05
N.Y. Kennedy (JFK)	0.00	0.01	0.03	0.03	0.03
Las Vegas (LAS)	0.17	0.17	0.00	0.00	0.00
Los Angeles (LAX)	0.20	0.19	0.00	0.47	0.22
N.Y. LaGuardia (LGA)	0.12	0.13	1.07	1.07	0.91
Orlando (MCO)	0.00	0.00	0.00	0.00	0.00
Memphis (MEM)	0.01	0.10	0.00	0.05	0.03
Miami (MIA)	0.04	0.06	0.08	0.07	0.08
Minneapolis (MSP)	0.21	0.32	0.13	0.15	0.15
Chicago O'Hare (ORD)	0.00	0.00	0.17	0.26	0.18
Philadelphia (PHL)	0.01	0.01	0.00	0.14	0.06
Phoenix (PHX)	0.00	0.18	0.00	0.47	0.24
Pittsburgh (PIT)	0.02	0.02	0.00	0.11	0.05
Seattle (SEA)	0.13	0.16	0.00	0.01	0.03
San Francisco (SFO)	0.10	0.08	0.17	0.16	0.15
Salt Lake City (SLC)	0.00	0.02	0.00	0.02	0.01
St. Louis (STL)	0.13	0.06	0.09	0.22	0.15

Economic Analysis

The daily traffic delay data are extrapolated to annual cost savings by airport using detailed aircraft operating costs and airport traffic and meteorological factors. Calculation of potential annual delay cost savings follows Equation (1.2):

$$\textit{Annual Savings} = (\textit{Annual Ops}) \times (\textit{Average Delay Savings per Op}) \times (\textit{Delay Cost Rate}) \quad (1.2)$$

where: *Annual Ops* = Annual airport operations (IMC & VMC) (Appendix B)
Average Delay Savings Per Op = Average delay savings per airport operation (min) (Table 1.5)
Delay Cost Rate = Fleet-weighted flight cost ($/min) (departure & arrival rates) (Appendix C)

This formulation is evaluated for four operation types:

IFR Arrivals & Departures - Accounting for historic airport-specific persistence and occurrence of IMC.
VFR Arrivals & Departures - Accounting for historic airport-specific occurrence of VMC.

This general formula is followed for EDA, relative to the Baseline case, at each of the airports under study. Equation (1.2) delay data, for each of the four operation types, are found in Table 1.5 and aircraft cost rates and annual traffic levels are identified in Appendices. Aircraft direct operating cost rates including crew, maintenance, oil, and fuel costs and are evaluated as an airport fleet-wide average. Departure fuel costs are less as departure delays are assumed to be held on the ground, rather than the airborne holding of arrivals. Per Operation delay savings for the eight airports not simulated was assumed equivalent to the closest simulated airport, based on FAA delay data [31], also included in Appendix B. Table 1.7 and Figure 1.5 identify the 1996 estimated annual cost savings (in 1998 dollars) due to EDA for the 37 NAS-wide airports. Table 1.7 gives the assumed annual ops, historical IMC share, and "equivalent airport" relationships, as reference. The capacity constrained large hub airports of LGA, LAX, and ORD accrued the most significant benefit estimates.

Table 1.7 EDA Airport Throughput Benefits

Airport	Annual Airport Ops (000s)	Historical Share of IMC	"Equivalent" Airport (1)	EDA Annual Cost Savings ($000, 1998)
Atlanta (ATL)	773	14.2%		3.21
Nashville (BNA)	226	9.5%		0.03
Boston (BOS)	463	15.6%		2.52
Bradley (BDL)	161	14.6%	DEN	0.03
Baltimore (BWI)	270	12.4%		0.41
Cleveland (CLE)	291	15.6%	SEA	0.20
Charlotte (CLT)	457	12.5%		0.58
Cincinnati (CVG)	394	15.0%		0.25
Washington National (DCA)	310	10.7%		0.20
Denver (DEN)	454	6.0%		0.10
Dallas – Ft. Worth (DFW)	870	8.4%		0.46
Detroit (DTW)	531	16.6%		0.88
Newark (EWR)	443	16.6%		0.52
Ft. Lauderdale (FLL)	236	3.0%	DEN	0.04
Houston Hobby (HOU)	252	13.5%	SLC	0.07
Washington Dulles (IAD)	330	11.7%		0.17
Houston – Intercontinental (IAH)	392	12.7%		0.48
N.Y. Kennedy (JFK)	361	15.0%		0.40
Las Vegas (LAS)	480	0.3%		0.03
Los Angeles (LAX)	764	22.2%		5.70
N.Y. LaGuardia (LGA)	343	16.4%		8.28
Orlando (MCO)	342	5.9%		0.00
Chicago Midway (MDW)	254	15.1%	MIA	0.42
Memphis (MEM)	364	9.2%		0.30
Miami (MIA)	546	2.3%		1.11
Minneapolis (MSP)	484	11.6%		1.92
Oakland (OAK)	516	14.4%	MEM	0.27
Chicago O'Hare (ORD)	909	16.1%		5.12
Portland (PDX)	306	10.2%	DEN	0.06
Philadelphia (PHL)	406	15.0%		0.65
Phoenix (PHX)	544	0.5%		3.39
Pittsburgh (PIT)	447	24.6%		0.52
San Diego (SAN)	244	12.6%	SLC	0.09
Seattle (SEA)	398	14.9%		0.29
San Francisco (SFO)	442	12.5%		2.12
Salt Lake City (SLC)	374	5.6%		0.11
St. Louis (STL)	517	11.5%		2.02
37-Airport Total/Average	430	---	---	42.93

(1) Airports not simulated assumed the delays of an "Equivalent" simulated airport, based on FAA Delay data [31] in Appendix B.

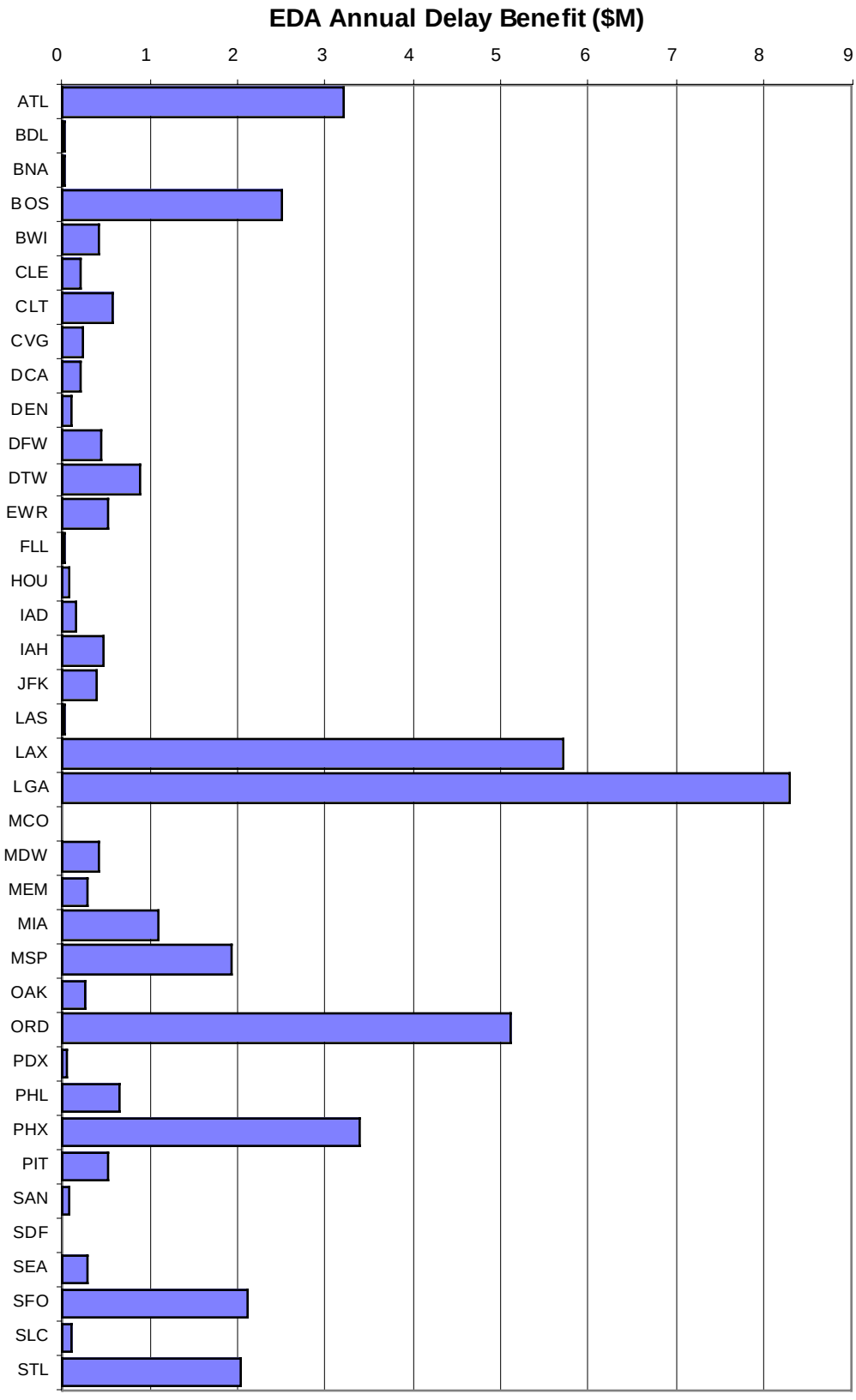

Figure 1.5 EDA Airport Throughput Benefits

Results Summary

This chapter evaluated EDA airport throughput benefits. Reduced runway threshold separations (in excess of minimums) are expected from EDA as a result of improved arrival metering fix delivery accuracy. The reduced variance in arrival metering fix crossing times leads to reduced runway gaps with associated airport throughput increases and aircraft delay and delay propagation reduction, especially during rush periods.

It was found that EDA saved an average 1-2 seconds of delay or $2.35 per operation (time and fuel), for a total NAS-wide deployment at 37-airports of 445 hours and $42.93M annually. These benefits reflect a reduction in the average runway threshold excess spacing buffer relative to a FFP1 Baseline, which includes TMA and pFAST. With no CTAS improvements, the average buffer was found to be approximately 31 seconds [32]. Thus, a rough indication of the relative benefits of EDA, TMA, and pFAST operations can be made by noting the airport delay savings in Figure 1.4 associated with the approximated 1-2 second TMA buffer improvement, 4 second pFAST improvement, and this study's 0.65 second EDA improvement.

It should also be noted that this analysis, an update of previous studies, was limited by the use of a runway demand and capacity modeling tool (AIRNET) which does not account for airspace constraints and subtleties of arrival scheduling embedded in proposed ATM DSTs. To address these limitations, Seagull has initiated development of a higher fidelity model, the Integrated Air Traffic (IAT) Model, which has been used in recent benefits assessments for TMA [33].

Additionally, there is some concern regarding the underlying schedule used to model LGA. Because of the high demand, delays are unable to be dissipated, and they build up without break over the full day. As a result, any improvement to LGA aircraft separation leads to significant savings. It is recommended that the IAT model be applied to refine these airport throughput benefits and the LGA flight schedule be updated to reflect existing operations.

2. Center/TRACON Delay Distribution Benefits

During busy periods, aircraft arrivals are metered to meet airport capacity restrictions. Controllers distribute overall arrival aircraft delay between Center and TRACON airspace during busy traffic periods. This allocation process performs a trade-off between the advantage of absorbing delay more efficiently in Center airspace, versus the advantage of packing more aircraft in the terminal airspace to ensure that aircraft are continually available to use the runway system. The TRACON delay allows controllers flexibility to absorb variability in arrival-metering fix crossing time. Excess allocation of delay to the Center airspace degrades runway system utilization. As trajectory prediction and control accuracy are improved, less delay is needed in the TRACON airspace to maintain high runway system throughput. An increase in the proportion of total delay taken in the Center provides cost savings due to the ability to absorb delay more efficiently in Center airspace.

Thus, separate from runway throughput impacts of the previous chapter, improved arrival metering fix (MF) timing accuracy with EDA can also allow ATM to improve how the aforementioned metering delays are absorbed. With improved MF arrival stream delivery timing, less TRACON delay or front-loading is needed to absorb metering fix crossing variations, while maintaining high runway system throughput. As a result, extra TRACON time currently imposed on peak-period arrivals for this purpose can be shifted upstream to ARTCC airspace for more efficient absorption and associated fuel savings. The estimated EDA fuel savings were tabulated at 3 airports, and extrapolated to annual and NAS-wide levels.

Analysis Process

The benefits assessment methodology process employed in previous research [33] and updated here for EDA, is described below. Previous EDA benefits for this mechanism, employing a more primitive analysis method are found in [13-14]. The sequence of analytical formulations and computer-based modelings follows the Figure S.1 approach (and numbering) of the introduction summary section. The Trajectory Prediction Accuracy Model (2) uses Baseline and EDA defined data parameter accuracies to calculate the expected timing error in CTAS' prediction of when the aircraft will cross the meter fix (MF). This timing error as well as airport-specific arrival routes, arrival procedures, and arrival rush schedules (3), are used to identify the optimum level of TRACON delay. A reduction in the TRACON delay setting relative to Baseline operations indicates the amount of delay that can be shifted upstream and absorbed in the more fuel-efficient ARTCC airspace. The resulting delay savings from the EDA case, at 3 airports (ATL, DFW, and LAX) are then converted to user direct operating cost savings (fuel) and extrapolated to annual and NAS-wide levels (4). These model components are discussed in more depth with the analysis results in the following sections.

Delay Distribution

CTAS includes a delay distribution function, which allocates aircraft delay between Center and TRACON airspace during busy traffic periods. As discussed above, the allocation process is designed to achieve an optimum balance between fuelburn savings and runway system throughput. CTAS TMA and EDA, allow for this optimal distribution of delay between Center and TRACON airspace through a TRACON delay setting parameter. During rush periods, the parameter is increased to allow TRACON the controllability needed to fully utilize runway system throughput, at a fuel penalty of absorbing some of the delay in the TRACON airspace.[4] As arrival fix crossing accuracy or predicted TRACON flight time improves, a lower TRACON delay setting is necessary to maintain runway system throughput, leading to associated fuelburn savings. Figure 2.1 shows the fuelburn penalty (ΔFuel) and runway utilization cost of increasing the TRACON delay setting parameter.

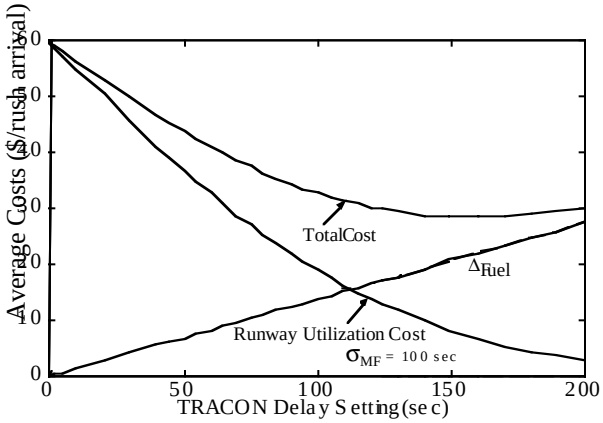

Figure 2.1 Runway Utilization and Fuelburn Penalty Costs Vary with TRACON Delay Setting

Runway utilization costs reflect the delay impact of arrivals unable to meet their landing slot, despite the TRACON Delay Setting, as a result of arrival fix delivery variation. Previous research has analytically derived Equation (2.1) to calculate the optimum TRACON Delay Setting as a function of arrival fix delivery accuracy (σ_{MF}), fuelburn cost rates in the TRACON and Center (C_{FT}, C_{FC}), time costs, rush size (N), and a calibration factor (k_{Slot}). Equation (2.2) gives the EDA TRACON Delay Setting fuelburn savings for a flight relative to the FFP1 Baseline system, which includes TMA. These savings would be zero, if the optimum setting exceeds the maximum setting, based on the controllability window of each TRACON arrival route at each airport.

$$TRACON\ Delay\ Setting\Big|_{OPT} = \sigma \sqrt{-2\ln\left[\frac{\sqrt{8}\sigma\,(C_{FT}-C_{FC})}{(N+1)k_{Slot}\,(C_T+C_{FT})}\right]} \tag{2.1}$$

$$FuelSavings = (C_{FT}-C_{FC})\,(TRACON\ Delay\ Setting\Big|_{FFP1} - TRACON\ Delay\ Setting\Big|_{EDA}) \tag{2.2}$$

[4] Current operations front-load the TRACON during rush periods, which entails pushing several minutes of the total flight delay into the TRACON (e.g. longer final approach flight segments) in order to address metering fix delivery and other flight uncertainties.

Figure 2.2 illustrates how the optimal TRACON Delay setting (y-axis) declines with improved arrival metering fix delivery accuracy (x-axis). Note that the maximum delay absorption capability of a route (typically 100-300 seconds) may require a setting below optimal when the MF delivery error is large (shaded area of figure). Pre-TMA, TMA, and EDA MF delivery accuracies are shown for reference. Note that only small Center/ TRACON delay distribution benefits would be expected under TMA, since despite the large improvement in delivery accuracy, the TRACON delay setting did not change much. More benefits would be expected with post-TMA improvements.

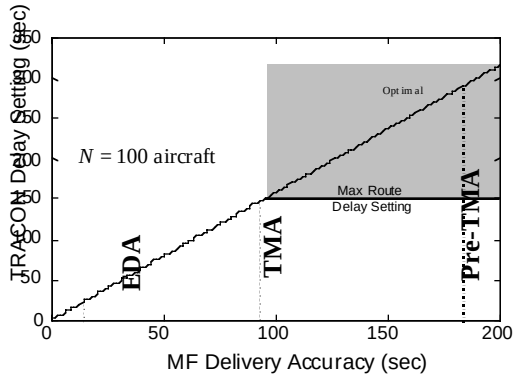

Figure 2.2 Optimal TRACON Delay Setting as a Function of Arrival Metering Fix Delivery Error

Equation Parameters

Equations (2.1-2.2) require case-specific metering fix delivery accuracy values (σ_{MF}). These values were obtained using the Trajectory and Traffic Spacing Model and case-specific input errors as used in Chapter 1, Airport Throughput Benefits, and discussed in Appendix A. This model incorporates case-specific errors that contribute to arrival metering fix delivery accuracy, which were calibrated to match TMA [30] and EDA [10] prototype field test observations. The resulting assumed arrival metering fix trajectory accuracies are repeated in Table 2.1.

Table 2.1 Assumed Arrival Trajectory Accuracy

	Units	FFP1 Baseline	EDA
MF uncertainty (σ_{MF})	Sec	86.1 (1)	17.9 (2)

(1) Calibrated to approximate 90 second (1-sigma) metering fix delivery error of TMA prototype field tests [30].
(2) Calibrated to approximate 15-20 second (1-sigma) metering fix delivery error of EDA prototype field tests [10].

Airport-specific parameters that apply to all study cases were identified through evaluation of the airport TRACON procedures and typical traffic operations. The maximum delay that could be absorbed in each TRACON route category was identified based on ATM facility-provided data [34] as well as geographic airspace and adjacent operations limitations, per discussions with each facility. Straight-in approaches in general have a smaller controllability window (i.e., less room to maneuver) and thus a lower maximum TRACON Delay Setting than the longer downwind-turn-to-base routes. Additionally at LAX, two arrival fixes are often used to hold primarily non-jet aircraft for up to several minutes to fill holes on final approach, increasing their delay absorption capability.

Additionally, evaluation of a typical day's ETMS-based traffic operations at each of these facilities [35] was used to identify and characterize the arrival rushes at each facility. The assumed attributes are shown in Table 2.2

Table 2.2 ATL, DFW, LAX Assumed Airport Rush Operations

	Approach Procedure	Max TRACON Delay (sec)	Airport Arrival Rushes Start Time, Duration, Operations									
			Rush 1	Rush 2	Rush 3	Rush 4	Rush 5	Rush 6	Rush 7	Rush 8	Rush 9	Rush 1
ATL	Straight-In	150	07:20	08:43	10:38	12:14	14:10	15:41	17:35	19:36	21:47	
	Downwind	300	33 min	51 min	55 min	63 min	67 min	94 min	79 min	89 min	55 min	
			40	62	64	79	77	116	99	109	63	
DFW	Straight-In	180	06:48	08:19	09:41	11:34	13:11	14:28	15:54	17:34	18:48	20:2
	Downwind	360	13 min	24 min	25 min	46 min	26 min	47 min	31 min	52 min	63 min	53 min
			17	27	35	78	47	75	53	85	107	64
LAX	Straight-In	100	09:17	10:40	13:53	16:50	18:45					
	Downwind	300	29 min	102 min	71in 80	71 min	193 min					
	PropHolding	360	31	122		83	216					

Note: LAX Prop Holding Fixes are DARTS and SLI

The cost parameter values used in Equations (2.1-2.2) are shown in Table 2.3. Airport-specific costs of time and fuel (Center and TRACON) were weighted by the average airport fleet mix. Note the key assumption that TRACON fuelburn during arrival delay absorption is 1.5 times ARTCC fuelburn rate. This may be optimistic and representative of costs under optimal conditions. In fact under current operations, rush arrival flights are typically delayed in the ARTCC with vectoring, which does not fully leverage more fuel-efficient speed control methods for delay absorption. Thus, the Center/TRACON fuelburn rate assumption may be more representative of the EDA en route metering delay strategies (Chapter 3).

Table 2.3 Fleet-Weighted Time and Fuel Costs

	Airport Cost Rates ($/min)		
Cost Type	ATL	DFW	LAX
Time	$20.63	$17.78	$18.01
Fuel – ARTCC	$10.89	$9.19	$9.51
Fuel – TRACON	$16.34	$13.78	$14.27

TRACON Delay Settings

In the FFP1 Baseline case, TMA sets the TRACON time-to-fly during rushes to include the minimum TRACON to MF time-to-fly plus the TRACON Delay Setting. Since the MF delivery accuracy in today's operations is typically quite large, the maximum TRACON Delay Setting is used. This has the effect of maximizing runway system utilization, at the expense of less fuel-efficient trajectories. As the MF delivery accuracy improves, this delay can be shifted to more fuel-efficient to ARTCC airspace.

For each airport's rush/approach categories, optimum TRACON delay settings are defined from Equation (2.1) for the each case, with the parameter values of Tables 2.1 through 2.3. The optimal setting is then compared with the maximum settings defined in Table 2.2. Because the FFP1 Baseline settings are all less maximum, the optimal setting can be used, and thus all rush arrival operations are able to shift the full amount of delay from the TRACON to the Center airspace. The calculations of fuel savings per arrival and per rush are shown in Tables 2.4 relative to the FFP1 Baseline.

Table 2.4a ATL Center/TRACON Delay Distribution Fuel Savings Calculation

ATL	Approach Procedure	Rush Ops	Optimal TRACON Delay Setting (sec) FFP1 Baseline	Optimal TRACON Delay Setting (sec) EDA	EDA Fuelburn Savings ($)	
Rush 1	All	40	138	29	Per Arr	$9.89
					Per Rush	$396
Rush 2	All	62	160	33	Per Arr	$11.53
					Per Rush	$715
Rush 3	All	64	162	34	Per Arr	$11.62
					Per Rush	$743
Rush 4	All	79	171	36	Per Arr	$12.25
					Per Rush	$968
Rush 5	All	77	170	35	Per Arr	$12.25
					Per Rush	$943
Rush 6	All	116	187	39	Per Arr	$13.43
					Per Rush	$1558
Rush 7	All	99	181	38	Per Arr	$12.98
					Per Rush	$1285
Rush 8	All	109	185	38	Per Arr	$13.34
					Per Rush	$1454
Rush 9	All	63	161	33	Per Arr	$11.62
					Per Rush	$732

Table 2.4b DFW Center/TRACON Delay Distribution Fuel Savings Calculation

DFW	Approach Procedure	Rush Ops	Optimal TRACON Delay Setting (sec) FFP1 Baseline	Optimal TRACON Delay Setting (sec) EDA	EDA Fuelburn Savings ($)	
Rush 1	All	17	78	16	Per Arr	$4.75
					Per Rush	$81
Rush 2	All	27	115	24	Per Arr	$6.97
					Per Rush	$188
Rush 3	All	35	131	27	Per Arr	$7.96
					Per Rush	$279
Rush 4	All	78	171	36	Per Arr	$10.33
					Per Rush	$775
Rush 5	All	47	147	31	Per Arr	$8.88
					Per Rush	$417
Rush 6	All	75	170	35	Per Arr	$10.33
					Per Rush	$775
Rush 7	All	53	153	32	Per Arr	$9.26
					Per Rush	$491
Rush 8	All	85	175	36	Per Arr	$10.64
					Per Rush	$904
Rush 9	All	107	185	38	Per Arr	$11.25
					Per Rush	$1204
Rush 10	All	64	162	34	Per Arr	$9.80
					Per Rush	$627

Table 2.4c LAX Center/TRACON Delay Distribution Fuel Savings Calculation

LAX	Approach Procedure	Rush Ops	Optimal TRACON Delay Setting (sec) FFP1 Baseline	EDA	EDA Fuelburn Savings ($)	
Rush 1	All	31	123	26	Per Arr	$7.69
					Per Rush	$238
Rush 2	All	122	189	39	Per Arr	$11.89
					Per Rush	$1450
Rush 3	All	80	172	36	Per Arr	$10.78
					Per Rush	$862
Rush 4	All	83	173	36	Per Arr	$10.86
					Per Rush	$901
Rush 5	All	216	211	44	Per Arr	$13.24
					Per Rush	$2859

Economic Analysis

The fuelburn savings from shifting delay from the TRACON to the Center airspace is determined for each arrival rush and multiplied by the frequency of using each approach category in each rush. The savings are calculated for each rush period, as the TRACON delay setting is dependent upon the rush size (*N*). Table 2.5 summarizes the daily savings of all airports. Note that LAX and ATL show more benefit due to their larger number of aircraft per rush. A three-airport average is calculated for use in annual/NAS-wide extrapolation.

Table 2.5 EDA Center/TRACON Delay Distribution Fuel Savings Summary

	EDA Daily Center/TRACON Delay Distribution Benefits			
	ATL	DFW	LAX	Airport Average
Rush Operations Rate (per 100 Airport ops)	35.7	27.0	27.0	30.4*
ARTCC Delay Shift (sec)	137 sec	128 sec	150 sec	138 sec
Average Fuel Savings ($)	$12.40/op	$9.82/op	$11.86/op	$11.42/op
	$977/rush	$577/rush	$1,262/rush	$939/rush
	$8,794/day	$5,772/day	$6,311/day	$6,959/day

* Assumes average delayed arrival rates from reference [12] to maintain consistency between EDA benefit estimates.

The daily DFW savings are extrapolated to an annual level and to other NAS airports by accounting for the total number of 1996 operations at each facility. NAS benefits are calculated based on EDA deployment in the Center airspace surrounding 37 candidate airport sites. This set was chosen to represent high-demand NAS airports, include FAA FFP1 and phase 2 deployment locations. The simple extrapolation used here employs Equation (2.3) to estimate benefits, as employed in other studies [12].

$$\textit{Annual Savings} = (\textit{Annual Ops}) \times (\textit{Rush Arrivals}_{DFW}) \times (\textit{Apt Factor}) \times (\textit{Savings Per Interrupt}) \quad (2.3)$$

where: *Annual Ops* = Annual airport operations (00s) (Appendix B)

Rush Arrivals$_{DFW}$ = DFW number of rush arrivals per 100 daily airport operations (Appendix B)

Apt Factor = Factor accounting for local airport rush arrival frequency relative to DFW, based on FAA delay data (Appendix B)

Savings Per Interrupt = Average cost savings per rush arrival (Table 2.6)

As in the other evaluations, DFW rush arrival rates were adjusted by an *Airport Factor* to account for variations in congestion at each facility. Airports with less overall delays are assumed to require disproportionately fewer metering conformance actions. Thus, airports with less demand-capacity congestion are assumed to delay fewer en route arrival and

departure aircraft to meet airport-scheduling constraints. An individual airport's assumed delayed arrival rate is adjusted from the nominal DFW value of Table 2.6, using FAA delay data [31]. These data records delays at each airport in excess of 15 minutes in CY1996, including both arrivals and departures. This metric hides the significant number of smaller delays during an arrival rush period and includes delayed departures, making it a gross indicator of the airport's level of delayed arrival flights. Despite these limitations, this data provided a reasonable factor for extrapolating the detailed traffic analyses (at 3 airports) to the 37-NAS airports. To do so, the NAS airports were broken into five delay categories. Engineering judgement was used to assign each category a rush arrival rate relative to DFW. Simulated rates [12] of 130%, 115%, 100%, 80%, and 60% for airport delay classes 1, 2, 3, 4, and 5 were used, as shown in Table 2.6. The FAA delay data and criteria used to assign delay classes are included in Appendix B.

The three-airport average rush arrival rates and cost savings observed in the daily simulation are summarized in Table 2.5 and used in Equation (2.3). Note that the average rush arrival rate was increased slightly to match metered arrival frequencies identified in previous studies in order to be consistent with the other benefits assessments in this report.

The annual airport operations [36] and resulting annual savings by airport using Equation (2.3) are shown in Table 2.6. The annual savings are plotted graphically by airport in Figure 2.3. The large hub airports, ORD, DFW, ATL, and LAX, achieved significant gain with EDA, saving over $2.5M per year relative to the FFP1 Baseline. Benefits at all 37 NAS-deployment airports, representing NAS-wide deployment, totaled $47.73M annually.

Table 2.6 EDA Center/TRACON Delay Distribution Benefits

Airport	Annual Airport Ops (000s)	Apt Delay Delays/Category		Rush Arrival Rate (per 100 Airport Ops)	EDA Annual Cost Savings ($M, 1998)
Atlanta (ATL)	773	23.88	3	30.4	2.68
Nashville (BNA)	226	1.36	5	18.2	0.33
Boston (BOS)	463	0.73	2	18.2	0.47
Bradley (BDL)	161	26.37	5	34.9	1.84
Baltimore (BWI)	270	3.67	5	18.2	0.56
Cleveland (CLE)	291	4.68	5	18.2	0.61
Charlotte (CLT)	457	6.55	4	24.3	1.27
Cincinnati (CVG)	394	10.38	4	24.3	1.09
Washington National (DCA)	310	6.53	4	24.3	0.86
Denver (DEN)	454	1.90	5	18.2	0.94
Dallas – Ft. Worth (DFW)	870	19.59	3	30.4	3.01
Detroit (DTW)	531	9.10	4	24.3	1.47
Newark (EWR)	443	65.25	1	39.5	2.00
Ft. Lauderdale (FLL)	236	1.53	5	18.2	0.49
Houston Hobby (HOU)	252	2.57	5	18.2	0.52
Washington Dulles (IAD)	330	6.81	4	24.3	0.92
Houston – Intercontinental (IAH)	392	11.45	4	24.3	1.09
N.Y. Kennedy (JFK)	361	29.53	2	34.9	1.44
Las Vegas (LAS)	480	3.68	5	18.2	1.00
Los Angeles (LAX)	764	24.13	3	30.4	2.65
N.Y. LaGuardia (LGA)	343	46.22	1	39.5	1.54
Orlando (MCO)	342	4.59	5	18.2	0.71
Chicago Midway (MDW)	254	6.70	4	24.3	0.71
Memphis (MEM)	364	NA	5	18.2	0.76
Miami (MIA)	546	6.79	4	24.3	1.51
Minneapolis (MSP)	484	9.29	4	24.3	1.34
Oakland (OAK)	516	NA	5	18.2	1.07
Chicago O'Hare (ORD)	909	34.46	2	34.9	3.62
Portland (PDX)	306	2.41	5	18.2	0.64
Philadelphia (PHL)	406	17.95	3	30.4	1.41
Phoenix (PHX)	544	7.25	4	24.3	1.51
Pittsburgh (PIT)	447	6.60	4	24.3	1.24
San Diego (SAN)	244	3.31	5	18.2	0.51
Seattle (SEA)	398	6.37	4	24.3	1.10
San Francisco (SFO)	442	56.57	1	39.5	1.99
Salt Lake City (SLC)	374	3.53	5	18.2	0.78
St. Louis (STL)	517	34.04	2	34.9	2.06
37-Airport Total/Average	430	---		---	47.73

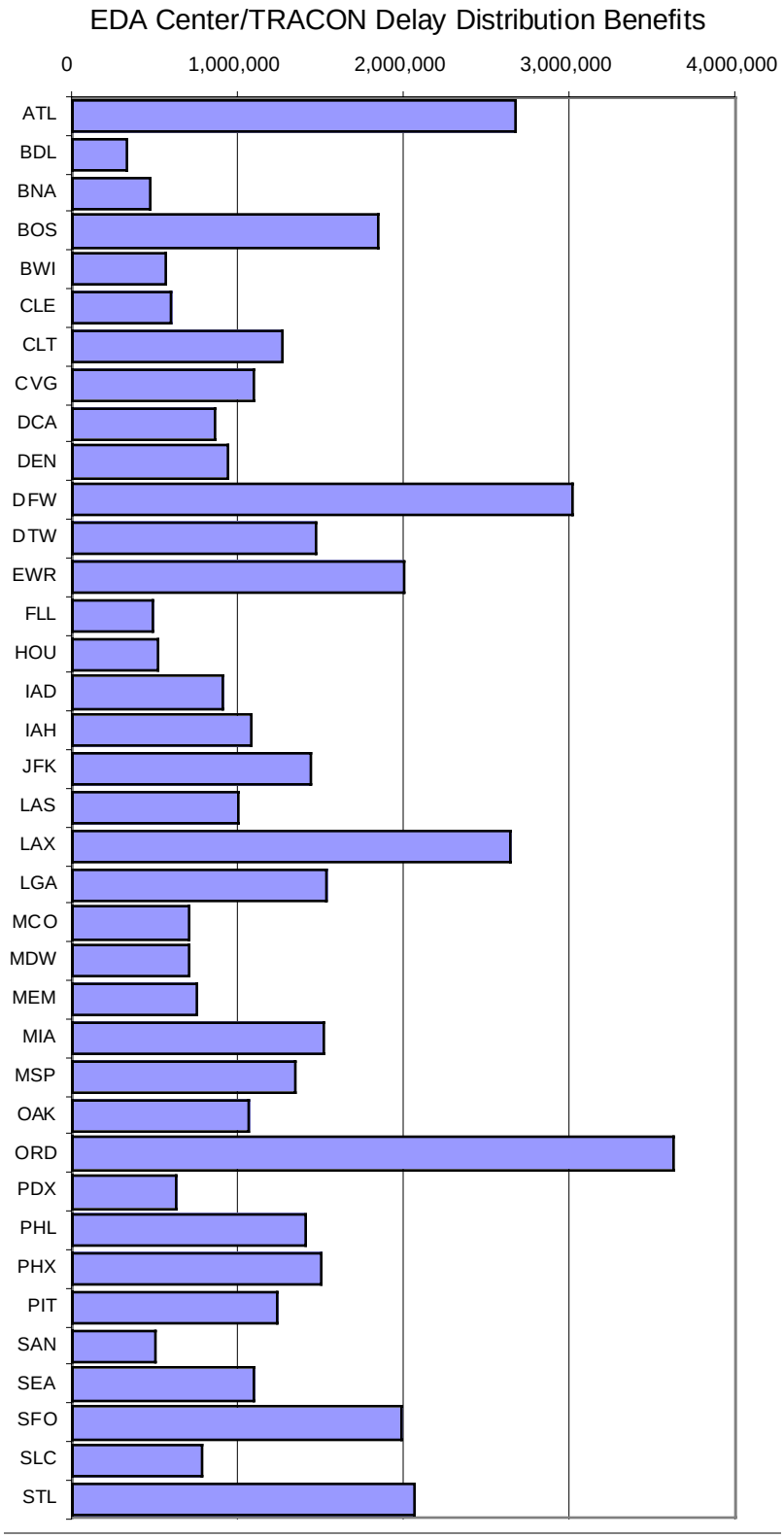

Figure 2.3 EDA Center/TRACON Delay Distribution Benefits

Results Summary

This chapter evaluated EDA Center/TRACON delay distribution benefits. Reduced variance in EDA arrival metering fix delivery accuracy results in arrival flight efficiency benefits due to the ability to absorb more efficiently upstream in Center airspace while still maintaining a given TRACON entry rate.

It was found that EDA shifted an average of 138 seconds of rush arrival delay from TRACON to Center airspace. This saved 114 lbs of fuel or $11.42 per rush arrival ($939 per average rush), with a total savings of $47.73M annually assuming NAS-wide deployment at 37-airports. This EDA benefit mechanism is used to model the general shift of delay from TRACON to Center airspace. EDA metering conformance efficiency, discussed in the next chapter, addresses more specifically the EDA efficiency of Center delay absorption, a separate advantage of EDA operations over TMA alone.

The EDA benefits were evaluated relative to a FFP1 Baseline, which includes TMA. The arrival metering fix delivery accuracy (1-sigma) was found to be approximately 180 seconds prior to TMA and 90 seconds with TMA [30]. EDA field tests found an accuracy of 15-20 seconds [10], modeled here as 17.9 seconds (Table 1.2). Using these values, a rough indication of the relative Center/TRACON delay distribution benefits of EDA and TMA can be made by using Figure 2.2. Note that for the FFP1/TMA Baseline, the maximum delay absorption capability of a route (typically 100-300 seconds) would likely require a TRACON delay setting below optimal. Thus, despite TMA's significant improvement in metering fix delivery accuracy, little change would occur in the TRACON delay setting, allowing only limited shifting of delay to more fuel-efficient ARTCC airspace, with associated limited benefits. Post-TMA, improvements to the metering fix accuracy, such as with EDA, enables a reduction in TRACON delay along the optimal line, resulting in significantly higher benefits per metering fix accuracy improvement.

To achieve these benefits, it is assumed that TRACON traffic managers would be comfortable in shifting delay upstream (i.e., less TRACON front-loading) with the more accurate metering fix delivery schedule adherence of these DSTs. Additionally, the study would benefit from a better understanding of the controllability window (minimum/maximum TRACON delay setting) of various TRACON arrival routes at various ATM facilities. Another key assumption driving these estimates is that aircraft fuelburn rates for absorbing delay are 1.5 times larger in the TRACON relative to ARTCC airspace. This assumption should be calibrated with field data, and may differ under Baseline and EDA metering conformance delay strategies. Alternatively, higher fidelity aircraft trajectory and fleet mix models could be employed to improve fuelburn estimates.

3 Arrival Metering Conformance Efficiency Benefits

Air traffic controllers deviate flights from the users' preferred trajectory to avert impending traffic conflicts and to conform to flow-rate restrictions. The efficiency and effectiveness of such controller-imposed deviations directly affect controller and flight crew workload as well as user costs. ATM En Route DSTs and their further enhancement with data exchange have the potential to reduce unnecessary deviations and improve the efficiency with which necessary deviations are implemented by more accurately predicting flight trajectories and supporting useful clearance decisions. We refer to these processes that the ATM system uses to interrupt the normal traffic flow in order to mechanize flow-rate conformance and separation assurance conflict resolution as "ATM interruptions," and the DST processes of reducing and imposing more efficient traffic interruptions as "ATM interruption benefits." This chapter evaluates EDA improvements to ATM arrival-metering conformance efficiency (i.e., reduction in costs related to ATM flight interruptions for arrival delay absorption). The following chapter evaluates EDA improvement to separation assurance flight interruptions as integrated with metering conformance.

During high-density airport arrival operations under the FFP1 Baseline, the CTAS Traffic Management Advisor (TMA) sets a meter-fix crossing schedule to optimize the arrival flow into the terminal area. The controller then meters arrival traffic according to this schedule, as necessary, to meet airport flow-rate restrictions. Arrival metering delay is absorbed en route, using a mix of airborne delay absorption methods including changes in speed (cruise and descent), cruise altitude, and routing (vector/path-stretching) of the arrival trajectory. Baseline delay strategy development entails controller cognitive processes. EDA automation assists controllers in formulating and executing an arrival delay strategy, by providing EDA-generated metering conformance maneuver advisories (i.e. conflict-free, fuel-efficient aircraft clearances to meet the TMA schedule). This EDA assistance allows the controller to assess quickly and accurately the impact of various delay methods. Earlier execution on the time horizon to the metering fix allows an increased use of fuel-efficient speed control delay methods and reduced reliance on the more expensive vectoring methods.

Additionally, the EDA built-in conflict prediction/resolution capability can assist controllers in accommodating user-requested arrival preferences, such as direct routes to a future waypoint or metering fix. To address the impact of arrival direct routing on metering conformance and separation assurance flight interruptions, two EDA cases were analyzed, standard terminal arrival routes (STARs) and direct arrival routes. Metering Conformance impacts are assessed here, while separation assurance impacts are addressed in the next chapter.

Specifically, this benefit mechanism concerns the fuel-efficiency of ATM strategies to absorb arrival metering delay under Baseline and EDA automation-assisted operations. The cost of ATM interruptions for metering conformance were calculated for both technology cases sensitive to the chosen delay strategies, their implementation accuracy, and the time horizon until metering fix crossing. EDA automation is shown to result in more fuel-efficient metering conformance actions.

Analysis Process

The benefits methodology process employed in previous research [11-12,16] is described below. The sequence of analytical formulations and computer-based modelings follows the Figure S.1 approach (and numbering) of the introduction summary section. After identifying the technologies and their parametric effects of the study case (1), the attributes of the particular Baseline and EDA metering conformance delay absorption strategies are defined (2). These strategies are then combined with a DFW daily traffic schedule in an

ATM Interruptions Model (3), shown in Figure 3.1. Initially, the model generates a set of air-traffic trajectories for a typical day within a block of Center airspace. This set of four-dimensional (4D) "undelayed" trajectories, represents what each flight would do if left alone to fly the users' filed route and preferred profile. The Metering Conformance model component analyzes the arrival traffic and determines aircraft-specific metering delay necessary to meet airport flow-rate restrictions. A new set of arrival flight trajectories is then generated, incorporating maneuvers necessary to absorb the metering delay, under Baseline and EDA metering conformance strategies. The aircraft-specific delay methods employed and their associated interruption costs are tabulated. The simulated daily interruption rates and costs are then extrapolated to annual and NAS-wide levels using economic models (4). These model components are discussed in more depth with the analysis results in the next section.

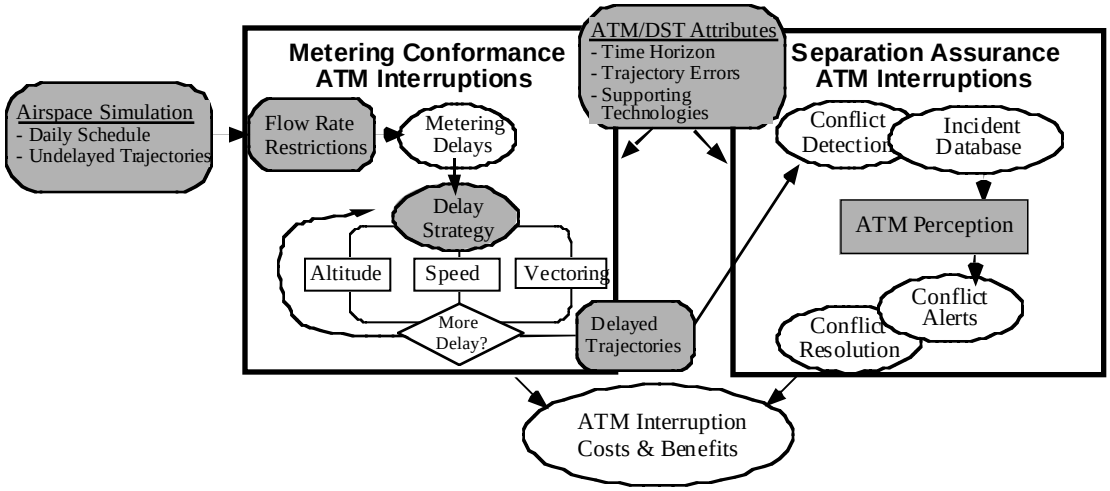

Figure 3.1 ATM Interruptions Model Approach

Metering Conformance Strategies

Figure 3.2 illustrates the general methodology employed in the model to clear an aircraft to meet a delayed arrival fix crossing time. Combinations of speed, altitude, and vectoring maneuvers are considered, where the maximum amount of delay is absorbed by each method before moving onto the next method. The affect of time horizon where the maneuver is initiated is also illustrated. Note that at larger time horizons (right figure), speed and altitude changes can absorb more delay. As the effective time horizon decreases (left figure), the need for more expensive vectors (path stretching) increases since the speed and altitude changes cannot absorb as much delay.

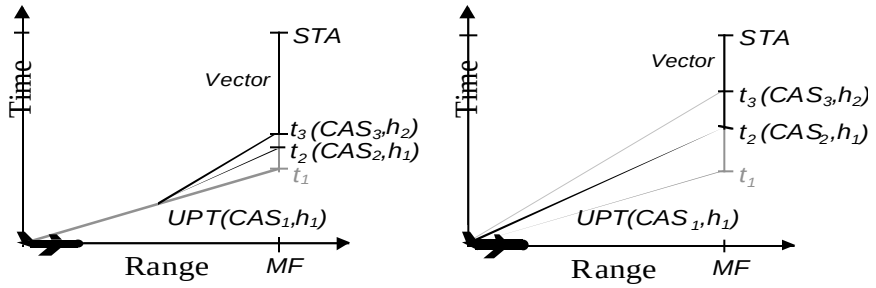

t_1 = User Preferred Trajectory (UPT) = Undelayed Metering Fix (MF) crossing time (CAS_1, h_1)
t_2 = Crossing time if cleared to minimum speed (CAS_2)
t_3 = Crossing time if cleared to minimum speed at a lower altitude (h_2)
STA = crossing time if cleared to minimum speed, lower altitude, and vectored

Figure 3.2 Metering Conformance Delay Absorption

The effectiveness of the delay absorption clearance depends on the amount of delay to be absorbed by any one flight, the time available to absorb the delay (i.e., effective time horizon), and the delay absorption strategy. Differences in delay-absorption performance are modeled through differences in the technology-specific time horizon and delay strategy.

In the model, four possible arrival metering conformance methods are used to alter the trajectory of particular flights so that the proper amount of delay is absorbed. The four methods are graphically illustrated in Figure 3.3.

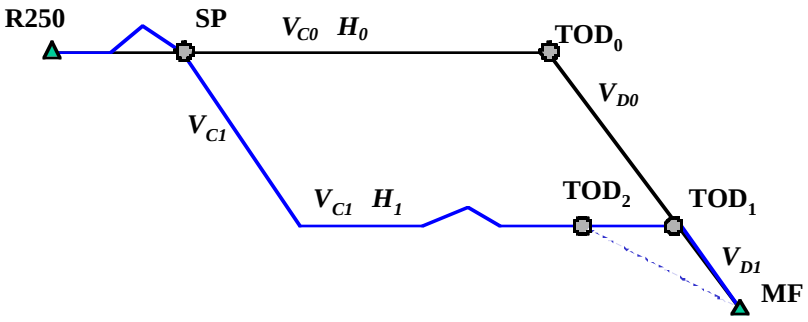

LEGEND

R250	= Airspace Outer Ring (250nm out)	TOD	= Top-of-Descent Location
MF	= Arrival Metering Fix	H	= Altitude (ft)
SP	= Meet-time Maneuver Start Point = *x* minutes before MF Crossing Time	V	= Speed CAS (kt)

Figure 3.3 ATM Interruption for Metering Conformance

- **Speed Control** - Reduce aircraft cruise and descent CAS speed along the initial routing and altitude profile. Chosen speeds are limited by aircraft performance-based minimum speeds, assumed to approximate best endurance speed under EDA, and subject to ATM controller rounding/ increment limitations. In this study, the descent speed is set to essentially "balance" cruise and descent CAS speeds. The higher of cruise/descent CAS is initially decremented until both speeds are equal. Then each speed is alternately decremented. Although actual controller techniques may not be so precise, this approach conservatively represents controller actions. Reduction in speed profile results in an earlier TOD location.

- **Altitude Change** – Descend and maintain a new cruise altitude (until final top of descent) down to floor of the high-altitude sector airspace (flight level (FL) 230/240). With future technology cases, speed may also be allowed to change at the new altitude, providing an optimal combined speed/altitude approach.

- **Vectoring**– Increase path length, using simple 1-sided out and back vector path stretching, at constant altitude and speed, up to a maximum heading change. The aircraft is vectored off the original path and than back to the top of descent (TOD). An error is imposed on the timing of the final return vector to reflect ATM clearance limitations that may lead to arrival fix STA deviations, as shown in Figure 3.4. A turn back error is modeled as a random sample from a distribution, with bounds reflecting ATM/DST accuracy.

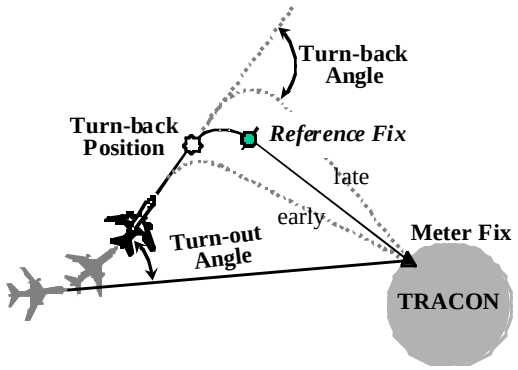

Figure 3.4 Modeled Vectoring Method

- **Time Shift Strategy** – A last resort method, assumes delay is absorbed by the controller issuing additional vectoring clearances for additional path stretching at cruise altitude/speed, essentially shifting ARTCC entry times to absorb any remaining delay.

A specific delay strategy is defined by the ordering of these methods in addition to time horizon and clearance accuracy parameters. These strategy orderings are an extreme simplification of the complexity of actual operations, which are restricted, especially in the Baseline case, by such issues as sector airspace boundaries, rush/non-rush conditions, in-trail separation constraints, and controller workload. Table 3.1 summarizes metering conformance delay strategy parameters for Baseline and EDA cases. Each case is summarized in the following paragraphs.

Table 3.1 Assumed Metering Conformance Delay Strategy Parameters

	FFP1	CTAS EDA
General		
Strategy Order	Altitude Speed Vectoring Time Shift	Speed Altitude/Speed Vectoring Time Shift
Time Horizon	16 min	18 min
Speed		
Speed Increments	10 kt	5 kt
Speed Error	+ 10 kt	None
Min Cruise Speed Min Descent Speed	BADA(1) BADA (1)	BADA(1) – 10 kts BADA(1) – 20 kts
Altitude (Jets only)		
Permitted Altitudes	Min Altitude	FAR Altitudes
Min Altitude	FL230/FL240	FL230/FL240
Vectoring		
Heading Increment	1°	1°
Max Vector Angle	60°	60°
Turn back Error	± 60 seconds	± 30 seconds

(1) Reflecting a lack of automation to help controllers identify efficient speeds, the minimum cruise/descent speeds for FFP1 used Eurocontrol BADA model [37] "low" cruise speeds included in Appendix D (e.g. 250 kts for jets). EDA minimum speeds were modeled as 10 kts (20 kts in descent) lower than BADA, a conservative estimate closer to best endurance speed.

FFP1 Baseline Strategy

The FFP1 Baseline delay strategy reflects current ZFW Center metering conformance methods, based on discussions with NASA ATM experts familiar with ZFW en route airspace [38]. A time horizon of 16 minutes (before the undelayed metering fix crossing time) is assumed, allowing a 3-minute lag after the TMA delay advisories are displayed to the controller. In this cognitively developed strategy, controllers are assumed to first employ altitude control by descending aircraft to the floor of the high-altitude sector airspace. Additional delay is absorbed using speed reductions, based on controller experience, down to a minimum speed applicable to most aircraft types. Without additional information/automation, controllers are unable to routinely identify acceptable lower speeds for clearance. A speed error is added to the optimal case to represent cognitive limitations in developing the metering conformance clearance without automation assistance. Finally, vectoring is implemented to absorb any residual delay. The magnitude of the vectoring turn back error [10] reflects controller cognitive limitations in identifying the optimal vector turn back location/time.

EDA Strategy

EDA delay strategies [6], employ high-fidelity trajectory modeling to predict future aircraft positions and generate metering conformance maneuver advisories. The maneuver advisories assist controllers in quickly formulating and executing a traffic delay strategy. As such, a longer 18 minutes time horizon (only a 1-minute lag after the TMA delay advisories are displayed) is assumed. With a longer time horizon, speed control can be implemented more effectively, and because of its fuel efficiency, is attempted first. EDA automation provides controllers with more efficient speeds that are closer to the aircraft's best endurance speed than manually possible. If speed control alone is not sufficient, a combination of altitude/speed adjustments are used instead. Here, EDA advises an optimal speed/altitude combination, difficult to calculate without EDA data and computational

assistance. Vectoring, the least precise and least efficient strategy is reserved for large delays. EDA vectoring advisories are designed to bring the flight within speed-control range using precise "turn-back" advisories to reduce uncertainty [10].

Arrival Metering Costs

ATM interruptions for metering conformance, which delay metering fix arrivals to meet airport capacity constraints, result in both time and fuel penalties. Time costs were calculated directly from the arrival metering delay combined with FAA-based airborne cost rates included in Appendix C. Time costs include both crew and maintenance components and vary by aircraft class.

Fuel costs were primarily calculated using Equation (3.1). Additional cost components were added to account for changing TOD location and turn back error corrections, not implemented geometrically in the delayed trajectories.

$$FuelCost = Fuelburn\ Rate \times Distance_{Cruise}/Speed_{Cruise} \quad (3.1)$$

Equation (3.1) essentially applies a fuelburn rate to the cruise flight time. This flight time is calculated as the distance flown during the case-specific time horizon. Arrival fuel rates were calculated based on cruise speed and altitude and an average aircraft weight per type. Time shift delays were evaluated as additional vectoring time at the vectoring cruise altitude and speed. Arrival fuelburn rates used in the cost model are included in Appendix D. The fuelburn rates were based on high-fidelity simulations [39] of a B737 aircraft under various conditions normalized to determine the fuelburn rates (lbs/min) at each altitude and airspeed. Thus delay strategies causing reductions in speed or altitude employed different fuelburn rates. Vectoring or time shift methods increased fuel costs by increasing the time or distance spent at constant speed/altitude with its associated fuelburn rate. The B737 simulation results were extrapolated to all aircraft classes by applying a scale factor, derived from FAA-based airborne fuel cost rate data found in Appendix C. As with departures, a fuel cost of $0.10 per pound was assumed, so results should be scaled to reflect future higher fuel costs. This approach assumes no fuel impact with speed changes on the descent segment, a simplification of the assumed idle descent conditions.

Additionally, the fuel impact of the vectoring turn back error was also added to the delayed arrival trajectory fuel cost. Vectoring turn back error impacted fuel costs as increased vectoring distance pre-TOD (late turn), or post-TOD on descent (early turn). Additional vectoring on descent was assumed at the descent speed and MF altitude using the B737-based fuelburn rates just discussed. A fuel and time penalty was imposed when vectoring turn back error caused the flight to arrive late to the metering fix. The impact of such arrival fix delivery error on inefficient metering fix throughput was not addressed.

Finally, the above speed change fuelburn estimate (jets only) was adjusted to account for the fuel impact of a modified TOD location under changing cruise speed. The fuel impact of the new TOD location leads to additional or reduction of fuel burned depending upon the extended (faster) or shortened (slower) cruise segment. The TOD location, relative to nominal, was calculated using Equation (3.2) for both undelayed and metered flights, with the difference representing the shift in TOD location due to metering conformance cruise speed changes.

$$TOD\ Shift = 0.00001 \times (Altitude_{Cruise} - Altitude_{MF}) \times (Speed_{Descent} - 280) \quad (3.2)$$

where: $Altitude_i$ = Arrival cruise and metering fix (MF) altitudes (ft)
$Speed_{Descent}$ = Descent speed (kt)

Equation (3.2) assumes a typical jet descent rate of 3 nm per 1000 vertical ft, at a nominal 280 kts CAS. The descent rate was assumed to shift by 0.1 nm per 1000 ft, for every 10 kt

deviation from the nominal descent speed. The fuelburn impact of this TOD location was calculated by applying the B737-based cruise fuelburn rates, to the cruise distance shift in TOD location. The speed fuelburn estimates were adjusted accordingly.

Traffic Scenario

Initially an en route set of air-traffic "demand" trajectories for a typical day within a block of en route airspace was defined. In this study the Fort Worth Air Route Traffic Control Center (ZFW) airspace was analyzed, including arrival, departure, and overflight traffic operations between 40 and 250 nautical miles (nm), at or above 10,000 ft from Dallas-Fort Worth International Airport (DFW). Enhanced Traffic Management System (ETMS)-based flight trajectories for a typical day (Friday, June 14, 1996) were used to generate "undelayed" trajectories, trajectories for approximately 2,500 DFW arrivals and departures [35], representing what each flight would do if left alone to fly the users' filed route and preferred profile. FFP1 filed routes were restricted to STAR routes, while two EDA traffic scenarios were generated representing filed STAR or direct arrival routing to the arrival-metering fix. The arrival trajectories, shown in red in Figure 3.5, define the arrival congestion traffic scenario. The figure also includes the study day departures (blue) and overflights (green). The various cases under study are shown in Table 3.2.

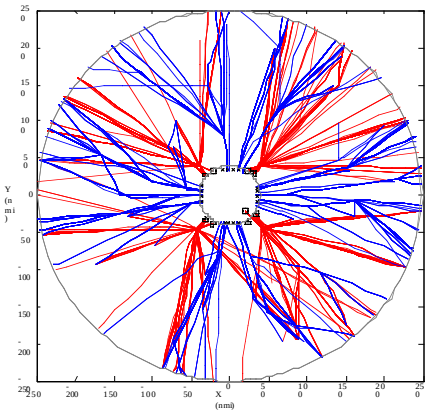

DFW

Figure 3.5 Plan and Profile View of DFW Study Day Operations

Table 3.2 Analysis Case Criteria

Case	Metering Conformance Strategy	Traffic Routing	
		Departures	Arrivals
FFP1 Baseline	FFP1	SID	STAR
EDA-STAR	EDA	SID	STAR
EDA-Direct	EDA	SID	Direct Arrivals

Arrival Metering Delay

During peak periods controllers meter DFW arrival flights to meet airport capacity restrictions. A simplified model of TMA metering was developed to estimate metering delays for each DFW arrival. Meter-fix scheduled times of arrival (STAs) at the TRACON boundary, and associated delays, were based on maximum TRACON entry rates and minimum inter-arrival fix separations, as shown in Table 3.3. Figure 3.6 shows a distribution of the delays imposed upon the 1,047 arrival flights in order to meet the Table 3.3 flow-rate constraints over the course of the sample day.

Table 3.3 DFW Scheduling Criteria

Scheduling Criteria	Assumed Value
Minimum Arrival Meter-Fix Separation	5.50 nm
Maximum TRACON Arrival Rate (4 Arrival	150 ac/hr

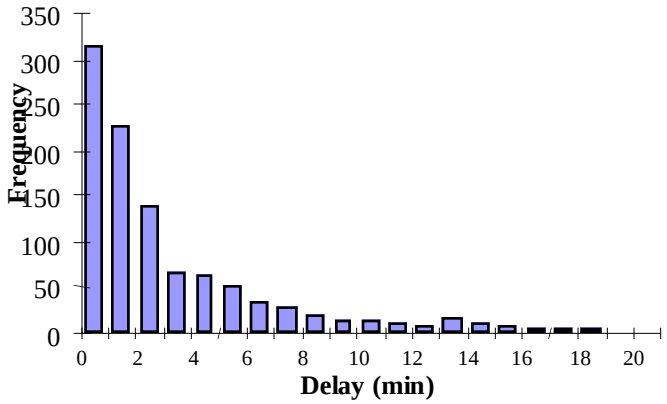

Figure 3.6 TMA Arrival Delays

EDA Metering Savings

The metering conformance cost model, discussed earlier, was used to calculate the total fuel expended for each simulated metered arrival flight. EDA metering conformance benefits were calculated as the difference between the total (time and fuel) arrival delay costs of the Baseline and EDA cases. The frequency and per operation rates from the daily simulation were then used to extrapolate annual and NAS-wide potential benefits.

The number of metering conformance interruptions and share of total delay absorbed by each method is shown in Table 3.4. Despite the different trajectories in the two EDA cases (arrivals on STAR or direct routing), there was no significant difference in metering conformance results. The EDA direct and STAR arrival routes are subject to the same arrival fix crossing schedule, but differ on the time they enter the en route ARTCC. Because of the similar results, the following discussion will address them jointly as EDA results. Note that the similar results imply that direct routing does not inhibit EDA metering conformance efficiency.

Table 3.4 Metering Conformance Delay Methods

	Number Delayed Arrivals	Delay (min)		Method Frequency (%)*			Share of Total Delay (%)		
		Ave.	Total	Altitude	Speed	Vector/TS	Alt/Spd	Vector	TimeShift
FFP1 Baseline	662	4.0	2682	41.2%	38.4%	84.9%	16.2%	47.2%	36.6%
EDA	662	4.0	2654	47.0%	74.0%	65.9%	31.8%	34.4%	33.8%

Note: In this table, EDA-STAR and EDA-Direct arrival cases produced identical results.
* Because multiple methods were applied to each flight, these columns sum to over 100 percent

Two arrival delay strategy breakdowns are shown in the table. The first shows the frequency of employing each method. The second identifies the share of total delay absorbed by each method. The frequency breakdown and Figure 3.7 clearly show that EDA replaces the Baseline's use of vectoring with less intrusive and more cost-effective speed control and altitude arrival delay methods.

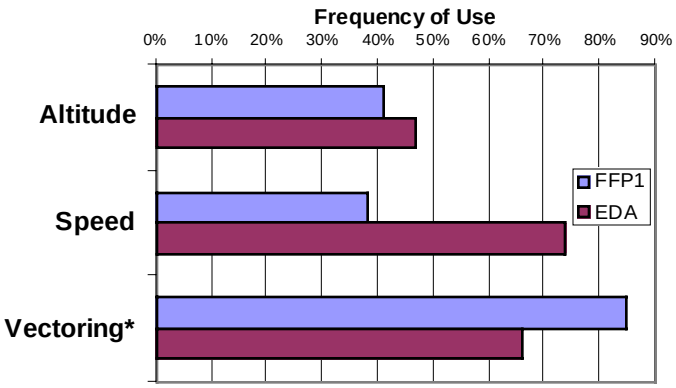

* Vectoring includes Time Shift method.

Figure 3.7 Comparison of Employed Metered Arrival Delay Strategies

As previously shown in Figure 3.6, both Baseline and EDA metered arrival flights were delayed typically 3-5 minutes, with an average of 4.0 minutes. The range of arrival delay absorbed with each delay method is shown in Table 3.5. The table compares the varying effectiveness of the delay absorption methods employed in both the Baseline and EDA cases

Table 3.5 Metered Arrival Delay Comparison

	Delay (minutes)					
	FFP1 Baseline			EDA – STAR*		
	Range	Ave	Total	Range	Ave	Total
Altitude	0-2.5	0.2	160	0-10.2	1.3	845
Speed	0-4.6	0.4	275			
Vectoring**	0-18.1	3.4	2,247	2.8-17.9	2.7	1,808

Note: In this table, EDA-STAR and EDA-Direct arrival cases produced identical results.
* CTAS EDA cases combine speed and altitude methods.
** Vectoring includes Time Shift method.

Table 3.6 compares the resulting arrival metering conformance fuel costs tied to the FFP1 Baseline and EDA cases. The table points out the fuel efficiency of speed delays, where delays absorbed with speed control can actually reduce the overall flight cost (i.e., note negative values in Table 3.6). Additionally, EDA with direct arrival routes (i.e., those marked "Direct") was found to have slightly lower altitude speed costs for a given delay (than those that followed the STAR routes), resulting in overall lower delay fuel costs under this scenario. This implies that direct routing does not inhibit EDA metering conformance efficiency. Overall, EDA saved approximately $4000 worth of fuel (at $0.10 per lb) in the daily simulation

Table 3.6 Simulated Metered Arrival Fuelburn Comparison

	FFP1 Baseline			EDA-STAR			EDA-Direct		
	Fuel (lbs)								
	Range	Ave	Total	Range	Ave	Total	Range	Ave	Total
Altitude/Speed	(168)-579	14	9,502	(533)-590	17	11,494	(753)-483	13	8,645
Vectoring*	0-2,659	244	161,422	0-2,440	182	120,205	0-2440	183	120,866
Total	(133)-2,793	258	170,924	(533)-2,773	199	131,700	(533)-1,870	196	129,511
	Total Fuel Cost ($) **								
Total	$(13)-279	$25.82	$17,092	$(53)-277	$19.89	$13,170	$(53)-187	$19.56	$12,951

* Vectoring includes Time Shift method.

** Assumes $0.10 per lb of fuel.

As both cases used the same traffic scenario and flow-rate constraints, each flight was subject to the same time delays in the Baseline FFP1 and EDA cases. As a result, EDA savings primarily reflect improved fuel efficiency in absorbing the common metering delay. However, a vectoring turn back error was applied which, in some cases, increased the flight time to the arrival fix. Less error was applied in the EDA case, based on prototype EDA observations [10]. This increased the FFP1 time by 1 percent (see Table 3.4) increasing EDA daily cost savings by $500 ($740 with direct route case). Figure 3.8 graphically shows the distribution of total (time and fuel) per operation EDA metering conformance fuel savings.

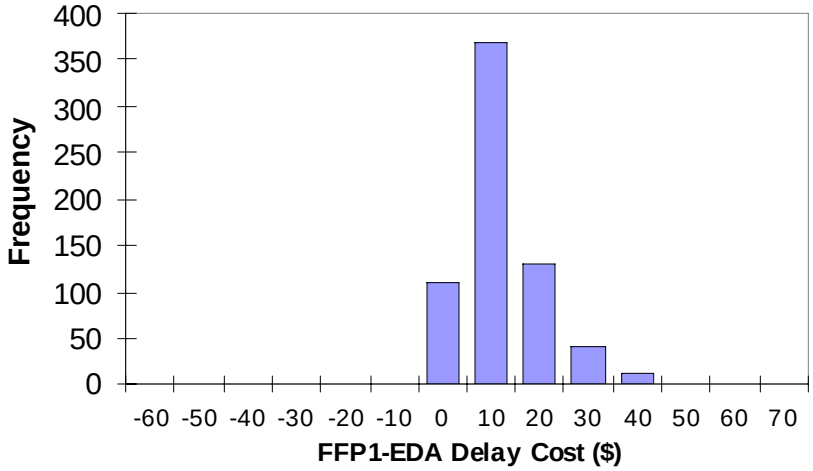

Figure 3.8 EDA Metering Conformance Savings Per Operation

Economic Analysis

As with other benefit mechanisms in this report, these daily DFW savings were extrapolated to an annual NAS-wide level by accounting for the total number of 1996 operations at each facility. As in other chapters, the simple extrapolation employs Equations (3.3) and (3.4) to estimate benefits.

$$\textit{Annual Cost} = (\textit{Annual Ops}) \times (\textit{Rush Arrivals}_{DFW}) \times (\textit{Apt Factor}) \times (\textit{Cost Per Interrupt}) \quad (3.3)$$

$$\textit{Annual Savings} = \textit{Annual Cost}_{FFP1} - \textit{Annual Cost}_{EDA} \quad (3.4)$$

where: *Annual Ops* = Annual airport operations (00s) (Appendix B)
Rush Arrivals$_{DFW}$ = DFW number of rush arrivals per 100 daily airport operations (Appendix B)
Apt Factor = Factor accounting for local airport rush arrival frequency relative to DFW, based on FAA delay data (Appendix B)
Cost Per Interrupt = Average cost savings per rush arrival (Table 3.7)

The average rush arrival rates and cost savings observed in the daily simulation are summarized in Table 3.7.

Table 3.7 DFW Interruption Rates and Costs

	FFP1 Baseline	EDA-STAR	EDA- Direct
Metered Arrival Rate (per 100 ops)	30.4	30.4	30.4
Cost Per Interrupt ($/op)	$104.66	$97.86	$97.50

As in the other evaluations, DFW rush arrival rates were adjusted by an *Airport Factor* to account for variations in congestion at each facility. Airports with less overall delays are

assumed to require disproportionately fewer metering conformance interruptions. Thus, airports with less demand-capacity congestion are assumed to delay fewer en route arrival and departure aircraft to meet airport-scheduling constraints. An individual airport's assumed delayed arrival rate is adjusted from the nominal DFW value of Table 3.7, using FAA delay data [31]. These data record delays at each airport in excess of 15 minutes in CY1996, including both arrivals and departures. This metric hides the significant number of smaller delays during an arrival rush period and includes delayed departures, making it a gross indicator of the airport's level of delayed arrival flights. Despite these limitations, this data provided a reasonable factor for extrapolating the detailed DFW traffic analyses to the 37-NAS airports. To do so, the NAS airports were broken into five delay categories. Engineering judgement was used to assign each category a rush arrival rate relative to DFW. Simulated rates [12] of 130%, 115%, 100%, 80%, and 60% for airport delay classes 1, 2, 3, 4, and 5 were used, as shown in Table 3.8. The FAA delay data and criteria used to assign delay categories are included in Appendix B. Note that by using the DFW simulated per interrupt savings, we implicitly assume a DFW distribution of delay, despite some adjustment for the total number of delayed/rush operations by airport. Because EDA metering conformance benefits appear to be largest for small delays, an airport with a larger share of smaller delays may save more per average metering conformance interrupt than observed in the DFW simulation.

The annual airport operations and annual savings by airport using Equations (3.3)-(3.4) are also shown in Table 3.8 and plotted graphically by airport in Figure 3.9. The annual EDA benefits at any one airport ranges from $0.18M at BDL to nearly $2M at ORD, with all 37 airports totaling an annual benefit of over $25M, slightly more under EDA with arrival direct routing. The airports with larger operations fared best, including ORD, DFW, ATL, and LAX, each saving nearly $1.5 per year. For consistency across EDA benefit mechanisms, only the EDA-STAR results are shown in the summary chapter benefits matrix. The EDA-STAR values are more conservative.

It should be noted that the similar benefits estimated for STAR and direct arrival routing implies that direct routing does not inhibit EDA metering conformance efficiency. Indeed, the results indicate that automation may allow aircraft to file for their user-preferred direct routes, with ATM DST-assisted management and monitoring interrupting these routes only as required for metering conformance and separation assurance. During non-rush periods, user-preferred direct arrival routes would save both time and fuel. During metering, no time savings would accrue due to delays but, as the results in this chapter show, the metering conformance direct arrival route actions have a slight fuel advantage, without adverse impact on metering conformance workload. Indeed, as discussed in the next chapter, separation assurance conflicts are also reduced relative to the FFP1 Baseline under direct arrival routes. Such direct arrival routing benefits are enabled by EDA automation, allowing controllers to dynamically adhere to metering constraints without restricting aircraft to common arrival paths.

It should also be noted that the estimates do not include the controller and occasional flight crew workload benefits. EDA maneuver advisories embody an efficient inter-sector approach to metering restrictions, easing controller strategy and clearance development. By identifying an appropriate strategy as well as magnitude, EDA reduces controller workload. Indeed, in early EDA testing, over two-thirds of the EDA clearances provided to controllers required no modification, being acceptable in both method (speed, heading, altitude) and magnitude [23-24]. Additionally, the use of a high-fidelity model to develop the EDA maneuver advisories improves their accuracy over cognitively-developed interruptions, reducing the need for additional corrective interruptions closer to the restriction, and limiting vectoring which requires two clearances (i.e., turnout and turn back).

Current TMA-based arrival metering conformance procedures typically include the following clearances [40]:

Clearance 1: Altitude, speed, and vectoring heading change to conform to arrival metering schedule. This clearance may split into two under busy conditions with an initial altitude clearance, followed later by a vectoring/speed clearance. Additionally, multiple altitude clearances may be given to step descend aircraft in order to de-conflict merging arrival streams that have been vectored, or avoid crossing traffic streams.

Clearance 2: Heading turn back to Fix/Navaid, with the timing of this clearance assisted by TMA delay count-down. That is, TMA displays a dynamic delay value for each metered aircraft, indicating its conformance to the metering schedule, if turned back now.

Clearance 3: Appraise pilot of arrival metering fix crossing restrictions and instruct pilot to begin descent (typically at pilot discretion).

Table 3.8 EDA Metering Conformance Benefits

Airport	Annual Airport Ops (000s)	Apt Delay Delays/Category		Rush Ops Rate (/100 Ops)	Annual Savings ($M, 1998) EDA-STAR	EDA-Direct
Atlanta (ATL)	773	23.88	3	30.4	1.41	1.49
Nashville (BNA)	226	1.36	5	18.2	0.18	0.19
Boston (BOS)	463	0.73	2	18.2	0.25	0.26
Bradley (BDL)	161	26.37	5	34.9	0.97	1.03
Baltimore (BWI)	270	3.67	5	18.2	0.30	0.31
Cleveland (CLE)	291	4.68	5	18.2	0.32	0.34
Charlotte (CLT)	457	6.55	4	24.3	0.67	0.71
Cincinnati (CVG)	394	10.38	4	24.3	0.57	0.61
Washington National (DCA)	310	6.53	4	24.3	0.45	0.48
Denver (DEN)	454	1.90	5	18.2	0.50	0.53
Dallas – Ft. Worth (DFW)	870	19.59	3	30.4	1.58	1.68
Detroit (DTW)	531	9.10	4	24.3	0.77	0.82
Newark (EWR)	443	65.25	1	39.5	1.05	1.11
Ft. Lauderdale (FLL)	236	1.53	5	18.2	0.26	0.27
Houston Hobby (HOU)	252	2.57	5	18.2	0.28	0.29
Washington Dulles (IAD)	330	6.81	4	24.3	0.48	0.51
Houston – Intercontinental (IAH)	392	11.45	4	24.3	0.57	0.61
N.Y. Kennedy (JFK)	361	29.53	2	34.9	0.76	0.80
Las Vegas (LAS)	480	3.68	5	18.2	0.52	0.56
Los Angeles (LAX)	764	24.13	3	30.4	1.39	1.47
N.Y. LaGuardia (LGA)	343	46.22	1	39.5	0.81	0.86
Orlando (MCO)	342	4.59	5	18.2	0.37	0.40
Chicago Midway (MDW)	254	6.70	4	24.3	0.37	0.39
Memphis (MEM)	364	NA	5	18.2	0.40	0.42
Miami (MIA)	546	6.79	4	24.3	0.80	0.84
Minneapolis (MSP)	484	9.29	4	24.3	0.70	0.75
Oakland (OAK)	516	NA	5	18.2	0.56	0.60
Chicago O'Hare (ORD)	909	34.46	2	34.9	1.90	2.02
Portland (PDX)	306	2.41	5	18.2	0.33	0.35
Philadelphia (PHL)	406	17.95	3	30.4	0.74	0.78
Phoenix (PHX)	544	7.25	4	24.3	0.79	0.84
Pittsburgh (PIT)	447	6.60	4	24.3	0.65	0.69
San Diego (SAN)	244	3.31	5	18.2	0.27	0.28
Seattle (SEA)	398	6.37	4	24.3	0.58	0.61
San Francisco (SFO)	442	56.57	1	39.5	1.05	1.11
Salt Lake City (SLC)	374	3.53	5	18.2	0.41	0.43
St. Louis (STL)	517	34.04	2	34.9	1.08	1.15
37-Airport Total/Average	430	---	---	---	25.09	26.59

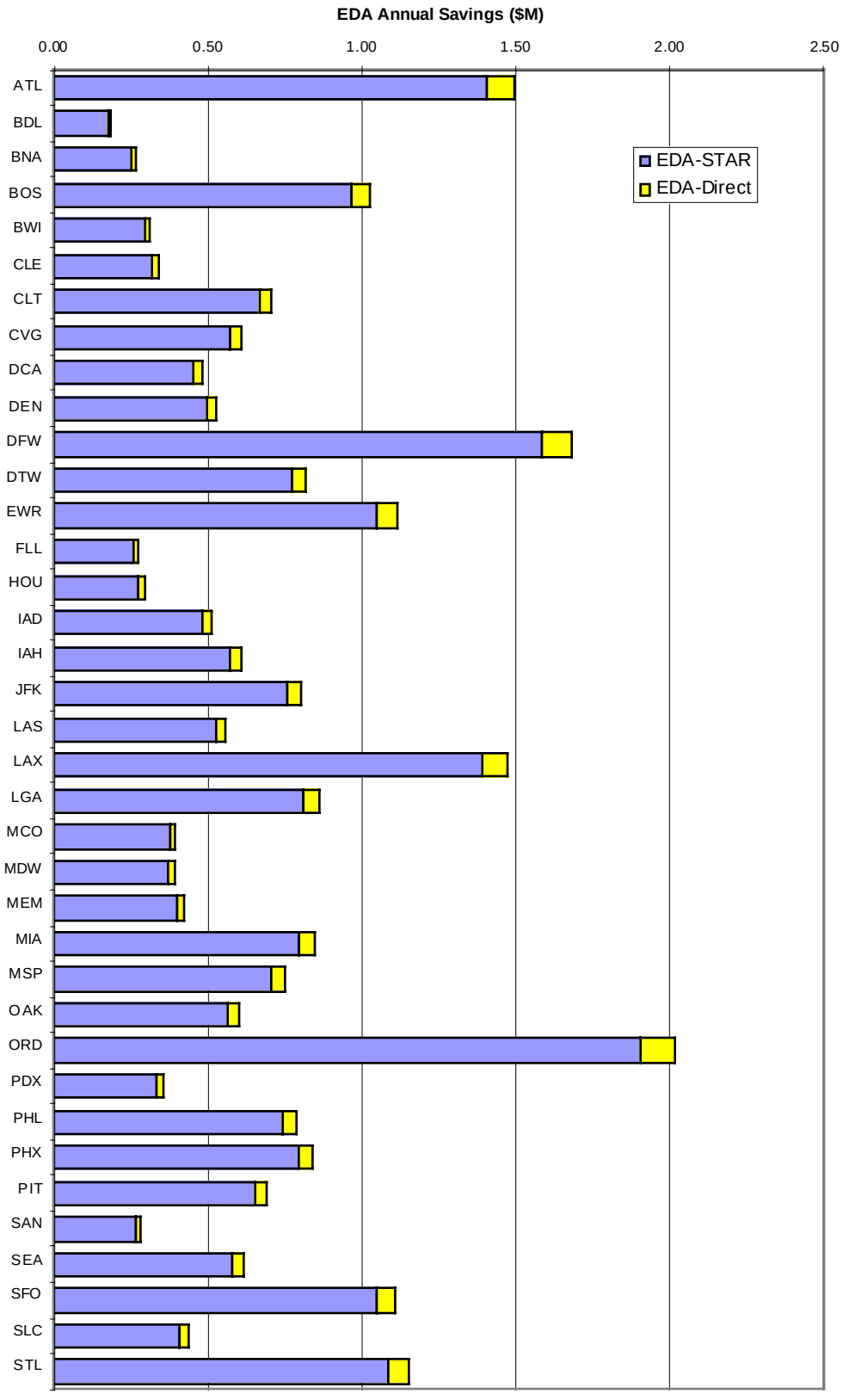

Figure 3.9 EDA Metering Conformance Benefits

EDA poses several advantages to this Baseline metering conformance procedure:

- Clearance 1 will more frequently not be split into multiple clearances, due to EDA's ability to provide initial conflict-free advisories that conform to arrival metering constraints;
- Clearance 2 turn back, may be required less frequently, with EDA's replacement of vectoring with speed and altitude methods for smaller delays.
- Arrival metering fix delivery accuracy will improve with more accurate Clearance 2 vector turn back under EDA, plus the ability of EDA to fine-tune descent speeds in Clearance 3.

EDA maneuver advisories are set up to auto-load into a datalink message format for uplink to pilots, which will speed up clearance delivery/read back, enhancing controller workload.

Results Summary

This chapter evaluated EDA metering conformance efficiency benefits. ATM interruptions for metering conformance delay arrival aircraft to meet airport capacity constraints. EDA maneuver advisories assist controllers in formulating and executing a traffic delay strategy to meet the specified arrival metering fix crossing schedule. EDA allows controllers to quickly and accurately assess the impact of various delay strategies, and more effectively use fuel-efficient strategies, such as speed control, resulting in lower cost metering conformance interruptions.

It was found that EDA saved an average of 59 lbs and 2.6 seconds or $6.80 per arrival metering conformance interruption, for total savings of $25.09M annually assuming NAS-wide deployment at 37-airports. This fuel efficiency benefit was slightly increased under arrival direct routing over conventional STAR routing. In addition, the EDA metering conformance procedures are more strategic and require less overall workload (fewer downstream controller corrections to conform to metering times) than under the FFP1 Baseline.

These benefit estimates are sensitive to the amount of metering delay per flight. A typical DFW day was analyzed with per operation savings extrapolated to other airports. Although some adjustment was made for the number of metered arrival flights at each airport, no adjustment was made in the per operation savings. If airport have smaller per operation delays, EDA may result in larger per operation savings because current vectoring operations can be fully replaced with EDA speed/altitude maneuvers. Thus, NAS-wide EDA benefit estimates would improve with evaluation of detailed simulations at additional airports.

4 ATM Separation Assurance Benefits

As discussed in the previous chapter, air traffic controllers issue clearances that deviate flights from the users' preferred trajectory, to avert impending traffic conflicts and conform to flow-rate restrictions. We refer to these processes of flow-rate conformance and separation assurance conflict resolution as "ATM interruptions," and the DST processes of reducing and imposing more efficient traffic interruptions as "ATM interruption benefits." This chapter evaluates EDA improvement to separation assurance flight interruptions. The process includes integration of metering conformance and conflict probe DSTs. The preceding chapter evaluated EDA improvements to ATM arrival-metering conformance flight interruptions.

ATM relies on accurate predictions of future flight positions within conflict probe DSTs to accurately identify and alert ATM of the location and nature of pending conflicts. Within a conflict probe, trajectory prediction capabilities determine whether ATM would perceive a predicted future encounter (i.e., predicted point of closest approach between two aircraft being less than some standard separation distance) as a conflict requiring intervention. This includes ATM/DST's ability to correctly infer the pending conflict, including its timing (conflict start) and severity (minimum separation of the event). It also includes the controller's use of excess spacing buffers (that the controller uses to effect an extra margin of safety), beyond the FAA minimum aircraft protected airspace zone (PAZ) constraint, imposed to account for such conflict uncertainties.

With DST reduction in trajectory prediction uncertainties, controllers can become confident in the consistency of more accurate conflict predictions, and PAZ buffers can be assumed to shrink while maintaining the current level of safety in both the horizontal and vertical dimensions. Indeed, current operations impose significant vertical PAZ buffers around aircraft in climb and descent phases of flight due to limitations in ATM knowledge of aircraft state, intent, and aircraft climb/descent performance during the transition flight maneuvers. With a reduction in both horizontal and vertical buffers, ATM would less frequently perceive aircraft to be in conflict, resulting in fewer ATM flight interventions, and associated conflict resolution fuel and workload penalties. The integration of trajectory maneuvers to effect metering conformance (referred to here as metering conformance flight intent) with the conflict probe tool, in particular, could significantly reduce conflict probe prediction inaccuracies. Incorrect knowledge of route intent, such as not knowing that a flight is being expedited (e.g. direct routing) and/or that a flight is being delayed to meet airport or flow-rate constraints without filing a flight plan amendment, can lead to incorrect or inaccurate DST conflict predictions and increased false and missed alert rates. Finally, improved DST conflict prediction will include more accurate estimation of conflicting aircraft geometry and speeds, which may lead to more efficient resolution maneuvers.

This chapter summarizes ATM interruption benefits expected with EDA, as derived in previous efforts [11-12]. These benefits accrue due to more accurate conflict alerts and improved controller confidence, leading to reduced (e.g., fewer false alerts) and more efficient (e.g., fewer missed alerts) ATM interruptions of user preferred trajectories.

Analysis Process

The benefits methodology process employed in previous research [11-12, 45] is described below. The sequence of analytical formulations and computer-based modelings follows the Figure S-2 approach (and numbering) of the introduction summary section. After the technologies of the study case are defined (1), the Trajectory Prediction & Accuracy Model (2) uses Baseline and EDA defined data parameter accuracies to calculate the expected position error in CTAS' conflict probe prediction. This timing error is then converted into

ATM perception values of miss distances and associated spacing buffers, that would be imposed by air traffic controllers to limit separation minima violations.

These modeled controller spacing buffers, defined for Baseline and EDA cases, are then combined with a DFW daily traffic schedule in the same ATM Interruptions Model discussed in Chapter 3, Arrival Metering Conformance Benefits (3). As shown in Figure 4.1, the separation assurance ATM interruption modeling components initially identify and record conflicts and near-conflicts from the metered (delayed) traffic scenario (output from the metering conformance model) in a conflict incident database. Near-conflicts are included to allow the analysis of false alerts. These incidents are then filtered through an ATM perception model to identify whether ATM would perceive the incident as a conflict requiring resolution. This perception model reflects the level of conflict probe accuracy as derived from the Trajectory Prediction & Accuracy Model (2).

A resolution is identified for each separation assurance ATM interruption and is tabulated over the daily simulation. The simulated daily interruption rates and resolution costs are then extrapolated to annual and NAS-wide levels using the economic modeling (4). These model components are discussed in more depth with the analysis results in the next section.

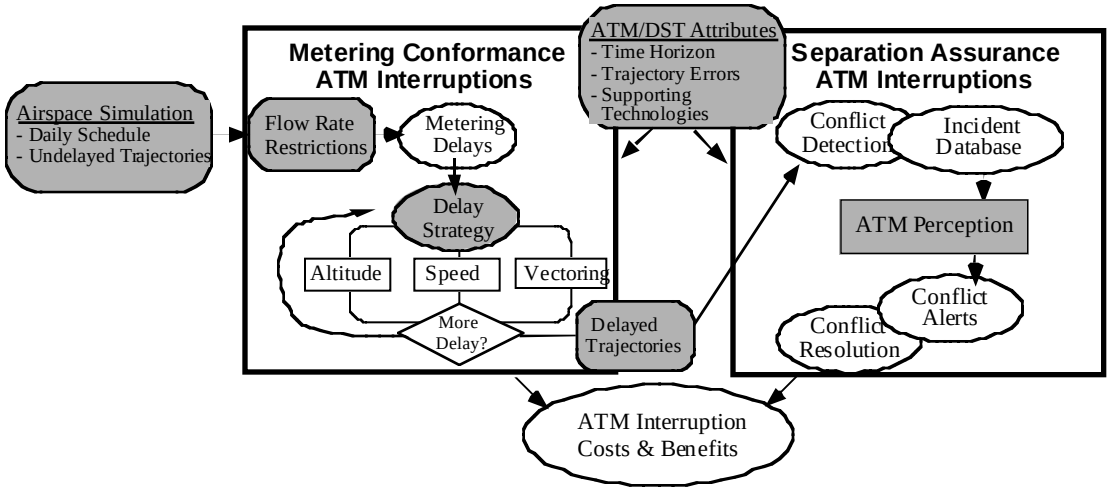

Figure 4.1 ATM Interruptions Model Approach

Conflict Detection

Initially a set of air-traffic "demand" trajectories for a typical day within a block of Center airspace was defined. In this study the Fort Worth Air Route Traffic Control Center (ZFW) airspace was analyzed, including the same arrival, departure, and overflight traffic operations as discussed in Chapter 2, Center/TRACON Delay distribution, and Chapter 3 Arrival Metering Conformance Benefits [35]. These data represent what each arrival, departure, and overflight trajectory would do if left alone to fly the users' filed route and preferred profile, with EDA assumed to enable direct routing to the arrival-metering fix. Both DFW arrival and departure trajectories were modified to impose delays necessary to meet airport capacity restrictions. These delayed trajectories, shown in Figure 4.2 define the conflict probe traffic scenario. Departure delays were absorbed on the ground, as ground holds. Arrival delays were absorbed en route by speed control, altitude, and/or vectoring maneuvers.

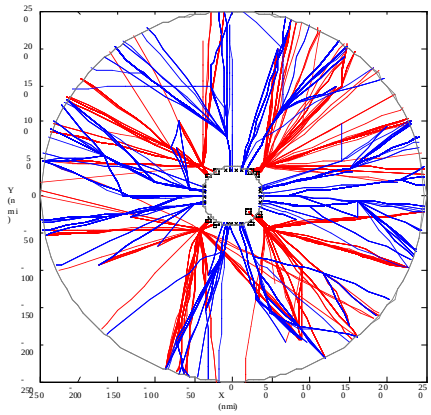

DFW

Figure 4.2 Plan and Profile View of DFW Study Day Operations

A conflict detection algorithm was used to identify actual and potential conflicts that would occur without ATM intervention(referred to as "incidents"). From the trajectory simulation, all potential conflict pairs were identified using a stepping algorithm, which uses inputs of trajectory data and Protected Airspace Zone (PAZ) bounds. In creating the incident database, a PAZ larger than the minimum FAA separation requirement was assumed to allow a margin of safety imposed by controllers as well as to facilitate analysis of false alerts. A "conflict" is identified if an aircraft enters the PAZ of another aircraft. The resulting Incident Database identifies all aircraft pairs that could be perceived by ATM as requiring intervention. The database also identifies information about the conflict including the separation at the point of closest approach (PCA).

ATM Perception

ATM is assumed to intervene and alter conflicting trajectories that are perceived by the operating conflict probe tool to violate Acceptable Controller Spacing (or the controller's PAZ). With improved perception, fewer incidents will be perceived as requiring intervention. ATM perception of conflict is characterized by four metrics that vary between Baseline and EDA cases and by phase of flight:

- Trajectory Prediction Accuracy
- Acceptable Controller Spacing
- Perceived Miss Distance
- Probability of Perceived Conflict

Trajectory Prediction Accuracy is defined as a combination of position and velocity error terms that are combined as a function of the time horizon used for the particular study case. The process of computing trajectory accuracy, whether it is represented as timing error or position error at a fixed point in time, is developed in Appendix A. This includes calibration of descent metering fix timing error resulting from application of TMA [30] or EDA [10] through field observations.

Table 4.1 shows the resultant trajectory prediction error in climb, cruise, and descent segments as combined for arrival, overflight and departure flight operations. These categories represent the flight phase of the aircraft at the conflict point of closest approach (PCA). A 12-minute time horizon was chosen to represent all cases. Note that shading of a cell in Table 4.1 indicates improvement with application of EDA.

Table 4.1 Assumed ATM Trajectory Prediction Accuracy

	Units	FFP1 Baseline					EDA				
		DEP		OVR	ARR		DEP		OVR	ARR	
		CL	CR	CR	CR	D	CL	CR	CR	CR*	D
12-minute Trajectory Prediction Accuracy											
Predicted Position Error $\sigma_{p,pred}(\tau)$	nm	13.8	4.7	4.7	4.7	4.5	13.8	4.7	4.7	3.74	4.0

* Applies to metered arrivals only.

Acceptable Controller Spacing indicates at what separation values (lateral and vertical miss distances) ATM controllers would perceive a projected encounter as a conflict requiring intervention. These are functions of the required minimum separation and an intentional excess spacing buffer. This buffer is used by controllers to prevent violation of the FAA separation minima, given trajectory uncertainties. This concept is displayed in Figure 4.3 for the lateral dimension. As trajectory uncertainties are reduced and controllers become confident in the consistency of more accurate trajectory predictions, this buffer is assumed to shrink, while maintaining the current level of safety.

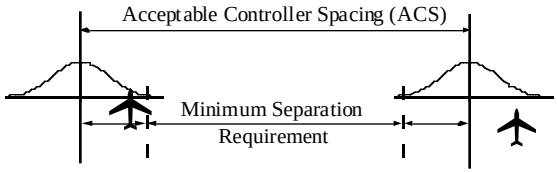

Figure 4.3 Acceptable Controller Spacing (ACS) Results from Predicted Position Accuracy.

To be in conflict, aircraft must violate Acceptable Controller Spacing (ACS) in either the horizontal or vertical dimensions. ACS is assumed to be dependant upon position accuracy. Equation (4.1) is used to relate position accuracy to horizontal and vertical ACS. The minimum separation fraction values for each flight mode are estimated based on current system operations ACS values [30].[5]

$$ACS = n\sigma_{p.pred} + Rule \tag{4.1}$$

where: *Rule* = En route minimum separation requirement [42]
= 5 nm horizontally, 2000/1000 ft vertically >FL290/≤FL290
$\sigma_{p.pred}$ = Trajectory prediction position accuracy (Table 4.1)
n = Minimum separation fraction
= (0.22, 0.67, 0.60) horizontal and (72.5, 0.0, 200.0) vertical for (climb, cruise, descent) flight segments

Using Equation (4.1), Table 4.2 shows the Baseline and improvement in ACS assumed with the EDA case. Again, shaded cells show improvement due EDA when compared to the previous case. Note that the arrival-cruise vertical ACS does not improve, since the vertical ACS values are already at the FAA minimums.

[5] That is the FFP1 ACS values (shown in Table 4.3) are combined with FFP1 trajectory prediction position accuracy values of Table 4.2 and FAA minimum en route separation (*Rule*) to derive the minimum separation fraction (n). Using this minimum separation fraction, EDA ACS values (Table 4.3) are generated reflecting Table 4.2 improved EDA/EDX trajectory prediction position accuracies.

Table 4.2 Acceptable Controller Spacing

	Units	FFP1 Baseline					EDA				
		DEP		OVR	ARR		DEP		OVR	ARR*	
		CL	CR	CR	CR	D	CL	CR	CR	CR	D
Horizontal ACS											
En Route	nm	**8.00**	**8.00**	**8.00**	**8.00**	**8.00**	8.00	8.00	8.00	7.37	6.07
Vertical ACS											
>FL290	Ft	**3000**	**2000**	**2000**	**2000**	**3000**	3000	2000	2000	2000	2357
<=FL290	Ft	**2000**	**1000**	**1000**	**1000**	**2000**	2000	1000	1000	1000	1357

Note: Bold values assumed to reflect current system operations [41].
* Applies to metered arrivals only.

Perceived Miss Distance indicates the accuracy to which ATM perceives the extent and degree of the potential conflict. Inaccurate perception may lead to false or missed interventions because the conflict may be perceived as more or less severe than in actuality. This concept is illustrated in Figure 4.4 where actual aircraft tracks and miss distance (r_f) are shown with bold (_) lines. Dashed (--) lines show inaccurately predicted flight tracks due to ATM prediction errors in heading and speed. These errors result is a range of perceived conflict miss distances which may be more or less severe than the actual miss distance.

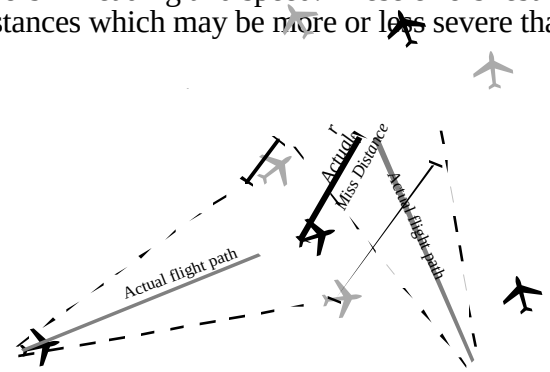

Figure 4.4 Perceived Miss Distance results from Actual Miss Distance & Trajectory Prediction Accuracy.

Equation (4.2) describes the incident-specific variation in ATM perceived miss distance as a function of the technology-specific trajectory prediction accuracies of the conflicting aircraft pair:

$$\sigma_{r_f} = \sqrt{\sigma^2_{p,pred,aci} + \sigma^2_{p,pred,acj}} \qquad (4.2)$$

where: $\sigma_{p,pred,\,acx}$ = Predicted trajectory position accuracy at point of closest approach for aircraft *x* (nm)

For each incident in the Incident Database, the flight mode of each aircraft at the conflict point of closest approach (PCA) is identified. The associated 12-minute trajectory prediction accuracies (prior to conflict start), drawn from Table 4.1, are used in Equation (4.2) to define ATM perception miss distance error. The result is a Gaussian distribution of miss distance for each conflict under each technology case. The mean value of this distribution is equivalent to the actual uninterrupted Incident Database miss distance. The miss distance distribution is compared with ACS to determining the ATM's probability of perceived conflict and subsequent intervention.

A *Probability of Conflict*, or probability of ATM interruption, is calculated by comparing the ACS with the conflict probe perceived attributes and actual Incident Database attributes for each incident. This probability indicates the likelihood that a controller would perceive

the incident as a conflict requiring intervention. Because the perceived miss distance is stochastic in nature, it takes the form of a Gaussian distribution, as shown in Figure 4.5, with a mean value equal to the actual miss distance. The ACS bounds (±ACS) are overlaid onto the perceived miss distance curves. The shaded region between ±ACS is the probability that ATM would perceive this incident as equal or less than the ACS, and intervene to resolve the perceived conflict. The unshaded region represents the probability that no conflict was perceived nor intervention made at the strategic conflict probe time horizon.

Figure 4.5 shows three curves representing three possible outcomes, the actual miss distance is: *(i)* less than the minimum separation requirement (±M); *(ii)* larger than minimum but less than the ACS (±ACS); or *(iii)* larger than the ACS. Because ATM perception is not completely accurate, intervention or lack of intervention may be an incorrect action. In general, ATM interruptions fall into three categories: correct, missed, and false alerts, defined as:

- **Correct Alert** (CA) - Conflicts correctly perceived by ATM (i.e., minimum aircraft separation falls below the Acceptable Controller Spacing). As a result of correct perception, ATM is able to resolve the impending conflict at the strategic time horizon.
- **Missed Alert** (MA) - Conflicts *not* correctly perceived by ATM. Due to conflict probe inaccuracies, the tool identified no projected conflict. As a result of ATM misperception, conflict detection, and the initiation of a conflict resolution maneuver, will be delayed resulting in a tactical resolution and economic penalty.
- **False Alert** (FA) - Erroneous conflicts detected by the conflict probe tool despite an acceptable miss distance. False alerts result in extra workload, for controllers and pilots, and add additional flight costs for deviations that are not necessary.

In Figure 4.5, intervention is the correct course of action in the top two scenarios because the actual miss distance (between aircraft symbols) is less than the ACS. In these cases, a missed alert would result if no 12-min. intervention were made. Once ATM *did* perceive these incidents, a tactical intervention would be required with a shorter time horizon at a higher cost. Conversely, intervention in the last scenario of Figure 4.5 would be a false alert, and would lead to an unnecessary ATM interruption and its associated costs and workload. Improved accuracy of the conflict probe tool would lead to a tightening of the Perceived Miss Distance curve about the mean value. As a result, the shaded region would be modified, reducing the number of false and missed alerts.

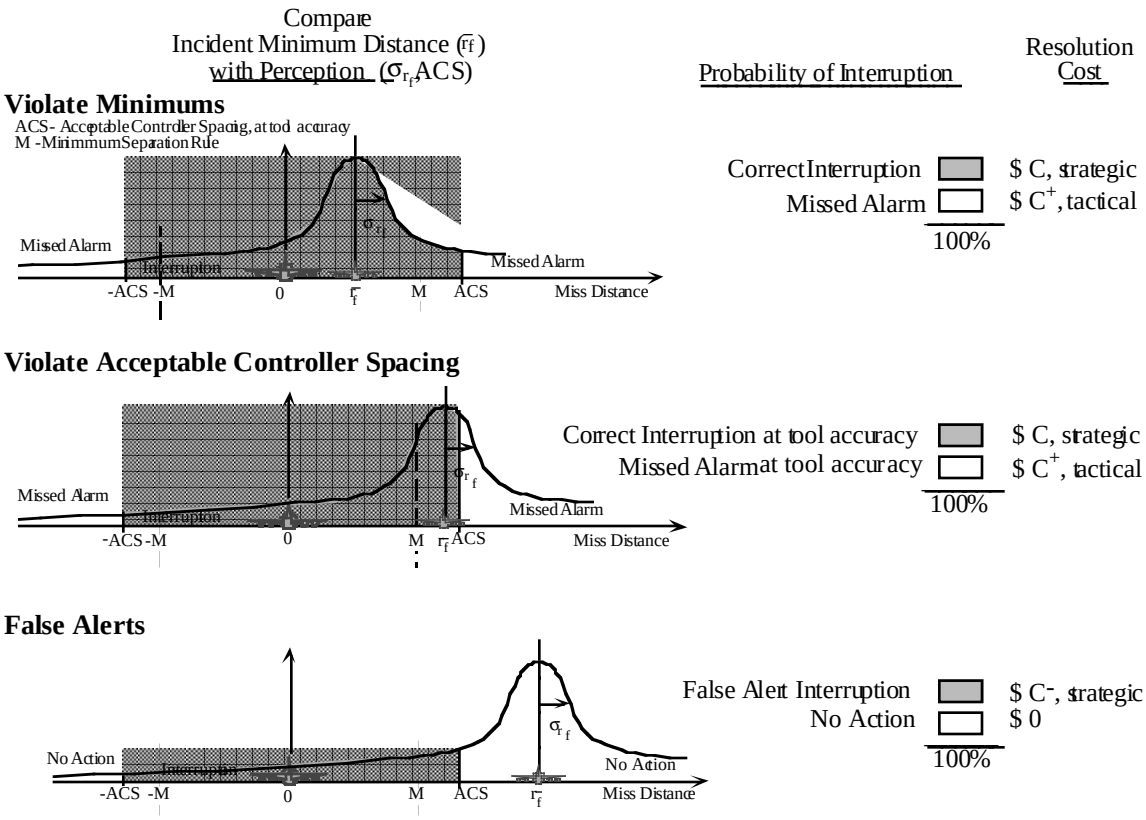

Figure 4.5 Comparison of Perceived Miss Distance Curves and Acceptable Controller Spacing (ACS) results in Probability of Conflict and Resolution Costs for Each Type of Incident

The probability of perceived conflict, which determines the likelihood of ATM interruption of an incident, is equivalent to the area under the perceived miss distance curve between ±ACS, calculated using Equation (4.3):

$$P(conflict) = \frac{1}{2} erf\left(\frac{ACS + r_f}{\sqrt{2}\sigma_{r_f}}\right) + \frac{1}{2} erf\left(\frac{ACS - r_f}{\sqrt{2}\sigma_{r_f}}\right) \quad (4.3)$$

where: r_f = Actual miss distance at point of closest approach

ACS = Acceptable Controller Spacing (ACS)

σ_{r_f} = Miss distance error from Equation (4.2)

$erf(x)$ = Integral of the standardized Gaussian distribution function from (0, x)

$erf(x) = \frac{2}{\sqrt{\pi}} \int_0^x e^{-u^2} du$ and $\frac{1}{2} erf\left(\frac{-x}{\sqrt{2}}\right)$ = Integral of the normal probability distribution function

This probability determines the likelihood of ATM interruption of this incident.

Impact of Off Flight Plan/Incorrect Intent

In the current system, flights are frequently diverted off the filed flight plan for a variety of reasons including metering conformance, conflict avoidance, and accommodation of requests for direct routes. If these deviations are not recorded as a flight path amendment, ATM and conflict probe DSTs are unaware of the changed aircraft intent. The lack of updated intent degrades conflict probe trajectory prediction, frequently resulting in a false alert for the original conflict, and/or a missed alert on the new route. Future integrated conflict probe, direct routing, and metering conformance tools will assist controllers in recording these intent changes. Alternatively, aircraft downlink of its next few waypoints could correct conflict probe aircraft intent errors. In both cases, the improved knowledge of aircraft intent leads to conflict probe performance benefits.

Figure 4.6 illustrates a situation where an eastbound aircraft's filed flight plan route supposedly conflicts with a southeast flight (actually a false alarm). To avoid this, the controller vectors the eastbound aircraft for spacing conformance but fails to record this change as a flight plan amendment. As a result, the initial presumed conflict is avoided (false alert), but is replaced by a new undetected conflict (missed alert) with a second southeast flight.

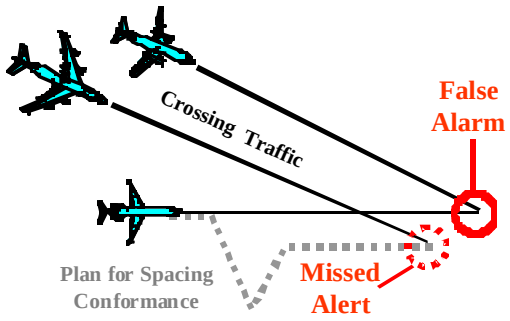

Figure 4.6 Off-flight Plan Effect on ATM Perception

The analysis accounted for inaccurate intent information as part of ATM perception. If an aircraft is off-flight plan, the bad intent data changes the ATM perception attributes of Figure 4.5 slightly, as shown in Figure 4.7. The key change is the shift of the second aircraft's actual location, reflecting a gap between the perceived (flight plan) and actual (off flight plan) miss distance. Thus, the perceived miss distance curve is still centered about the flight plan intent, which no longer matches the actual intent of the aircraft. Per the scenario of Figure 4.7, bad intent results in a significantly higher probability for the, now false alert, conflict than would occur with good intent information.

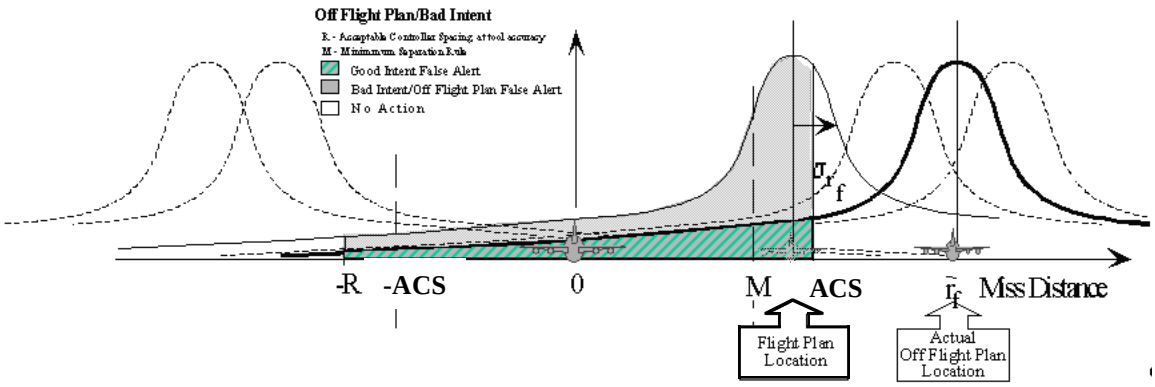

Figure 4.7 Off-Flight-Plan Probability of Conflict Estimation

For this study, it is assumed that a controller would clear the aircraft to a route that would avoid any original flight plan-based conflict, while not creating any new conflicts. This approach implies that the off-flight plan route would avoid the flight-plan-based conflict, converting it to a false alert. The off-flight plan location of the second aircraft was assumed to be outside the ACS (±R) by a distance equal to the horizontal ACS safety buffer (ACS – FAA minimum Rule). This results in the solid off-flight plan curve of Figure 4.7 (regardless of the original miss distance attributes). Thus, under erroneous intent, ATM's perceived probability of conflict would not change, implied by the area under the original Flight Plan-based location between the ACS bounds, but it would now represent a false alert, as the off-flight plan route avoided the conflict and thus no intervention is necessary.

Using this approach, a lack of accurate intent data will result in a higher frequency of false alerts. Probability of conflict is calculated for both accurate and inaccurate intent situations and combined based on the weighted frequency of inaccurate intent information.

The frequency of aircraft off-flight plan intent errors is assumed to vary by case, as shown in Table 4.3. In the FFP1 Baseline, full intent errors are assumed in all flight modes, reflecting the lack of integration of the metering (TMA) and the conflict probe tools and no downlinked aircraft intent. The frequency of inaccurate intent was assumed to be 15% for all flight modes, based on discussions with conflict probe experts [41] and Indianapolis Center observations that only 18% of all route clearances are documented [43]. With the integration of arrival metering/conflict probe in the EDA case, metered arrival intent errors are assumed to be removed, while departure and overflight intent inaccuracy remains unchanged.

Table 4.3 Frequency of Off-Flight-Plan Route Intent Error

	Units	FFP1 Baseline					EDA				
		DEP		OVR	ARR		DEP		OVR	ARR*	
		CL	CR	CR	CR	D	CL	CR	CR	CR	D
Off Flight Plan Route Intent Error Frequency											
Inaccurate Intent		15%	15%	15%	15%	15%	15%	15%	15%	0%	0%
Accurate Intent		85%	85%	85%	85%	85%	85%	85%	85%	100%	100%

* Applies to metered arrivals only.

FFP1 Perception Limitations

Additional processing was performed on the FFP1 Incident database to account for its unique ATM perception limitations. As discussed previously, the conflict probe tool assumed in the FFP1 case, has access only to the originally filed aircraft flight plans. As such, it's ATM perception is hindered, increasing the missed and false alerts that either are avoided or encountered when the flights are delayed to meet the TMA schedule. Because the EDA conflict probe tool has access to the CTAS-developed advisories supplied to the controllers to meet the TMA schedule, these misperceptions are removed.

To reflect the degraded FFP1 Perception, Incident Databases were developed from both the original (filed flight plan) and metered (delayed) trajectories. These two Incident Databases were then combined, by adjusting the probability of conflict and resolution costs, as appropriate.

Conflict Resolution

For each perceived conflict recorded in the Incident Database, a resolution cost was defined. This fuel cost penalty represents the cost just to avert a conflict, at the given time horizon. ATM shaded (interrupt) and unshaded (no interrupt) action probabilities of Figure 4.5 are tied to resolution costs, resulting in a weighted resolution cost for each conflict or predicted conflict. The costs of the shaded and unshaded actions are conceptually noted in Figure 4.5. In general, correct alerts incur a resolution cost initiated at the technology's expected time horizon. Missed alerts incur a more expensive resolution cost, initiated at a shorter time horizon (i.e., 5 minutes). False alerts were assigned a small cost related to resolving a non-conflict that would not actually have occurred.

The conflict resolutions are achieved with heading changes, sensitive to conflict geometry and severity, with the resolution maneuver split between the involved aircraft. The trajectories were not changed to implement the ATM intervention action; rather, the intervention was used to identify a representative cost penalty for the interruption. Three types of ATM intervention costs were identified: correct, false, and missed alerts. As previously discussed, the resolution cost of each type differs in its time horizon and conflict severity.

The resolution maneuver includes heading changes and steady level flight segment components. Conflict resolutions from altitude or speed changes were not examined. The fuel costs of executing these flight segments were summed and compared to the fuel costs of uninterrupted flight. For all maneuvers, the resolution of the conflict resulted in an increase in path distance with constant speed. The change in path distance was converted to a time value based on the aircraft speed, multiplied by a fuelburn rate (per unit time), and a Baseline cost of fuel ($0.10/lb). The fuelburn rates, included in Appendix E, were based on Eurocontrol's BADA performance data [37], sensitive to altitude, flight mode (climb, cruise, and descent), and aircraft class.

Economic Analysis

The number and cost of ATM interruptions was tallied for each scenario by applying the ATM resolution strategies to conflicts, as perceived by ATM. The probability of conflict, based on scenario-specific ATM perception, was used to weight the overall interruption cost for each incident of the Incident Database. Fuel costs for resolving all ATM perceived conflicts from the 24-hour incident database were tabulated. By comparing the costs of changes in ATM interruptions to a Baseline system, expected daily fuel cost savings were identified.

Table 4.4 summarizes the number and type of ATM perceived conflicts simulated under each case, categorized as correct (CA), missed (MA), and false (FA) alerts. Table 4.5

identifies only the perceived conflicts involving arrival flights. Each conflict implies interrupting one or both flights to maintain separation. These ATM interruptions resolve conflicts between aircraft pairs of various types including DFW arrivals (ARR), DFW departures (DEP), and overflights (OVR, including satellite airport operations) within the DFW en route/transition airspace. Arrival-Arrival and Departure-Departure alerts with PCAs larger than the FAA minimum separation rule (5 nm) were not included (NAs in Table 4.4). Because controllers closely monitor these streams at tight in-trail spacing during rush periods (assumed to be 5.5 nm for this study), conflict alerts between these aircraft can be a nuisance and is frequently deactivated [41]. Additionally, it should be noted that although EDA metering conformance maneuver advisories are designed to be conflict-free, where possible with all other traffic, this de-confliction was not fully accounted for in the modeling of EDA trajectories. Thus, EDA conflict alerts involving metered arrivals (over 80 percent of all identified arrival conflicts) would likely be significantly lower than identified in Tables 4.4 and 4.5.

As comparison of the scenarios in Table 4.5 shows, the total number of conflicts declines with EDA enhancements by 5-7 percent. Additionally the number of false and missed alerts declines, a 24-30 percent improvement for missed and 19-21 percent for false alerts, with missed and false alert rates improving by 15- 20 percent. Indeed, the number of arrival-arrival missed alerts decline by over 60 percent. A key controller workload benefit, the reduced false and missed alerts are largely due to the integration of metering conformance flight changes with conflict probe functions.

A comparison of EDA-STAR and EDA-Direct cases in Tables 4.4 shows that either EDA case provides significant improvement over the FFP1 Baseline. Under the EDA-Direct arrivals case, the results show a slightly smaller number of conflicts less than the FAA minima (PCA<Rule), but slightly more missed and false alerts.

Table 4.4 Number and Category of Separation Assurance Conflicts

	Number of ATM Resolutions						Metrics	
	PCA<Rule		Rule<PCA<ACS		PCA >ACS			
	CA	MA	CA	MA	FA	Total	R_{MA}	R_{FA}
FFP1 Baseline								
OVR-OVR	122	86	170	180	291	848	48%	52%
OVR-ARR	39	44	62	119	185	449	62%	70%
OVR-DEP	26	56	47	142	227	498	73%	84%
ARR-DEP	4	9	7	34	55	110	80%	102%
DEP-DEP	13	24	NA	NA	NA	37	NA	NA
ARR-ARR	58	87	NA	NA	NA	145	NA	NA
Total	263	307	286	474	758	2.087	59%	67%
EDA – STAR Arrivals								
OVR-OVR	131	77	156	159	259	782	45%	50%
OVR-ARR	64	27	93	72	124	380	39%	48%
OVR-DEP	48	35	79	93	161	416	50%	63%
ARR-DEP	7	8	18	23	54	110	56%	98%
DEP-DEP	18	20	NA	NA	NA	37	NA	NA
ARR-ARR	173	32	NA	NA	NA	205	NA	NA
Total	440	198	346	347	599	1.930	46%	56%
EDA – Direct Arrivals								
OVR-OVR	131	77	156	159	259	782	45%	50%
OVR-ARR	67	30	94	82	120	392	41%	44%
OVR-DEP	48	35	79	93	161	416	50%	63%
ARR-DEP	15	19	34	50	76	195	58%	65%
DEP-DEP	18	20	NA	NA	NA	37	NA	NA
ARR-ARR	142	25	NA	NA	NA	167	NA	NA
Total	421	205	364	383	617	1.989	47%	53%

Note: EDA arrival conflicts do not reflect EDA *conflict-free* metering conformance advisories, which would limit separation assurance conflict alerts.

PCA = Point of Closest Approach distance, Rule = FAA minima, ACS = Acceptable Controller Spacing
ARR = DFW Arrival, DEP = DFW Departure, OVR = Overflight/Satellite

Table 4.5 looks in detail at the arrival conflicts. Unlike Table 4.4, it includes conflicts exceeding FAA minimums (PCA>Rule). The changes between scenarios reflect the differences in arrival metering conformance flight changes under Baseline and EDA operations (per Chapter 3), the EDA integration of these flight changes with conflict probe, and the EDA reduction in the ACS. Despite this complex interplay of changes, the overall picture is a reduction in arrival conflicts by 9 percent and a halving of the missed and false alert rates, signaling significant controller workload savings. The number of conflicts above FAA minimums but below ACS declines, and in both categories EDA shows a significant shift from missed to correct alerts. Additionally, the number of arrival missed and false alerts are reduced by 62 and 35 percent, respectively. These changes all contribute to sharp fall in missed/false alert rates from 62/61 percent to 31/37 percent. It should be noted that these benefits appear to be diluted by the fact that the *modeled* EDA arrival metering conformance flight changes lead to more arrival conflicts than Baseline metering strategies, as shown by the EDA increase of 70 conflicts below FAA minimums (PCA < Rule). In fact, a more accurate modeling of EDA metering conformance flight changes would show a reduction in conflicts, since EDA attempts to advise conflict-free metering conformance maneuvers [44]. Despite the EDA modeling limitation, the Table 4.5 results indicate that the EDA improvements in Arrival-Arrival conflict rates (59/48 to 22/22 for missed and false alerts respectively) may allow controllers to better utilize the conflict probe for such conflicts. Under existing uncertainties, the conflict probe is

generally de-activated for high-density arrival flows due to excessive workload issues related to conflict probe errors [41].

Table 4.5 DFW Arrival Separation Assurance Conflicts Detail

	Number of ATM Resolutions						Metrics	
	PCA<Rule		PCA<ACS		PCA >ACS			
	CA	MA	CA	MA	FA	Total	R_{MA}	R_{FA}
FFP1 Baseline								
OVR-ARR	39	44	62	119	185	449	62%	70%
ARR-DEP	4	9	7	34	55	110	80%	102%
ARR-ARR	58	87	86	124	172	527	59%	48%
Total	101	140	156	277	412	1.086	62%	61%
EDA – STAR Arrivals								
OVR-ARR	64	27	93	72	124	380	39%	48%
ARR-DEP	7	8	18	23	54	110	59%	98%
ARR-ARR	173	32	143	57	90	494	22%	22%
Total	244	67	254	152	268	984	31%	37%

Note: EDA arrival conflicts do not reflect EDA *conflict-free* metering conformance advisories, which would limit separation assurance conflict alerts.

Table 4.6 summarizes the number of EDA separation assurance interruptions and the associated average and daily resolution costs from the DFW simulation. The interruption rate is based on the interruptions per 8,003 total simulation daily operations (arrival, departure and overflight). Note that only fuel costs were tabulated in the horizontal vectoring resolution maneuvers. Additionally, despite a slightly higher interrupt rate in the EDA-Direct case relative to EDA-STAR case, the smaller per operation resolution cost resulted in lower daily interruption costs.

Table 4.6 DFW Separation Assurance Conflict Rates and Costs

	Interrupts		Resolution Cost	
	Number	Rate/100 ops	($/op)	($/day)
FFP1 Baseline	2,087	26.1	$1.98	$4,123
EDA - STAR	1,930	24.1	$1.90	$3,660
EDA - Direct	1,989	24.9	$1.79	$3,552

As with other benefit mechanisms in this report, these daily DFW savings were extrapolated to an annual NAS-wide level by accounting for the total number of 1996 operations at each facility. As in other chapters, the simple extrapolation employs Equation (4.4) and (4.5) to estimate benefits.

$$\textit{Annual Cost} = (\textit{Annual Ops}) \times (\textit{Interrupt Rate}) \times (\textit{Cost Per Interrupt}) \quad (4.4)$$

$$\textit{Annual Savings} = \textit{Annual Cost}_{\text{FFP1}} - \textit{Annual Cost}_{\text{EDA}} \quad (4.5)$$

where: *Annual Ops* = Annual ARTCC operations (00s) (Appendix B)
Interrupt Rate = Number of interruptions per 100 ARTCC operations (Table 4.6)
Cost Per Interrupt = Average cost per interruption (Table 4.6)

The interruption rates and costs observed in the daily simulation and used in Equation (4.4) are included in Table 4.6. The annual ARTCC operations [36] and annual savings by airport are shown in Table 4.6. The annual savings are plotted graphically by airport in Figure 4.8. The total annual EDA benefits at any one ARTCC ranges from under $0.10M in ZOA and ZSE to almost $0.20M at ZOB and ZAU, with NAS-wide ARTCC annual benefit of over $2M. EDA with direct route arrivals saved approximately 23 percent more than STAR routes.

It should be noted that the similar benefits estimated for the EDA-STAR and EDA-Direct cases implies that direct arrival routing does not inhibit EDA separation assurance interruption improvements. Despite a slightly higher interrupt rate in the EDA-Direct case, the smaller per operation resolution cost resulted in larger overall annual/NAS-wide benefits. These results indicate that automation may allow aircraft to file for their user-preferred direct routes with ATM DST assisted management and monitoring, interrupting these routes only as required for metering conformance and separation assurance interruptions. Thus, during non-rush periods user-preferred direct arrival routes would save both time and fuel. During metering, no time savings would accrue due to delays but, as the results in the previous chapter show, the metering conformance direct arrival route actions have a slight fuel advantage, without adverse impact on metering conformance workload. Such direct arrival routing benefits are enabled by EDA automation, allowing controllers to dynamically adhere to metering constraints without restricting aircraft to common arrival paths. For consistency across EDA benefit mechanisms, only the EDA-STAR results are shown in the summary chapter benefits matrix. The EDA-STAR values are more conservative.

It should also be noted that the estimates do not account for the significant controller workload. Controller workload is enhanced by EDA assistance in strategic planning to meet the dual objectives of separation assurance and compliance with flow-rate restrictions. The improved metered arrival prediction and integration of flow-rate conformance flight changes with conflict probe functions, greatly reduces the probability of missed or nuisance (false) conflict alerts. Indeed, the analysis identified a halving of the arrival missed and false alert rates under EDA, in addition to the EDA reduction in overall detected conflicts. Safety also benefits with enhanced surveillance under improved EDA metered arrival trajectory prediction capabilities.

Table 4.6 EDA Separation Assurance ATM Interruptions Benefits

Airport	ARTCC	Annual ARTCC Ops (000s)	Annual Savings ($M, 1998) EDA-STAR	EDA-Direct
Atlanta (ATL)	ZTL	2,453	0.14	0.18
Nashville (BNA)	ZBW	1,727	0.10	0.12
Boston (BOS)	ZME	1,978	0.11	0.14
Bradley (BDL)	ZBW	1,727	0.10	0.12
Baltimore (BWI)	ZDC	2,331	0.14	0.17
Cleveland (CLE)	ZOB	2,870	0.17	0.21
Charlotte (CLT)	ZTL	2,453	0.14	0.18
Cincinnati (CVG)	ZID	2,222	0.13	0.16
Washington National (DCA)	ZDC	2,331	0.14	0.17
Denver (DEN)	ZDV	1,527	0.09	0.11
Dallas – Ft. Worth (DFW)	ZFW	2,118	0.12	0.15
Detroit (DTW)	ZOB	2,870	0.17	0.21
Newark (EWR)	ZNY	2,040	0.12	0.15
Ft. Lauderdale (FLL)	ZMA	1,542	0.09	0.11
Houston Hobby (HOU)	ZHU	1,853	0.11	0.13
Washington Dulles (IAD)	ZDC	2,331	0.14	0.17
Houston – Intercontinental (IAH)	ZHU	1,853	0.11	0.13
N.Y. Kennedy (JFK)	ZNY	2,040	0.12	0.15
Las Vegas (LAS)	ZLA	1,981	0.12	0.14
Los Angeles (LAX)	ZLA	1,981	0.12	0.14
N.Y. LaGuardia (LGA)	ZNY	2,040	0.12	0.15
Orlando (MCO)	ZJX	1,878	0.11	0.13
Chicago Midway (MDW)	ZAU	2,894	0.17	0.21
Memphis (MEM)	ZME	1,978	0.11	0.14
Miami (MIA)	ZMA	1,542	0.09	0.11
Minneapolis (MSP)	ZMP	2,027	0.12	0.14
Oakland (OAK)	ZOA	1,368	0.08	0.10
Chicago O'Hare (ORD)	ZAU	2,894	0.17	0.21
Portland (PDX)	ZSE	1,393	0.08	0.10
Philadelphia (PHL)	ZNY	2,040	0.12	0.15
Phoenix (PHX)	ZAB	1,505	0.09	0.11
Pittsburgh (PIT)	ZOB	2,870	0.17	0.21
San Diego (SAN)	ZLA	1,981	0.12	0.14
Seattle (SEA)	ZSE	1,393	0.08	0.10
San Francisco (SFO)	ZOA	1,368	0.08	0.10
Salt Lake City (SLC)	ZLC	1,509	0.09	0.11
St. Louis (STL)	ZKC	1,986	0.12	0.14
37-Airport Total/Average	---	39,202	2.28	2.80

* Totals include only one instance of each ARTCC, excluding the shaded ARTCC operations separation assurance operations.

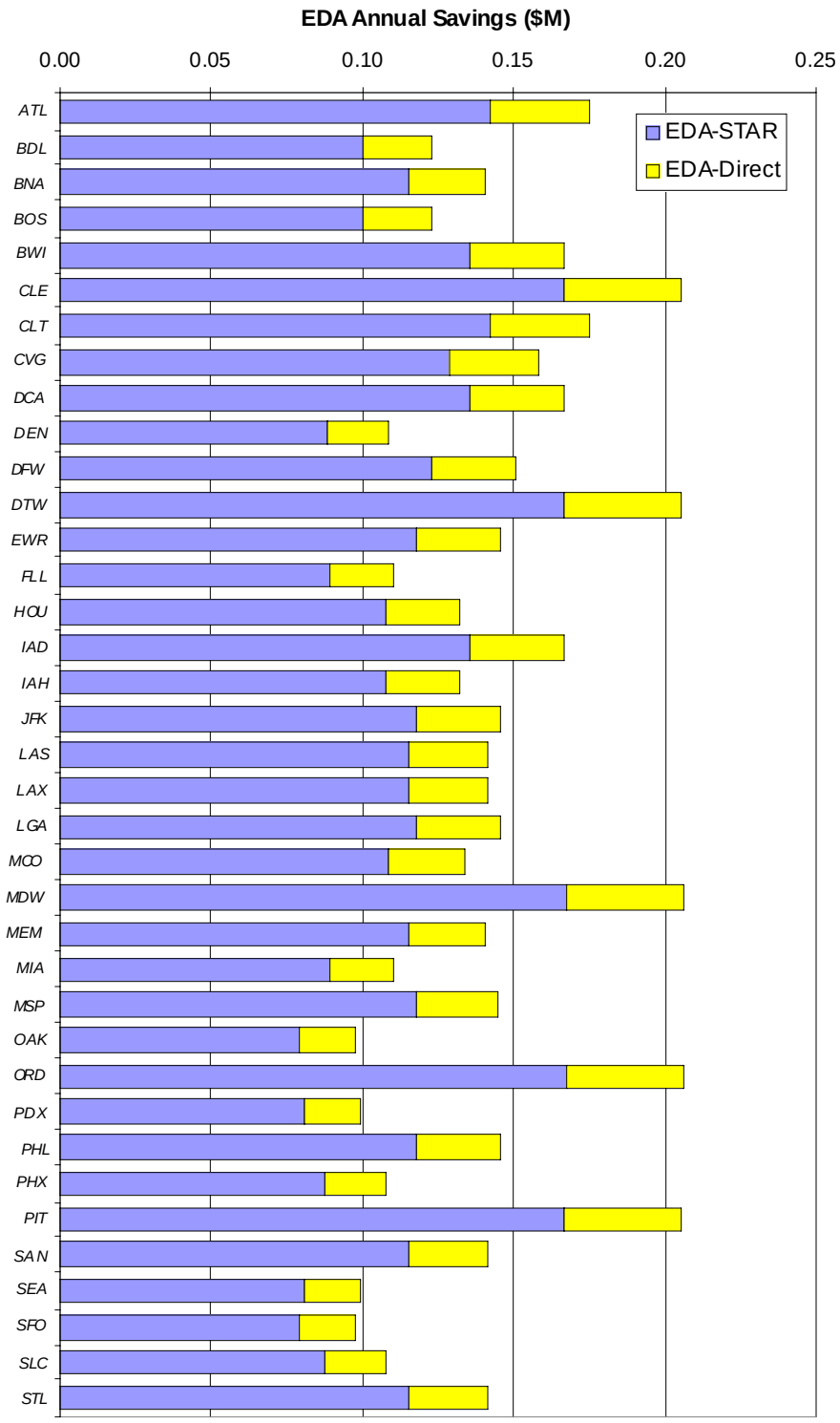

Figure 4.8 EDA Separation Assurance ATM Interruptions Benefits

Results Summary

This chapter evaluated EDA separation assurance interruption benefits. ATM relies on accurate predictions of flight trajectories within its conflict probe tool to accurately identify

the location and nature of pending separation assurance violations. With more accurate EDA arrival trajectory predictions (EDA advisories and updated intent), ATM perception errors (false and missed alerts) would be reduced, resulting in fewer ATM flight interventions and associated resolution fuel penalties. Additionally, improved traffic conflict prediction will include more accurate estimation of conflict geometry and speeds, leading to more efficient resolution maneuvers.

It was found that EDA reduced separation assurance interruptions by 5 percent with each interruption savings an average of 0.8 lbs or $0.08, for total savings of $2.80M annually assuming NAS-wide deployment at 37-airports. More significantly, use of the EDA tool requires less overall workload primarily because of the integration with metering conformance flight intent, reducing the number of missed and false alerts by 30 and 21 percent, respectively. As a result, EDA enhances overall safety, enables strategic controller planning across multiple sectors, and reduces nuisance conflict alerts.

These benefit estimates are sensitive to ARTCC traffic routing complexity. A typical day of ZFW Center activity was analyzed with interruption rates and per operation savings extrapolated to other airports. The NAS-wide EDA benefit estimates would be enhanced with more comprehensive evaluation of the en route traffic routing of various facilities.

5. Arrival Trajectory Optimization Benefits

Arrivals into high-density terminal airspace are currently subject to static restrictions and procedures that impact their en route trajectory efficiency. These restrictions are primarily imposed to manage and segregate arrival flows given arrival trajectory prediction uncertainty and arrival rate variability, as well as account for performance differences among aircraft types. These restrictions typically involve the use of ATM-defined Standard Terminal Arrival Routes (STARs), including altitude and speed restrictions at the metering fix (TRACON entry). Procedures typically merge flights into arrival streams upstream of the metering fix. EDA enables two general types of trajectory optimization benefits, relative to such operations: optimization to existing metering fix restrictions; and the relaxation of metering fix restrictions enabled by precise metering.

Given existing metering fix restrictions, EDA maneuver advisories can facilitate efficient conflict-free, arrival metering conformance without the need for merging arrivals upstream of the metering fix. EDA predicts and address any conflicts with crossing traffic and coordination among airspace sectors. Such optimization would allow aircraft to spend the maximum amount of time in cruise and provide a direct route to the arrival metering fix. These benefit mechanisms are referred to here as Top-of-Descent (TOD) optimization and arrival direct routing, respectively. Although controllers are currently able to facilitate such flight optimization under light traffic, arrival metering increases the complexity and uncertainty leading to more conservative controller clearances and increased arrival fuel consumption.

Additionally, EDA trajectory prediction and metering conformance accuracy could also enable the relaxation of existing static arrival restrictions, allowing greater fuel efficiency and user flexibility. Thus, it may no longer be necessary to force all arrivals to converge at the TRACON boundary (i.e. arrival metering fixes) at a common altitude, speed, and position when EDA maneuver advisories enable en route controllers to deliver aircraft to the TRACON in the required state and sequence for merging. Such a relaxation of constraints (horizontal/vertical anchor point concepts) would allow each aircraft to operate in a more efficient manner according to its performance characteristics. This dynamic movement of the metering fix or anchor point downstream into the TRACON is referred to here as the vertical and horizontal anchor point concepts. These concept effectively realize the industry [2] objective of delaying arrival merging as long as safely possible.

Four EDA mechanisms optimizing arrival trajectories were evaluated:

- Existing Metering Fix Restrictions - Top of Descent (TOD) Optimization,
- Existing Metering Fix Restrictions - Arrival Direct Routing,
- Relaxed Metering Fix Restrictions - Horizontal Anchor Point, and
- Relaxed Metering Fix Restrictions - Vertical Anchor Point.

The TOD optimization and vertical anchor point mechanisms shift the TOD location downstream, minimizing power-on flight at lower altitudes (early descents) and delaying

the start of the descent. The direct routing and horizontal anchor point mechanisms attempting to shorten aircraft flight path lengths. All mechanisms impact fuel consumption. Additionally, controller workload is also expected to benefit from the assistance of the EDA advisories, the enhanced situational awareness, and confidence in conflict-free clearances that meet separation requirements and flow-rate restrictions.

After an overview of the analysis process, this chapter begins by identifying the baseline (radar) data employed in the analysis of all four EDA trajectory optimization mechanisms. This is followed by four sections which assess per operation benefits of each mechanism. At the end of the chapter, all four mechanisms are extrapolated together to annual/NAS-wide levels.

Analysis Process

The overall sequence of analytical formulations and computer-based modelings follows a simplified approach relative to that of Figure S.1 in the introduction summary section. These findings were identified in past benefits studies of EDA, previously termed Sector Tool, mechanisms [18-20]. Initially, the technology requirements as well as Baseline and EDA trajectory profiles are defined (1). Flight improvements are identified by comparing Baseline operations, represented by radar track data from five airports (ATL, BOS, DFW, LAS, LAX), to EDA optimized trajectories (3). Per operation distance improvement is based on analysis of three hourly high-demand periods at each airport. In most cases, these EDA path distance savings were converted to fuel savings, assuming aircraft specific fuelburn rates from an analytical model. In the case of TOD optimization, theoretical fuel savings, using a higher fidelity aircraft performance model, were defined relative to an idle descent at the optimum TOD location (2). The resulting 5-airport average per operation EDA savings are then extrapolated to annual and NAS-wide levels (4). Mechanisms tied to existing metering fix restrictions are assumed to extend to metered arrivals only (non-metered arrival optimization currently practiced), while the new relaxed metering fix benefits are applicable to all arrival operations.

Note that for all mechanisms, it is assumed that the arrival flight trajectory could be changed without a significant increase doe to conflicts with traffic or restricted airspace. EDA would facilitate the efficient resolution of these conflicts while enabling the user-preferred optimal trajectory, as supported by Chapter 4, Separation Assurance Benefits, findings that EDA automation assistance improved separation assurance tasks. Additionally, only fuel efficiency are tabulated, despite the ability of path shortening to save time in non-metered conditions, leading to additional benefits.

Where applicable, an analytical model was used to determine fuelburn per nautical mile for over 20 aircraft types. This model applies performance and operating procedure coefficients for various aircraft types. The fuelburn results from this model were calibrated using a high-fidelity model. Note that the results of this investigation are differences in (modeled) fuelburn ascribed to actual (radar) and more-efficient EDA trajectories. The analytical aircraft models are sufficient to determine trends and differences in fuelburn. The aircraft types and input parameters (typical weight, airspeed, and cruise) used in this investigation are listed in Appendix F. The database of aircraft parameters, the Base of Aircraft Data (BADA), used in the model, was provided by the Eurocontrol Experimental Center [37]. Aircraft coefficients from BADA are used to calculate thrust, drag, and fuel flow. The results were used to determine the fuel-savings benefit of the vertical anchor point, horizontal anchor point, and direct routing mechanisms. Use of a higher-fidelity aircraft performance model is discussed with the TOD optimization mechanism.

The model components are discussed in more depth with the analysis results in the following sections. Note that the Baseline radar data used by all four trajectory optimization mechanisms is discussed initially, followed by the estimation of per operation savings for each mechanism, concluding with the extrapolation of all EDA trajectory optimization mechanisms to annual/NAS-wide benefit estimates.

Baseline Traffic & Trajectory Data

Radar-tracking data from the four Air Route Traffic Control Centers (ARTCCs) were used to determine Baseline arrival trajectories at five major airports to evaluate the four EDA Trajectory Optimization benefit mechanisms. Aircraft trajectories were studied to determine current en-route procedures and the potential for improvement. System Analysis Recording (SAR) radar track data were obtained for a 24-hour period from each Center. Three hours of data were then selected to represent pre-rush, rush, and post-rush conditions. These data, reflecting five major airports and a variety of airspace environments and traffic conditions, were processed to statistically identify information relevant to the EDA trajectories optimization mechanisms, included in later sections. By examining actual aircraft tracks, the degree, if any, to which these mechanisms could be applied was determined.

The chosen sites include the following:

- Dallas Ft. Worth International Airport (DFW), Ft. Worth Center (ZFW)
- Chicago O'Hare Airport (ORD), Chicago Center (ZAU),
- Boston Logan International Airport (BOS), Boston Center (ZBW),
- Las Vegas McCarran International Airport (LAS), Los Angeles Center (ZLA), and
- Los Angeles International Airport (LAX), Los Angeles Center (ZLA).

Figure 5.1 compares the total number of hourly radar operations at each study airport. The three study hours at each airport are also noted. The number of operations studied in this analysis may differ from actual operations due to incomplete and anomalous radar tracks, the fleet mix of the sample is given in Table 5.1.

Figure 5.2 illustrates actual arrival (red) and departure (blue) traffic for a representative peak hour over-layed on IFR En Route Low Altitude Charts. Note that LAS has large Special Use Airspace regions to the north, LAX is bordered to the West by the Pacific Ocean, and BOS is bordered to the East by the Atlantic Ocean.

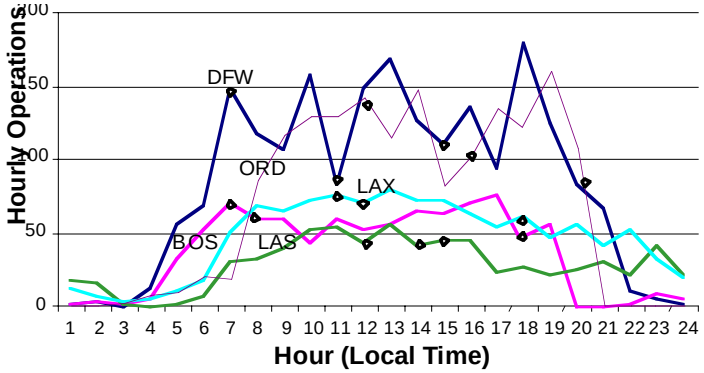

Figure 5.1 Radar Data Hourly Throughput by Airport

Table 5.1 Radar Sample Airport Fleet Mix

FAA Weight Class	Airport Fleet mix				
	BOS	**DFW**	**LAS**	**LAX**	**ORD**
Small	3%	2%	2%	5%	5%
Large	83%	84%	59%	42%	85%
Heavy	15%	13%	39%	53%	10%
Total	100%	100%	100%	100%	100%

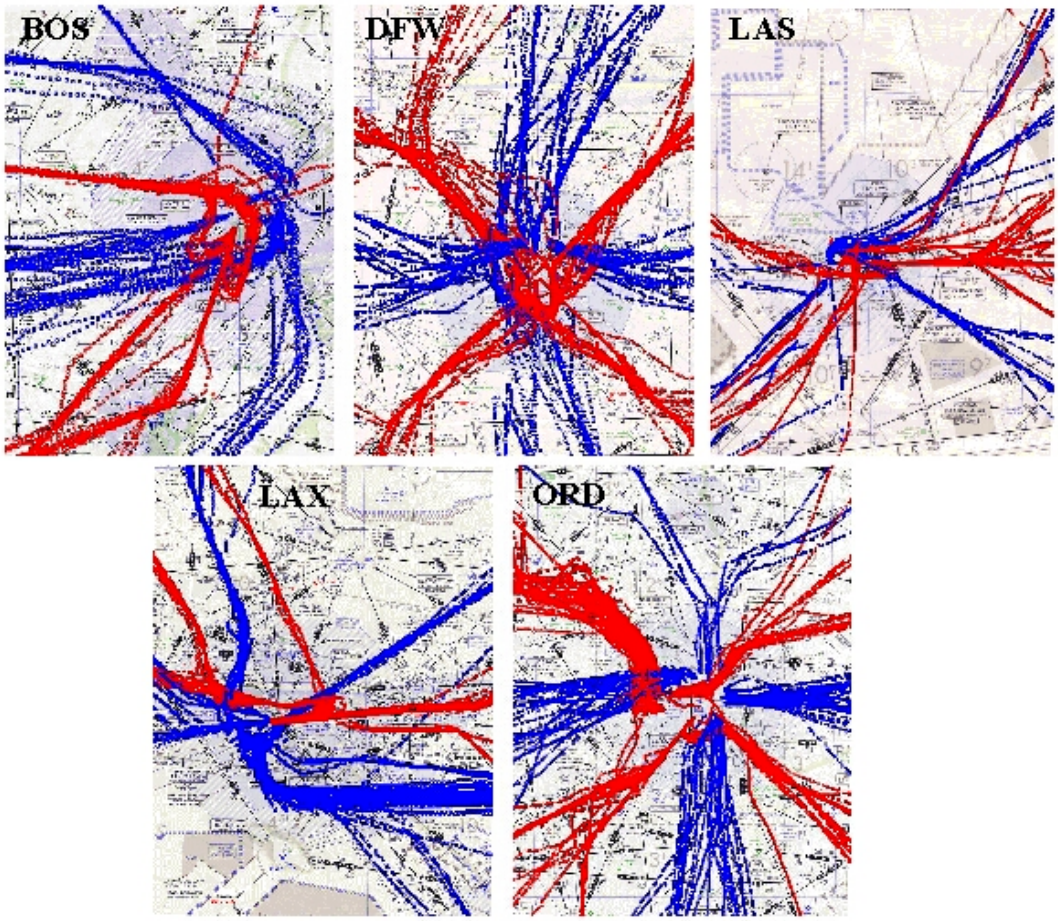

Figure 5.2 Arrival (Red) and Departure (Blue) Peak Period Traffic at Study Airports

Existing Metering Fix Restrictions - TOD Optimization

EDA provides fuel-efficiency benefits for metered arrival aircraft by facilitating aircraft optimal (idle thrust) TOD location. This analysis estimates the potential fuel savings per operation by comparing the fuelburn of flights under Baseline and idle-thrust Top-of-Descent (TOD) locations, enabled by EDA. Baseline operations reflect 1996 radar track observations at the five study airports. EDA idle-thrust descent fuelburn is derived from simulations of a single B727 aircraft, extrapolated fleet-wide using Eurocontrol Base of Aircraft Data (BADA) [37].

Baseline & EDA Descent Profiles

The Top-of-Descent (TOD) optimization mechanism affects the vertical-profile of an aircraft descent trajectory from cruise to the metering fix altitude, while maintaining current arrival metering fix restrictions. The vertical profile was assumed to be enhanced by moving the top of descent (TOD) location downstream to minimize power-on flight at lower altitude (i.e., early descents). Positioning of the TOD location is constrained such that the location of the bottom of descent (BOD) coincides with the existing metering fix. Ideally, the TOD is moved as far downstream as possible while still providing the aircraft with enough range to cross the metering fix at the bottom of descent under an idle descent starting at the cruise altitude. This results in a steep descent profile. Varying the TOD location, while fixing the BOD or metering fix, results in a set of continuous descent profiles ranging from early, gradual descent profiles to late, steep profiles, as shown in Figure 5.3. The steepest descent profile in the figure represents the optimal idle-thrust descent at a given speed. Different TOD locations reflect early descents at the given speed. Continuous descent profiles, supported by EDA, are preferable to step descent profiles because of their improved fuel efficiency.

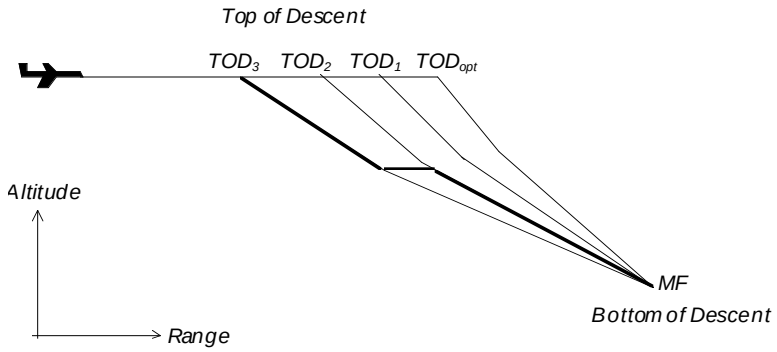

Figure 5.3 Early and Optimal (Idle) Descent TOD Locations for a Given Speed

Early descents may also take the form of step descents, as shown in bold in Figure 5.3. A step-descent profile may consist of one or more descent segments separated by level flight segments. Air traffic controllers may use step descents to ensure conflict avoidance. In this analysis descents (continuous or stepped) are modeled by an equivalent constant flight path angle. As the TOD location is moved downstream, the flight path angle, γ, becomes steeper, closer to the optimal idle-thrust descent profile.

EDA Optimal Vertical Profile

EDA-enabled TOD locations were assumed to be the latest point where an aircraft can begin an idle descent and hit the existing bottom of descent (BOD) location (and altitude), assumed to satisfy existing arrival metering fix restrictions. The aircraft-specific cruise to arrival metering fix altitude change (from the radar data), and nominal aircraft-specific descent speeds were used to identify the optimal TOD location for each flight under idle descent. Note that the trajectory of an idle-thrust descent does not have a constant flight path angle.

Baseline Vertical Profile

FFP1 Baseline TOD locations were determined from aircraft radar track data. The radar-tracking data were used to determine trajectory baselines for comparison with idle-thrust TOD trajectories, enabled with EDA. Observed DFW arrival trajectories from the cruise to metering fix altitude were studied to determine the frequency of early descents, i.e., earlier than necessary TOD locations, given existing speeds, winds, and metering fix restrictions. After accounting for variations due to cruise/MF altitudes and TOD/BOD range, the data revealed a spectrum of current aircraft TOD locations, which represent flights that could have benefited from a later TOD. Each observed (radar) descent trajectory, including both continuous and step descents, was characterized in the analysis with an equivalent constant flight path angle. This flight path angle was based on observed TOD and BOD flight range and altitudes, and assumed nominal descent speeds provided in Appendix F.

Evaluation of the radar data at the five airports resulted in a spectrum of actual TOD locations (i.e., equivalent flight path angles) for each airport. The airport variations in the radar-based flight path angles are shown in Figure 5.4. The three hour were combined as the observed vertical profiles did not vary significantly between the hours studied. Note that the observed flight path angles, despite the mix of aircraft, resemble a normal distribution with a mean of just over two degrees. BOS and LAS do not follow this trend, likely because of their smaller sample size.

Additionally, as discussed later in this section, the baseline flight path angles were limited to 2 degrees or greater, in order to conservatively account for the simplified fleet-wide extrapolation method used in this analysis.

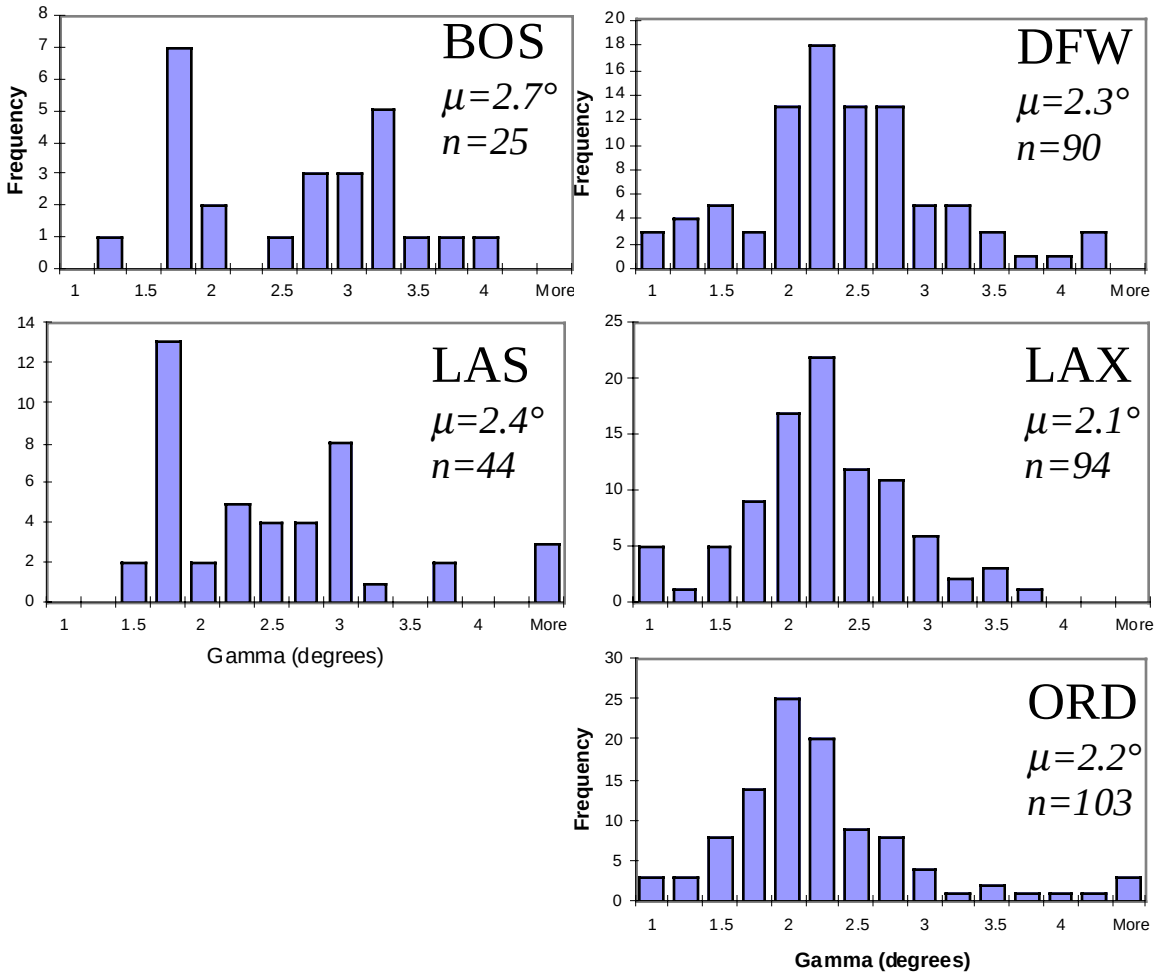

Figure 5.4 B727 Constant Flight Path Angle Descent Fuelburn Relative to Idle-Thruust Descent

Fuelburn by TOD Location

For this investigation, a set of high-fidelity simulations for a single aircraft were made to determine descent fuel consumption for a series of flight path angles and descent speeds, and extrapolated to reflect various aircraft types [18-20]. In the TOD optimization analysis, different constant flight path angle descent trajectories are assumed to reflect different Baseline TOD locations, and compared to the optimal EDA case of an idle-thrust descent.

The high-fidelity simulation results reflect a single 130,000 lb, B727-200 aircraft descending from 33,000 ft to 11,000 ft, with the speed schedules described in Table 5.2. Each trajectory was simulated over a range of 100 nm and was constrained to meet the same final arrival metering fix/bottom-of-descent (BOD) location, altitude and 250 kt airspeed restrictions. Constant Mach/CAS schedules were used in each simulation; therefore, either flight path angle or thrust was fixed, but not both. Figure 5.5 shows the simulated constant flight path angles and idle thrust descent trajectories.

Table 5.2 Assumed B727-200 Descent Simulation Speed Schedules

Constant Mach	Constant CAS (kt)
0.72	260
0.75	280
0.78	300
0.80	320
0.82	340
0.84	350

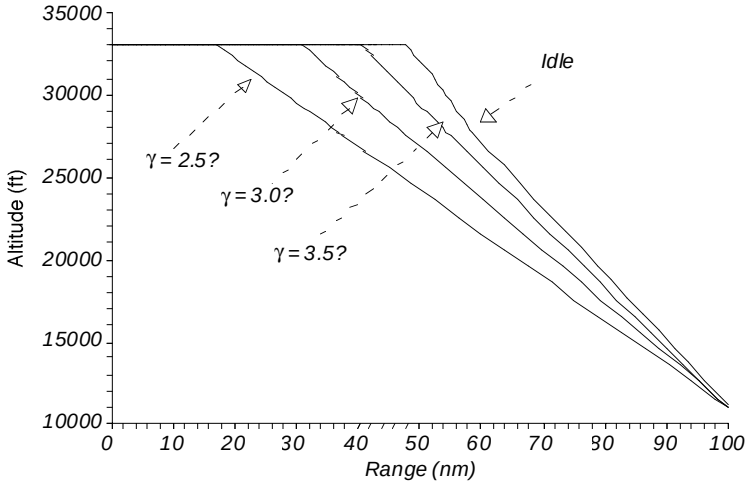

Figure 5.5 Simulated B727 Constant Flight Path Angle and Idle-Thrust Descent Profiles [18]

Figure 5.6 shows the amount of additional fuel consumed for each angle of descent relative to the idle descent case for the simulated B727-200 aircraft. The idle-thrust descent profile provided limited fuel savings over the case of the steepest constant flight path angle, $\gamma = 3.5°$. However, fuel consumption did increase notably with more shallow descents, with the most shallow case, $\gamma = 2.5°$ descent, consuming 18 percent more fuel than the idle descent. Note also, that B727 fuel savings decreased under slower descent speeds, for a given flight path angle, due to shallower idle-thrust descents at slower speeds.

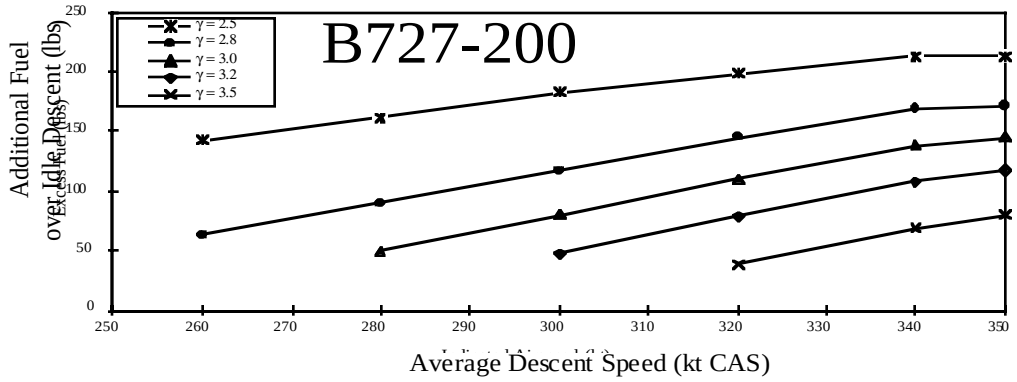

Figure 5.6 B727 Constant Flight Path Angle Descent Fuelburn Relative to Idle-Thrust Descent

To cover the spectrum of aircraft observed at the study airports, the high-fidelity B727 fuelburn results were extrapolated to over 20 aircraft classes using fuel-scale factors derived from Eurocontrol BADA aircraft performance characteristic data [37]. The fuel-scale factors, ranging from 0.15 to 5.75, can be found in Appendix F. Additionally, since this extrapolation method represents a significant simplification of actual descent fuelburn for these aircraft, the baseline flight path angle was limited to 2 degrees or greater.

TOD Optimization Fuel Savings

To estimate EDA TOD Optimization benefits, the spectrum of Baseline TOD locations (and equivalent constant flight path angles) as observed in the 3-hour radar track data for each airport, were compared to EDA idle-thrust flight-path angles to determine fuel savings. The data from Figure 5.6 were used to estimate the aircraft-specific fuel savings from shifting the observed equivalent constant flight path angle (i.e., TOD location) to the optimal idle-thrust TOD location at an assumed nominal descent speed (Appendix A). A fuel-scale factor was applied to scale the B727 savings to the particular aircraft type. The resulting benefit is measured in excess pounds of fuel used, over an idle-thrust descent. This fuelburn savings is an average, representative of the fleet observed during the 3-hourly periods studied at each airport.

The estimated average per operation savings for the EDA TOD optimization benefit mechanism at the five airports under study are summarized in Table 5.3. Note that since the TOD benefits for each of the three one-hour periods studied did not vary significantly, they are averaged together in Table 5.3. The table first identifies the observed average TOD to MF distance and equivalent constant flight path angle in descent from the baseline radar data. For a large aircraft with a 10-minute descent at an average descent speed of 350 kts, this implies that TOD optimization resulted in an average downstream shifting of the TOD by 36 nm. Table 5.3 next gives the range and average per operation fuel savings (lbs) assuming these aircraft were able to optimize their TOD location and fly EDA enabled idle descents. Fuel cost savings assumes a fuel cost of $0.10 per lb. Note that because this EDA benefit mechanism does not alter the flight time, only fuel benefits are included.

The results of Table 5.3 indicate that under EDA TOD optimization, aircraft would travel an additional 20-40 nm in cruise before beginning their descent, saving an average of 182 lbs or $18.16. LAX appears to have the highest level of per operation benefit, followed by ORD, then LAS. DFW and BOS, show significantly less benefit.

It should be noted that this analysis is only a first-cut estimate given the simple B727 fuelburn extrapolation method used in light of the large variation in descent fuelburn across aircraft types and at various altitudes. Additionally, the idle-thrust descent profiles are highly sensitive to assumptions of aircraft weight and speed. At a minimum future estimates should simulate a larger spectrum of aircraft, and be sensitive to the observed aircraft speeds.

In extrapolating this mechanism to annual/NAS-wide levels, benefits were only assumed to accrue to rush arrival operations. This implies that TOD optimization under existing metering fix restrictions would have little benefit during non-rush periods, when workload

is reduced, allowing controllers to accommodate user-preferred vertical profiles without EDA.

Table 5.3 EDA TOD Optimization Average Per Operations Savings

	Baseline Conditions		Per Operation Savings		
Airport	TOD to MF Distance (nm)	Average Flight Path Angle (degrees)	Fuel Savings Range (lbs/op)	Fuel Savings Average (lbs/op)	Fuel Cost Savings* ($/op)
BOS	82.81	2.7	0-433	107.16	$10.72
DFW	92.36	2.3	0-236	142.38	$14.24
LAS	89.72	2.4	0-621	188.82	$18.88
LAX	107.01	2.1	0-681	270.00	$27.00
ORD	97.89	2.1	0-298	199.84	$19.98
Average	93.96	2.3	–	181.64	$18.16**

* Assumes fuel cost of $0.10 per lb.
** 5-airport average used in annual/NAS extrapolation.

Existing Metering Fix Restrictions - Arrival Direct Routing

The EDA arrival direct routing mechanism attempts to improve flight efficiency by enabling user preferred routing to the arrival metering fix, while adhering to current day operational metering fix restrictions. Baseline operations typically require interception of a standard terminal arrival (STAR) route, which the aircraft follows to the metering fix (TRACON entry). Users are assumed to fly their preferred route (en route) with this EDA mechanism enabling a smooth transition directly to the metering fix. Direct routing shortens the actual path length flown by "cutting the corner" and flying directly to the metering fix, as shown in Figure 5.7.

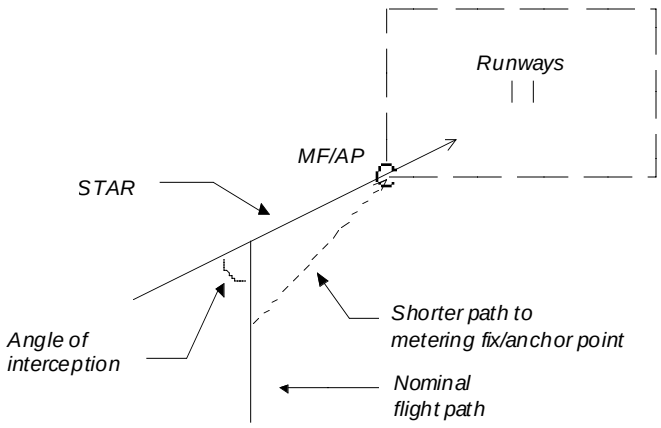

Figure 5.7 Arrival Direct Routing Shortens Arrival Flight Path

The potential benefits of direct routing will vary depending on the nominal or Baseline flight path. Baseline flight paths with multiple linear segments, or "dog legs," have the greatest potential for improvement. Currently-granted user-requested direct routes or straight-line paths reap little benefit from this mechanism. To account for the variation in

current operations, actual aircraft descent trajectories, based on radar track data from the five study airports, were used to represent the FFP1 Baseline trajectories.

Baseline Arrival Routing

Radar track data at five airports (BOS, DFW, LAS, LAX, and ORD) were examined to determine Baseline aircraft paths within the Center. The Baseline paths were characterized with respect to their directness to the TRACON including any indirect linear segments, or "dog legs." The path distance of each Baseline arrival route, extending from 140 nm from the airport to the arrival metering fix was tabulated. No direct routing benefit would accrue for trajectories already on direct routes. Note that the marginal benefits of direct routing decreases as you move farther away due to geometry.

EDA Arrival Direct Routing

EDA enabled user-preferred direct arrival routes were defined assuming aircraft could fly a route directly to the metering fix. This route took the aircraft location at 140 nm from the airport, and gave it a path directly to the arrival metering fix, assuming no change in descent profile.

Arrival Direct Route Fuelburn Savings

EDA Arrival direct routing benefits were based on the path length savings between Baseline (radar observations) and user-preferred (direct) arrival routings, each starting approximately 140 nm from the airport. The path difference was calculated for each flight within the 3-hourly periods studied at each airport. Fuel savings were calculated by assuming the shorter path distance represented fuelburn rate at a typical cruise altitude, weighted by airport fleet-mix during the hours studied.

The per operation fuel savings are summarized in Table 5.4. This table identifies the path distance savings of an average operation at each airport under EDA enabled direct routing. Although the individual savings would be highly variable, with some arrivals showing no benefits, the table value represents the average for all flights during the 3- hourly periods. This average is representative of the demand on the various arrival routes. The path distance savings is converted to fuel savings by calculating the fuel burned by an aircraft of that type flying the additional distance at a typical cruise altitude. The product of the distance and fuelburn is the average fuel saved by an average operation at each airport. Fuel cost savings assumes a fuel cost of $0.10 per lb.

The results of Table 5.4 indicate that under EDA direct route optimization, arrival aircraft would save 1-3 nm on average with direct routing, saving an average of 21 lbs of fuel or $2 per arrival operation. LAX shows the greatest potential for EDA arrival direct routing benefits, followed closely by DFW and LAS. Lower benefits are expected at ORD and BOS. This is reflective of the STAR routings at these locations and it should be noted that route restrictions (e.g. noise-abatement procedures, Special Use Airspace) were not taken into account and may attenuate these results.

In extrapolating this mechanism to annual/NAS-wide levels, benefits were only assumed to accrue to rush arrivals. This implies that arrival direct routing under existing metering fix

restrictions would have little benefit during non-rush periods, when workload is reduced, allowing controllers to accommodate user-preferred direct routing without EDA.

Table 5.4 EDA Arrival Direct Route Average Per Operation Savings

	Savings Per Arrival Operation		
Airport	Distance Savings (nm/op)	Fuel Savings (lbs/op)	Fuel Cost Savings* ($/op)
BOS	0.89	10.54	$1.05
DFW	2.17	23.05	$2.31
LAS	1.80	22.93	$2.29
LAX	2.54	36.67	$3.67
ORD	3.06	11.83	$1.18
Average	2.09	21.00	$2.10**

* Assumes fuel cost of $0.10 per lb.
** 5-airport average fuel cost savings used in annual/NAS extrapolation.

Relaxed Metering Fix Restrictions - Vertical Anchor Point Concept

Similar to TOD optimization, the EDA vertical anchor point concept affects the vertical-profile of an aircraft arrival trajectory, attempting to maximize aircraft flight time at cruise altitude. Aircraft descending into a TRACON airspace are currently directed by controllers to arrive at metering fixes approximately 30-40 nm from the runway threshold. EDA maneuver advisories can provide detailed traffic information that will allow the controller to safely direct an aircraft to a new bottom of descent, termed vertical anchor point (VAP), downstream of the current metering fix within TRACON airspace. Using this vertical anchor point as the new bottom of descent enables aircraft to spend more time at the more fuel efficient higher altitudes, as illustrated in Figure 5.8.

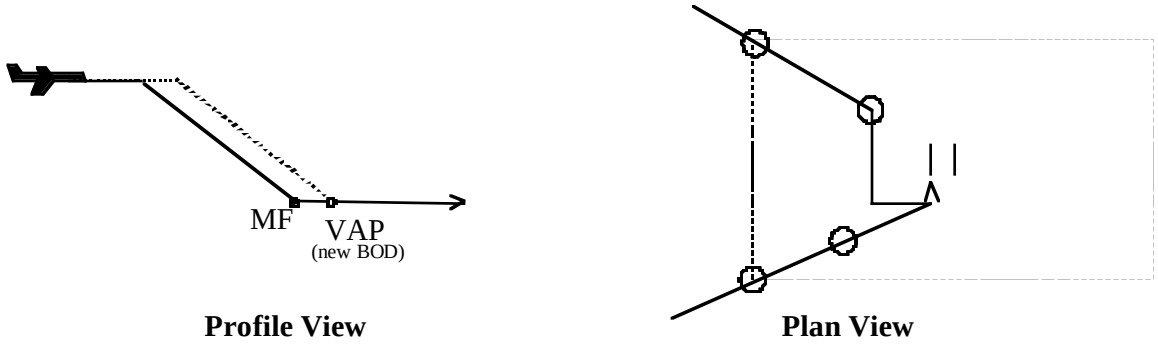

Figure 5.8 Plan and Profile View of the Vertical Anchor Point (VAP) Concept

The VAP concept may be expanded to specify aircraft-specific anchor points to accommodate differences in aircraft performance. That is, an aircraft-specific VAP would be defined by a 3D location and associated airspeed. For this investigation, the vertical anchor point is defined to be a location in space a set distance downstream of the original metering fix with the same altitude and speed restriction (250 kt maximum). Vertical and horizontal anchor point benefits may be more significant for long-side (LS) arrivals than short-side (SS) arrivals because of the additional high-altitude cruise length to be gained, as illustrated in Figure 5.8.

In this study, actual aircraft descent trajectories from the five study airport's radar track data were examined to determine the potential for using downstream vertical anchor points. Observed Baseline vertical trajectories into the TRACON were compared to user-preferred trajectories using the vertical anchor point concept to determine the EDA fuel benefits.

Baseline Vertical Anchor Point Location

Current Baseline metering fix or anchor point locations were determined from aircraft radar track bottom of descent (BOD) data. Current aircraft descents from the cruise to metering fix were studied to determine which aircraft would have benefited from shifting the BOD initially to the current metering fix location and then further into the TRACON.

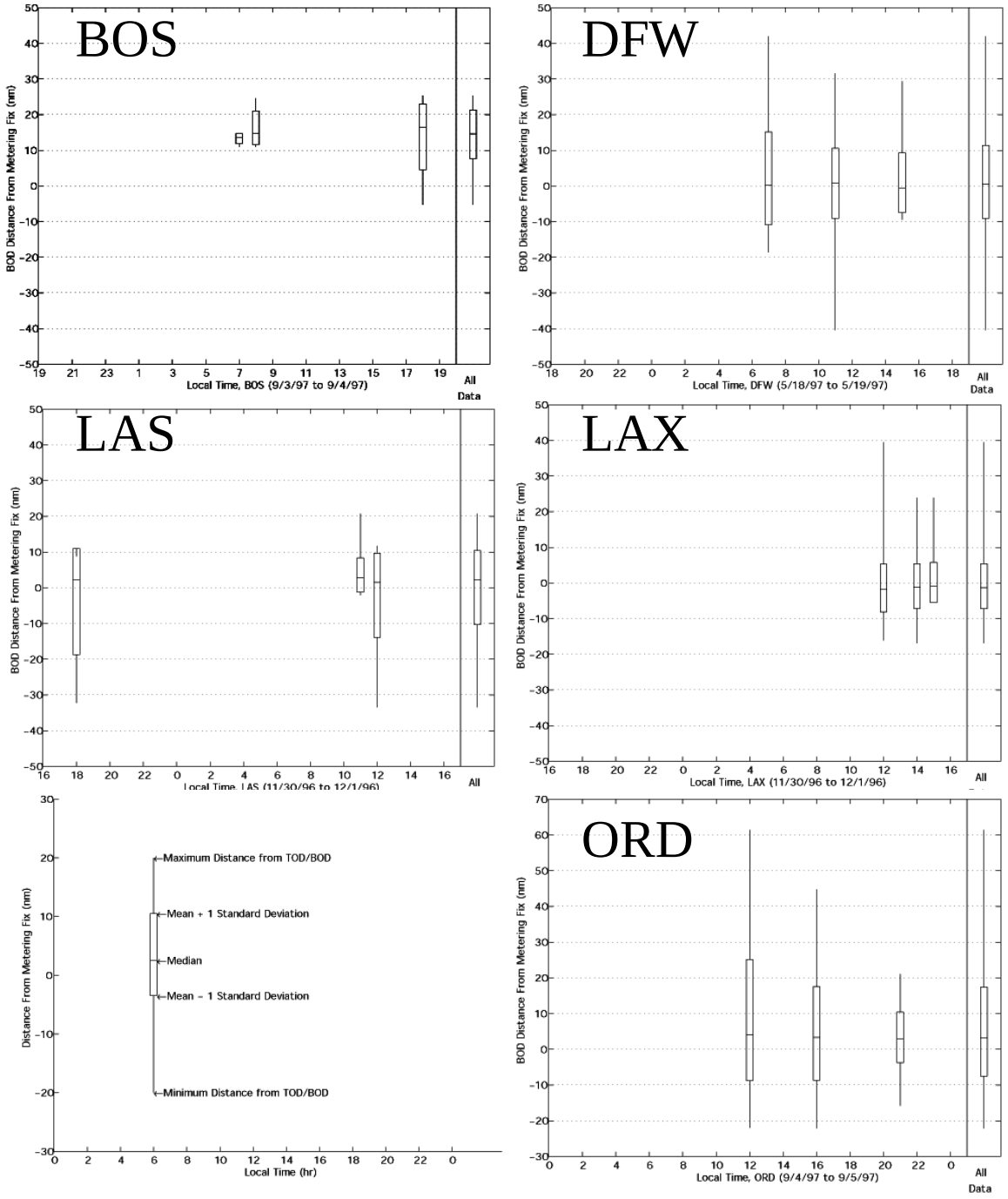

Figure 5.9 BOD Statistics at Five Study Airports

Evaluation of the radar data resulted in a spectrum of actual BOD locations for each airport. Radar track BOD statistics for each hour at each airport are shown in Figure 5.9, along with a key to interpreting these statistics. Since current procedures require aircraft to enter the TRACON at the arrival metering fix, most BOD locations fell upstream of the arrival metering fix, and have a tighter spread than the TOD locations, presented earlier. This finding also implies that controllers do not currently use the vertical anchor point concept. Generally, the BOD location varied by 10 to 20 nm (1-sigma) across all airports. The least

variation was found at BOS and LAX, with large variations at LAS and DFW, similar to the TOD findings.

EDA Vertical Anchor Point Location

The EDA enabled movement of the vertical anchor point was assumed to push the Baseline operations downstream. These included the existing arrival metering fix location as well as locations 5, 10, and 15 nm downstream into the TRACON. Note that the current location was assumed to be 35 nm from the airport, which in actuality varies by airport.

BOD Optimization Fuel Savings

The Bottom-of-Descent (BOD) statistics of Figure 5.9 were used to estimate average fuel savings at each airport, with the downstream shifting of the BOD or vertical anchor point into the TRACON. Table 5.5 summarizes the results of shifting the BOD by 0, 5, 10, and 15 nm downstream, relative to the observed BOD, as identified in the radar track data. Note that in all cases, it is assumed that EDA would enable the BOD to be moved downstream by accurately delivering arrivals on time for merging in the TRACON. Since the results did not vary significantly among the 3-hourly periods, the data were reduced to a single average for each airport. Table 5.5 initially identifies the distance saved by an average operation at each airport under the current and alternate VAP locations. The static MF case is included to isolate the observed level of BOD optimization occurring today, as exemplified in the radar data. The small negative values reflect either simplified arrival fix locations assumed in the analysis (35 nm from airport) and/or ATM allowance of flight hand-off within the TRACON airspace. Aircraft-specific fuelburn values for cruise and metering-fix altitudes were applied to determine the average VAP fuel savings per arrival operation at each airport. Fuel cost savings assumes a fuel cost of $0.10 per lb.

The potential for benefits is largely tied to the airport's existing ability to coincide the aircraft BOD with the existing MF location. LAS and LAX are optimized very closely, with less optimization at DFW. BOS and ORD have the largest optimization potential. These "static MF" benefits of Table 5.5 could accure without relaxation of the existing metering fix restrictions. Once these initial conditions are accounted for, any additional shift of the metering fix/vertical anchor point location downstream reaps the same per operation savings across all airports. Note that the results of Table 5.5 do not reflect attenuation due to the feasibility of the downstream shift in BOD location. However, in extrapolation to annual/NAS-wide levels, a conservative 5 nm VAP location was chosen to represent a realistically achievable downstream shift for both long-side and short-side approaches, allowing sufficient additional descent distance in the TRACON. It is possible that the VAP could be shifted further downstream, especially for long-side operations.

Table 5.5 EDA Vertical Anchor Point Average Per Operation Savings

		Average Per Operation Savings		
Airport	Scenario	Distance Savings (nm/op)	Fuel Savings (lbs/op)	Fuel Cost Savings* ($/op)
BOS	Static MF	14.48	132.55	$13.26
	5nmVAP	19.48	178.34	$17.83
	10nmVAP	24.48	224.12	$22.41
	15nmVAP	29.48	269.90	$26.99
DFW	Static MF	1.16	10.03	$1.00
	5nmVAP	6.16	53.37	$5.33
	10nmVAP	11.16	96.71	$9.67
	15nmVAP	16.16	140.05	$14.01
LAS	Static MF	0.02 (1)	0.22 (1)	$0 (1)
	5nmVAP	5.02	52.47	$5.25
	10nmVAP	10.02	104.72	$10.47
	15nmVAP	15.02	156.97	$15.70
LAX	Static MF	(0.91) (1)	0 (1)	$0 (1)
	5nmVAP	4.09	46.66	$4.67
	10nmVAP	9.09	103.63	$10.36
	15nmVAP	14.09	160.61	$16.06
ORD	Static MF	4.94	43.94	$4.39
	5nmVAP	9.94	88.44	$8.84
	10nmVAP	14.94	132.94	$13.29
	15nmVAP	19.94	177.45	$17.75
Average**	5nmVAP	*8.94*	*74.96*	*$7.50*

Note: Static MF benefits could accrue without relaxation of existing metering fix restrictions.
(1) Negligible savings due to current BOD optimization at LAS and LAX.
* Assumed fuel cost of $0.10 per lb
** Average used in annual/NAS extrapolation, reflects no benefit in peak hour at DFW and ORD.

In extrapolating this mechanism to annual/NAS-wide levels, benefits were assumed to apply to all arrivals. This reflects the fact that the proposed anchor point concept is not attempted today, as it requires a relaxation of existing metering fix restrictions only available with EDA metering fix delivery accuracy improvement.

Relaxed Metering Fix Restrictions - Horizontal Anchor Point Concept

The EDA horizontal anchor point (HAP) concept, as with the arrival direct routing, affects the horizontal-profile of an arrival flight trajectory and attempts to improve the efficiency of the trajectory by shortening the path length. However, the HAP, as with the VAP, lifts the restriction of a single metering fix or anchor point, allowing arrivals to enter the TRACON offset from the existing metering fix location (e.g., inside the TRACON). Ideally the HAP would be placed along the straight-line path from the Center entry point to the runway. Although the Center-TRACON boundary is generally not circular, the horizontal anchor point is assumed to be moved along an arc to ensure that the aircraft has sufficient range to descend to the runway. Aircraft would be metered to scheduled times along this arc (at a pseudo-metering fix), although the aircraft would not merge into a single stream until reaching the HAP. For this investigation, the radius of the arc was based on an average distance between metering fix locations and the runway threshold. Figure 5.10 illustrates the HAP concept and the potential reduction in the arrival's path distance. Crossing traffic may preclude the use of the optimal HAP due to conflicts with departure operations, which may attenuate the results.

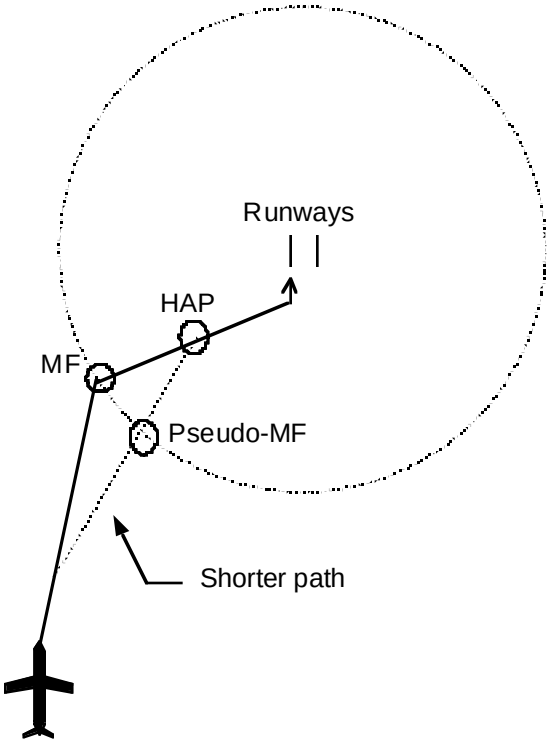

Figure 5.10 Plan View of the Horizontal Anchor Point (HAP) Concept

In this study, actual aircraft descent trajectories at the five study airports were examined to determine the fuel savings available using the EDA horizontal anchor point concept.

Baseline Horizontal Anchor Point Location

Radar-tracking data were examined to characterize the horizontal path of aircraft entering the TRACON. The Baseline is represented by routing along a STAR directly over an existing metering fix location.

The applicability and benefit of this mechanism was determined by evaluating the horizontal route of each trajectory and noting the angle and distance at which the path intersects the STAR and metering fix, respectively. No HAP benefit accrued to trajectories already using this mechanism.

EDA Horizontal Anchor Point Location

EDA-enabled user-preferred trajectories using horizontal anchor points were determined by assuming that aircraft could fly directly to a point 15 nm downstream of the metering fix, without passing through the metering fix. The difference in path length was calculated between user-preferred HAP and actual trajectories and the resulting fuel savings calculated. Time of arrival at the Center/TRACON boundary was not constrained in this analysis.

Horizontal Anchor Point Fuel Savings

Similar to the arrival direct routing mechanism, the benefit of horizontal anchor points was determined by comparing actual arrival trajectories with optimized trajectories, each starting approximately 140 nm from the airport. As with arrival direct routing, the marginal benefit decreases as you move farther away due to geometry. Actual trajectories were graphically characterized with their Center/TRACON-boundary-crossing location relative to the metering fix. Trajectories that did not use the metering fix to cross the Center/TRACON boundary and, instead, flew direct to the runway, were not assumed to benefit from this mechanism. Only aircraft that clearly diverted from a direct path to fly through the metering fix were assumed to benefit from this mechanism. Direct path length was compared to actual path length and resulting differences in fuelburn computed.

These results were used to determine annual fuel and cost savings at each airport, summarized in Table 5.6. This table identifies the distance saved by an average operation at each airport using the horizontal-anchor-point mechanism. Results from the 3 hours studied were averaged together in the calculation of annual savings. This distance saved is converted to fuel consumption by modeling the expected fuelburned by an aircraft flying that distance at a typical cruise altitude. The fuelburn rates reflect the fleet types observed during the 3 hours studied at each airport. LAX shows the greatest potential with this mechanism. Noise-abatement procedures may attenuate these results. ORD reaps the least benefit. From the radar data, it appears that ORD Baseline paths represent a smooth stream of traffic, gaining little from the corner cutting of the HAP mechanism.

Since DFW and ORD, as observed from the radar data, showed significantly high volumes of delays, no benefit was assumed for the rush hour at these airports. This is reflected in the fuel savings for those airports.

In extrapolating this mechanism to annual/NAS-wide levels, benefits were assumed to apply to all arrivals. This reflects the fact that the proposed anchor point concept is not attempted today, as it requires a relaxation of existing metering fix restrictions only available with EDA metering fix delivery accuracy improvement.

Table 5.6 EDA Horizontal Anchor Points Average Per Operation Savings

	Per Operation Savings		
Airport	Distance Savings (nm/op)	Fuel Savings (lbs/op)	Fuel Cost Savings* ($/op)
BOS	2.60	32.58	$3.26
DFW	4.19	45.88	$4.59
LAS	3.15	44.40	$4.44
LAX	3.82	51.99	$5.20
ORD	1.49	6.12	$0.61
Average	3.05	36.20	$3.62**

* Assumes $0.10 per lb fuel.
** Average used in annual/NAS extrapolation

Economic Analysis

As with other analyses in this report, the detailed per operation results based on a few airports were extrapolated to an annual NAS-wide level by accounting for the total number of annual operations at each facility and the frequency of operations expected to benefit from each mechanism. The NAS-wide annual benefits of the four EDA trajectory optimization mechanism are estimated in the rest of this section, following the simple extrapolation of Equation (5.1), as used in other chapters.

$$\textit{Annual Savings} = (\textit{Annual Ops}) \times (\textit{Frequency}) \times (\textit{Savings Per Interrupt}) \qquad (5.1)$$

where: *Annual Ops* = Annual airport operations (00s) (Appendix B)
Frequency = Number of applicable arrivals per 100 daily airport operations
Savings Per Interrupt = Average cost savings per applicable arrival (Table 5.7)

The relaxed metering fix benefit mechanisms were applied to all arrival operations. This reflects the fact that the proposed anchor point concept requires a relaxation of existing metering fix restrictions only available with EDA metering fix delivery accuracy improvement. Conversely, the existing metering fix benefit mechanisms are applied only to rush arrivals. This assumes these mechanisms would have little benefit during non-rush periods, when workload is reduced, allowing controllers to accommodate user-preferred TOD and (en route) routing without EDA.

Rush arrival frequency was estimated for each airport using a simulated DFW rush arrival rate ($\textit{Rush Arrivals}_{DFW}$) [12] adjusted by an *Airport Factor* to account for variations in congestion at each facility, as shown in Equation (5.2). Airports with less overall delays are assumed to meter disproportionately fewer arrival flights to meet airport-scheduling constraints. An individual airport's assumed delayed arrival rate is adjusted from a nominal DFW value from Reference [12], using FAA delay data [31]. These data record delays at each airport in excess of 15 minutes in CY1996, including both arrivals and departures. This metric hides the significant number of smaller delays during an arrival rush period and includes delayed departures, making it a gross indicator of the airport's level of delayed

arrival flights. Despite these limitations, this data provided a reasonable factor for extrapolating the detailed per operation benefits of the five study airports to the 37-NAS airports. To do so, the NAS airports were broken into five delay categories. Engineering judgement was used to assign each category a rush arrival rate relative to the DFW. Simulated rates [12] of 130%, 115%, 100%, 80%, and 60% for airport delay classes 1, 2, 3, 4, and 5 were used. The FAA delay data and criteria used to assign delay categories are included in Appendix B.

$$\text{Frequency} = (\textit{Rush Arrivals}_{DFW}) \times (\textit{Apt Factor}) \qquad (5.2)$$

where: $\textit{Rush Arrivals}_{DFW}$ = DFW number of rush arrivals per 100 daily airport operations [12]
Apt Factor = Factor accounting for local airport rush arrival frequency relative to DFW, based on FAA delay data (Appendix B)

Table 5.7 gives the applicable operation frequency and 5-airport average savings per operation for each EDA Arrival Trajectory Optimization mechanism, assuming a conservative fuel cost of $0.10/lb.

Table 5.7 Five-Airport Average Frequency and Cost Savings

Parameter	TOD Optimization	Arrival Direct Routing	Vertical * Anchor Point	Horizontal Anchor Point
ATL – Atlanta Hartsfield International Airport	$10.72	$1.05	$17.83	$3.26
DFW – Dallas Ft. Worth International Airport	$14.24	$2.31	$5.33	$4.59
LAS – Las Vegas McCarren International Airport	$18.88	$2.29	$5.25	$4.44
LAX – Los Angeles International Airport	$27.00	$3.67	$4.67	$5.20
ORD – Chicago O'Hare International Airport	$19.98	$1.18	$8.84	$0.61
Average Savings Per Applicable Operation	$18.16	$2.10	$7.50	$3.62
Applicable Operations Rate (per 100 Airport ops)	30.4**	30.4**	50.0	50.0

* Assumes VAP 5 nm downstream from existing anchor point location, no benefit in peak hour at DFW and ORD due to delays.
** DFW rush arrival rate from reference [12], airport factor (based on FAA delay data [31]) applied to extrapolate to other airports.

The Table 5.7 results reflect the specific airport runway and airspace configuration at each airport and the expectation that the 3 hours analyzed at each airport is representative of existing conditions. The primary factors affecting the TOD optimization benefit are the frequency of early descents in the Baseline trajectories. Likewise, the BOD location of current trajectories as well as the relative demand of long-side and short-side operations effect the vertical anchor point benefit. Both horizontal anchor point and arrival direct routing benefits depend on the horizontal geometry of the local airport STARs and the current ability of controllers to grant direct route requests. Indeed, ORD showed a very smooth Baseline operation, reaping little benefit from more direct ARTCC (direct routing mechanism) and TRACON (horizontal anchor point mechanism) routing. Differences among the 3-hourly periods studied at each airport is hidden by the airport averages. Little hourly difference was observed in the evaluation of TOD optimization and vertical anchor points. However, implementation of horizontal anchor points and arrival direct routing was diminished by the large volume of delays during rush hours. Vertical anchor point benefits were decreased to account for the delay limitations at DFW and ORD, as reflected in the Table 5.7 VAP average. It should be noted that part of the VAP benefit involves a shift in TOD to merge BOD and existing metering fix location. This portion of the VAP benefits do not require relaxation of existing metering fix restrictions.

Note that the frequencies in Table 5.7 are given per daily *airport* operation, which includes both arrivals and departures. Thus, a rate of 50 per 100 airport operations is assumed to represent all arrival operations. Since the existing metering fix restriction TOD optimization

and arrival direct routing mechanisms were applied only to rush arrivals, their rate is less than the other mechanisms, as discussed above.

The annual airport operations [36] and savings for 37 NAS airports are shown in Table 5.8. The annual savings are also plotted graphically by airport in Figure 5.11. The combined savings range from $1.5M to nearly $11.5M per year, at BDL and ORD, respectively, with a total annual benefit of almost $173M. Large hub airports showed the most promise, particularly ORD, DFW, ATL, and LAX. The greatest benefit came from EDA TOD optimization under existing metering fix restrictions, followed by the EDA mechanisms that relaxed the metering fix restrictions (Vertical/Horizontal Anchor Point concept). Approximately half of the total trajectory optimization benefits accrue under existing metering fix restrictions. Shifting flights to idle-thrust descent profiles, under EDA TOD optimization saved the gamut (44 percent overall), with the arrival direct routing benefits saved just 5 percent of the overall benefits. The high TOD optimization benefits are first-cut estimates, given the simple fuelburn extrapolation method and nominal speed assumptions. The second half of the total benefit is attributed to the relaxation of metering fix restrictions, with two thirds of that due to the VAP, despite the conservative 5 nm VAP location. More benefit would be expected if the VAP could be moved further into the TRACON. Again, this anchor point concept is made possible because EDA metering advisories result in accurate TRACON delivery/merging that reduces the need for conservative TRACON entry restrictions in use today.

Table 5.8 EDA Trajectory Optimization Benefits

Airport	Annual Airport Ops (000s)	Apt Delay Delays/Category		Rush Arrival Rate (/100 Ops)	Annual Savings ($M, 1998) TOD Optimization	Arrival Direct Routing	Vertical * Anchor Point	Horizontal Anchor Point
Atlanta (ATL)	773	23.88	3	30.4	4.26	0.49	2.90	1.40
Nashville (BNA)	226	1.36	5	18.2	0.53	0.06	0.60	0.29
Boston (BOS)	463	0.73	2	18.2	0.75	0.09	0.85	0.41
Bradley (BDL)	161	26.37	5	34.9	2.93	0.34	1.73	0.84
Baltimore (BWI)	270	3.67	5	18.2	0.89	0.10	1.01	0.49
Cleveland (CLE)	291	4.68	5	18.2	0.96	0.11	1.09	0.53
Charlotte (CLT)	457	6.55	4	24.3	2.02	0.23	1.71	0.83
Cincinnati (CVG)	394	10.38	4	24.3	1.74	0.20	1.47	0.71
Washington National (DCA)	310	6.53	4	24.3	1.37	0.16	1.16	0.56
Denver (DEN)	454	1.90	5	18.2	1.50	0.17	1.70	0.82
Dallas – Ft. Worth (DFW)	870	19.59	3	30.4	4.80	0.55	3.26	1.57
Detroit (DTW)	531	9.10	4	24.3	2.34	0.27	1.99	0.96
Newark (EWR)	443	65.25	1	39.5	3.18	0.37	1.66	0.80
Ft. Lauderdale (FLL)	236	1.53	5	18.2	0.78	0.09	0.89	0.43
Houston Hobby (HOU)	252	2.57	5	18.2	0.83	0.10	0.95	0.46
Washington Dulles (IAD)	330	6.81	4	24.3	1.46	0.17	1.24	0.60
Houston – Intercontinental (IAH)	392	11.45	4	24.3	1.73	0.20	1.47	0.71
N.Y. Kennedy (JFK)	361	29.53	2	34.9	2.29	0.26	1.35	0.65
Las Vegas (LAS)	480	3.68	5	18.2	1.59	0.18	1.80	0.87
Los Angeles (LAX)	764	24.13	3	30.4	4.21	0.49	2.86	1.38
N.Y. LaGuardia (LGA)	343	46.22	1	39.5	2.46	0.28	1.28	0.62
Orlando (MCO)	342	4.59	5	18.2	1.13	0.13	1.28	0.62
Chicago Midway (MDW)	254	6.70	4	24.3	1.12	0.13	0.95	0.46
Memphis (MEM)	364	NA	5	18.2	1.20	0.14	1.36	0.66
Miami (MIA)	546	6.79	4	24.3	2.41	0.28	2.05	0.99
Minneapolis (MSP)	484	9.29	4	24.3	2.13	0.25	1.81	0.88
Oakland (OAK)	516	NA	5	18.2	1.71	0.20	1.94	0.93
Chicago O'Hare (ORD)	909	34.46	2	34.9	5.76	0.67	3.41	1.65
Portland (PDX)	306	2.41	5	18.2	1.01	0.12	1.15	0.55
Philadelphia (PHL)	406	17.95	3	30.4	2.24	0.26	1.52	0.74
Phoenix (PHX)	544	7.25	4	24.3	2.40	0.28	2.04	0.99
Pittsburgh (PIT)	447	6.60	4	24.3	1.97	0.23	1.68	0.81
San Diego (SAN)	244	3.31	5	18.2	0.81	0.09	0.91	0.44
Seattle (SEA)	398	6.37	4	24.3	1.75	0.20	1.49	0.72
San Francisco (SFO)	442	56.57	1	39.5	3.17	0.37	1.66	0.80
Salt Lake City (SLC)	374	3.53	5	18.2	1.24	0.14	1.40	0.68
St. Louis (STL)	517	34.04	2	34.9	3.28	0.38	1.94	0.94
37-Airport Total/Average	430	---	---	---	75.95	8.78	59.57	28.77

* Assumes VAP 5 nm downstream from existing anchor point locations.

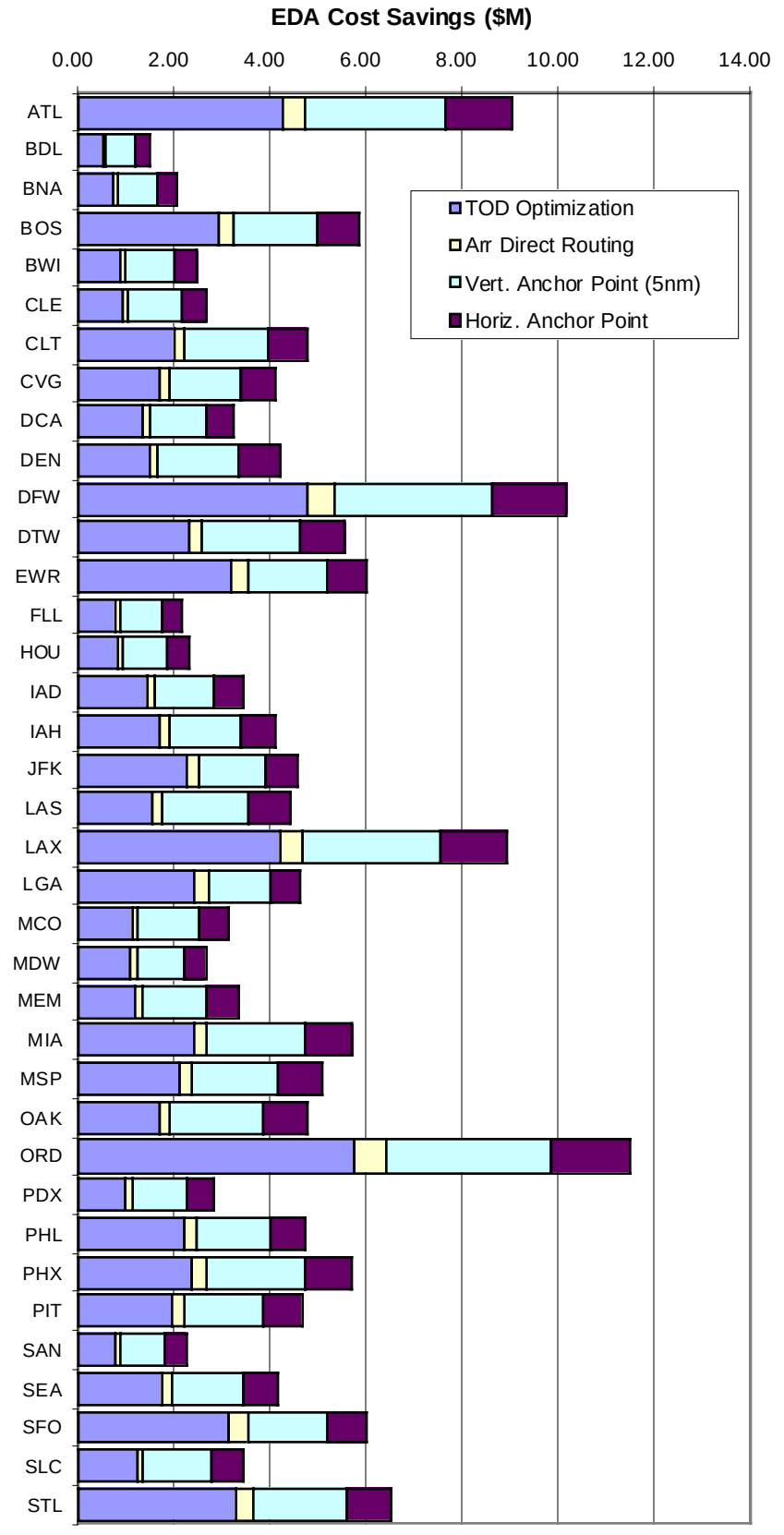

Figure 5.11 EDA Trajectory Optimization Benefits

Results Summary

This chapter evaluated EDA trajectory optimization benefits. Near-term optimization maintains existing arrival metering fix restrictions, while the far-term anchor point concept allows relaxing these restrictions on a per flight basis.

In the near-term, EDA maneuver advisories will enable the latest TOD and most direct horizontal route to the arrival metering fix. For these near-term mechanisms, EDA was found to shift the TOD an average of 20-40 nm downstream and shorten the path length by 2 nm, saving a total of 202 lbs or $20.26 per operation, for a total savings of $84.73M annually assuming NAS-wide deployment at 37-airports. Most of these benefits ($76M) result from improved TOD optimization. Due to limitations in the analysis method, further study is recommended to validate the TOD optimization findings, in particular.

For the relaxed metering fix restriction (anchor point) concept, EDA maneuver advisories provide conflict-free arrival trajectories that shift the BOD (vertical anchor point) downstream into the TRACON, while allowing the aircraft to cross the Center/TRACON boundary (horizontal anchor point) at a location in line with downstream runways. For these mechanisms, EDA was assumed to shift the BOD 5 nm downstream and horizontal routing was found to shorten by 3 nm, saving a total of 111 lbs or $11.12 per operation, for a total savings of $88.34M annually assuming NAS-wide deployment at 37-airports. Two-thirds of these relaxed metering fix benefits result from the vertical anchor point mechanism, despite the conservative 5 nm VAP shift.

These benefit estimates assume the three hours studied at each of five study airports is representative of the applicability of trajectory optimization mechanisms at these airports, and typical of other NAS airports. Additional benefits reflect only fuel savings. Potential time savings, due to horizontal path shortening in non-rush periods, was not evaluated. The TOD optimization results reflect a first-cut estimate employing a single aircraft fuelburn estimate, extrapolated fleet-wide, and assumed nominal descent speeds. The TOD results and assumptions should be validated with further study. The analysis of relaxed metering fix (anchor point) concept also assumes significant procedural changes for TRACON entry. The resulting benefits rely on the validation of the EDA tool to gain controller acceptance of such changes. Direct routing and horizontal anchor point benefits also reflect current STAR and ATM-granted direct routings at the study airports, extrapolated NAS-wide. Vertical optimization benefits reflect the ability of ATM to optimize TOD location under current operations at the five study airports. Additional benefits due to time savings tied to horizontal path shortening could also be evaluated.

Further investigation into specific airspace constraints may also reveal factors that would limit the use of these mechanisms. User-preferred optimal trajectories may be blocked by airspace restrictions such as noise-abatement procedures, Special Use Airspace (SUA), and Center and TRACON crossing traffic. Indeed, since the objective of the anchor point concept is to move the merge point downstream into the TRACON, the data must be examined for potentially conflicting traffic inside the TRACON. Since these factors were not taken into account and may attenuate these results, further study is recommended to assess the impact of specific airspace restrictions at the 37 high-density NAS airports. Other factors taken into account at the five study airports, which may differ at other NAS airports include the ability of each mechanisms to impact rush/non-rush operations, and the proportion of short and long side arrivals.

Finally, as shown here, a primary goal of the EDA tool is to dynamically solve separation and metering problems in high-density arrival airspace and thereby relax procedural/route

restrictions that prevent users from operations on their preferred trajectory. EDA accuracy may allow other existing arrival restrictions to be relaxed.

6. Conclusions/Recommendations

This report identifies the potential benefits of various EDA benefit mechanisms relative to common FFP1 Baseline assumptions. As noted earlier, these analyses are summarized and extended from a number of previous efforts, which involve many assumptions, varying levels of analysis fidelity, and very limited technical and operational assessment using field data. Key findings of the individual EDA benefit mechanism including analysis assumptions and limitations are discussed, followed by specific recommendations for improving the analyses. Other recommendations can be found in the respective reference reports of each chapter.

Conclusions

Airport Throughput

Reduced runway threshold separations (in excess of minimums) are expected from EDA as a result of improved arrival metering fix delivery accuracy. The reduced variance in arrival metering fix crossing times leads to reduced runway gaps with associated airport throughput increases and aircraft delay and delay propagation reduction, especially during rush periods.

It was found that EDA saved an average 1-2 seconds of delay or $2.35 per operation (time and fuel), for a total NAS-wide deployment at 37-airports of 445 hours and $42.93M annually. These benefits reflect a reduction in the average runway threshold excess spacing buffer relative to a FFP1 Baseline, which includes TMA and pFAST. With no CTAS improvements, the average buffer was found to be approximately 31 seconds [32]. Thus, a rough indication of the relative benefits of EDA, TMA, and pFAST operations can be made by noting the airport delay savings in Figure 1.4 associated with the approximated 1-2 second TMA buffer improvement, 4 second pFAST improvement, and this study's 0.65 second EDA improvement.

It should also be noted that this analysis, an update of previous studies, was limited by the use of a runway demand and capacity modeling tool (AIRNET) which does not account for airspace constraints and subtleties of arrival scheduling embedded in proposed ATM DSTs. To address these limitations, Seagull has initiated development of a higher fidelity model, the Integrated Air Traffic (IAT) Model, which has been used in recent benefits assessments for TMA [33]. Additionally, there is some concern regarding the underlying schedule used to model LGA. Because of the high demand, delays are unable to be dissipated, building up without break over the full day. As a result, any improvement to LGA runway separation leads to significant savings. It is recommended that the IAT model be applied to refine these airport throughput benefits and the LGA flight schedule be updated to reflect existing activity.

Center/TRACON Delay Distribution

Reduced variance in EDA arrival metering fix delivery accuracy results in arrival flight efficiency benefits due to the ability to absorb more efficiently upstream in Center airspace while still maintaining a given TRACON entry rate.

It was found that EDA shifted an average of 138 seconds of rush arrival delay from TRACON to Center airspace. This saved 114 lbs of fuel or $11.42 per rush arrival ($939 per average rush), with a total savings of $47.73M annually assuming NAS-wide deployment at 37-airports. This EDA benefit mechanism is used to model the general shift of delay from TRACON to Center airspace. EDA metering conformance efficiency,

discussed in the next chapter, addresses more specifically the EDA efficiency of Center delay absorption, a separate advantage of EDA operations over TMA alone.

The EDA benefits were evaluated relative to a FFP1 Baseline, which includes TMA. The arrival metering fix delivery accuracy (1-sigma) was found to be approximately 180 seconds prior to TMA and 90 seconds with TMA [30]. EDA field tests found an accuracy of 15-20 seconds [10], modeled here as 17.9 seconds (Table 1.2). Using these values, a rough indication of the relative Center/TRACON delay distribution benefits of EDA and TMA can be made by using Figure 2.2. Note that for the FFP1/TMA Baseline, the maximum delay absorption capability of a route (typically 100-300 seconds) would likely require a TRACON delay setting below optimal. Thus, despite TMA's significant improvement in metering fix delivery accuracy, little change would occur in the TRACON delay setting, allowing only limited shifting of delay to more fuel-efficient ARTCC airspace, with associated limited benefits. Post-TMA, improvements to the metering fix accuracy, such as with EDA, enables a reduction in TRACON delay along the optimal line, resulting in significantly higher benefits per metering fix accuracy improvement.

To achieve these benefits, it is assumed that TRACON traffic managers would be comfortable in shifting delay upstream (i.e., less TRACON front-loading) with the more accurate metering fix delivery schedule adherence of these DSTs. Additionally, the study would benefit from a better understanding of the controllability window (minimum/maximum TRACON delay setting) of various TRACON arrival routes at various ATM facilities. Another key assumption driving these estimates is that aircraft fuelburn rates for absorbing delay are 1.5 times larger in TRACON relative to ARTCC airspace. This assumption should be calibrated with field data, and may differ under Baseline and EDA metering conformance delay strategies. Alternatively, higher fidelity aircraft trajectory and fleet mix models could be employed to improve fuelburn estimates.

Metering Conformance Efficiency

EDA maneuver advisories assist controllers in formulating and executing a traffic delay strategy to meet arrival metering fix crossing schedule. EDA allows controllers to quickly and accurately assess the impact of various delay strategies, and more effectively use fuel-efficient strategies, such as speed control, resulting in lower cost metering conformance interruptions.

It was found that EDA saved an average of 59 lbs and 2.6 seconds or $6.80 per arrival metering conformance interruption, for total savings of $25.09M annually assuming NAS-wide deployment at 37-airports. This fuel efficiency benefit was slightly increased under arrival direct routing over conventional STAR routing. In addition, the EDA metering conformance procedures are more strategic and require less overall workload (fewer downstream controller corrections to conform to metering times) than the FFP1 Baseline.

These benefit estimates are sensitive to the amount of metering delay per flight. A typical DFW day was analyzed with per operation savings extrapolated to other airports. Although some adjustment was made for the number of metered arrival flights at each airport, no adjustment was made in the per operation savings. If airport have smaller per operation delays, EDA may result in larger per operation savings because current vectoring operations can be fully replaced with EDA speed/altitude maneuvers. Thus, NAS-wide EDA benefit estimates would improve with evaluation of detailed simulations at additional airports.

Separation Assurance

ATM relies on accurate predictions of flight trajectories within its conflict probe tool to accurately identify the location and nature of pending separation assurance violations. With more accurate EDA arrival trajectory predictions (EDA advisories and updated intent), ATM

perception errors (false and missed alerts) would be reduced, resulting in fewer ATM flight interventions and associated resolution fuel penalties. Additionally, improved traffic conflict prediction will include more accurate estimation of conflict geometry and speeds, leading to more efficient resolution maneuvers.

It was found that EDA reduced separation assurance interruptions by 5 percent with each interruption savings an average of 0.8 lbs or $0.08, for total savings of $2.80M annually assuming NAS-wide deployment at 37-airports. More significantly, the EDA separation assurance conflicts required less overall workload primarily because of the integration with metering conformance flight intent, reducing the number of missed and false alerts by 30 and 21 percent, respectively. As a result, EDA enhances overall safety, enables strategic controller planning across multiple sectors, and reduces nuisance conflict alerts.

These benefit estimates are sensitive to ARTCC traffic routing complexity. A typical day of ZFW Center activity was analyzed with interrupt rates and per operation savings extrapolated to other airports. The NAS-wide EDA benefit estimates would be enhanced with more comprehensive evaluation of the en route traffic routing of various facilities.

Trajectory Optimization

This chapter evaluated EDA trajectory optimization benefits. Near-term optimization maintains existing arrival metering fix restrictions, while the far-term anchor point concept allows relaxing these restrictions on a per flight basis.

In the near-term, EDA maneuver advisories will enable the latest TOD and most direct horizontal route to the arrival metering fix. For these near-term mechanisms, EDA was found to shift the TOD an average of 20-40 nm downstream and shorten the path length by 2 nm, saving a total of 202 lbs or $20.26 per operation, for a total savings of $84.73M annually assuming NAS-wide deployment at 37-airports. Most of these benefits ($76M) result from improved TOD optimization. Due to limitations in the analysis method, further study is recommended to validate the TOD optimization findings, in particular.

For the relaxed metering fix restriction (anchor point) concept, EDA maneuver advisories provide conflict-free arrival trajectories that shift the BOD (vertical anchor point) downstream into the TRACON, while allowing the aircraft to cross the Center/TRACON boundary (horizontal anchor point) at a location in line with downstream runways. For these mechanisms, EDA was assumed to shift the BOD 5 nm downstream and horizontal routing was found to shorten by 3 nm, saving a total of 111 lbs or $11.12 per operation, for a total savings of $88.34M annually assuming NAS-wide deployment at 37-airports. Two-thirds of these relaxed metering fix benefits result from the vertical anchor point mechanism, despite the conservative 5 nm VAP shift.

These benefit estimates assume the three hours studied at each of five study airports is representative of the applicability of trajectory optimization mechanisms at these airports, and typical of other NAS airports. Additional benefits reflect only fuel savings. Potential time savings, due to horizontal path shortening in non-rush periods, was not evaluated. The TOD optimization results reflect a first-cut estimate employing a single aircraft fuelburn estimate, extrapolated fleet-wide, and assumed nominal descent speeds. The TOD results and assumptions should be validated with further study. The analysis of relaxed metering fix (anchor point) concept also assumes significant procedural changes for TRACON entry. The resulting benefits rely on the validation of the EDA tool to gain controller acceptance of such changes. Direct routing and horizontal anchor point benefits also reflect current STAR and ATM-granted direct routings at the study airports, extrapolated NAS-wide. Vertical optimization benefits reflect the ability of ATM to optimize TOD location under current operations at the five study airports. Additional benefits due to time savings tied to horizontal path shortening could also be evaluated.

Further investigation into specific airspace constraints may also reveal factors that would limit the use of these mechanisms. User-preferred optimal trajectories may be blocked by airspace restrictions such as noise-abatement procedures, Special Use Airspace (SUA), and Center and TRACON crossing traffic. Indeed, since the objective of the anchor point concept is to move the merge point downstream into the TRACON, the data must be examined for potentially conflicting traffic inside the TRACON. Since these factors were not taken into account and may attenuate these results, further study is recommended to assess the impact of specific airspace restrictions at the 37 high-density NAS airports. Other factors taken into account at the five study airports, which may differ at other NAS airports include the ability of each mechanisms to impact rush/non-rush operations, and the proportion of short and long side arrivals.

Finally, as shown here, a primary goal of the EDA tool is to dynamically solve separation and metering problems in high-density arrival airspace and thereby relax procedural/route restrictions that prevent users from operations on their preferred trajectory. EDA accuracy may allow other existing arrival restrictions to be relaxed.

General

The NAS extrapolation of EDA benefits estimated at a single airport (or limited number of airports), frequently requires the identification of other airport's rush arrival operations. This analysis assumed a simplified categorization of airports based on FAA delay data. The limitations of this method, and high-sensitivity of the overall EDA benefits to this assumption, calls for a more defendable metric. It is recommended that in future benefit analyses, the traffic patterns of individual airports be modeled and rush arrival estimates for these airports be used directly.

Recommendations

The following recommendations are made relative to future studies to refine the results of this work.

- **Expand Modeling Conditions and Calibrate Baseline with Field Data** - The analyses in this report relies on detailed study at a limited set of airports, applying the applicability and per operation savings found at these airport facilities to estimate NAS-wide benefits. The NAS-wide estimates would clearly benefit from detailed study at more airports reflecting the range of airport-specific characteristics and constraints and their impact on applicability and per operation savings. Additionally, field data, such as that being collected by the FFP1 program office, could also be employed to calibrate the baseline case to match observed ATM performance, including the number and amount of rush arrival delays.

- **Continue to Develop and Employ Higher-Fidelity Scheduling Models** – The EDA airport throughput analysis applies a different modeling approach than has been used for assessing other EDA benefit mechanisms and evaluating other DST improvements. Since the original throughput studies were conducted, as summarized in this report (Chapter 1). Seagull initiated development of a higher-fidelity Integrated Air Traffic (IAT) Model. IAT addresses some of the limitations of the runway capacity model that was employed in the previous work (i.e. AIRNET). Additionally, the IAT model is set up to produce more refined Center/ TRACON Delay Distribution benefit assessments, and integrate them synergistically with the airport throughput mechanism. It is recommended that the IAT Model be completed to enable more accurate benefit assessments.

- **Combine Center/TRACON Delay Distribution and Metering Conformance Analyses** - Delay distribution changes the metered arrival time at the MF, forcing more delay in the ARTCC, less in the TRACON. Metering conformance ATM interruptions reflects the flight maneuvers made to conform to the arrival metering fix crossing time. It would be desirable to combine these in the future, in order to capture synergies/overlap and to check the assumed ARTCC/TRACON fuel consumption differential.

- **Enhance ATM Interruptions Model –** The ATM Interruptions Model (AIM) used to evaluate metering conformance and separation assurance benefits could be enhanced to improve benefit estimates. In the metering conformance modeling, this includes:

  (i) modifying the metered trajectories to include vectoring turn back error and TOD shift with descent speed changes;

  (ii) improved fuelburn models and parameters such as best endurance speeds;

  (iii) linking delay strategy errors with metering fix delivery error, to allow modeling of data exchange improvements;

  (iv) include the impact of arrival fix delivery errors on inefficient metering fix throughput.

  In the separation assurance interruptions modeling, suggested improvements include:

  (i) enhance conflict resolution strategies to including speed and altitude resolutions, as well as appropriate time benefit;

  (ii) improved off-flight plan inaccurate route intent modeling approach, to reflect aircraft-specific flight changes and the possibility of missed alerts resulting from the off-flight plan routing.

- **Improve Trajectory Optimization Analyses** – The trajectory optimization analyses used simplified methods to assess potential EDA benefits. The TOD optimization descent fuelburn model would benefit from high-fidelity simulation of *several* aircraft and knowledge of actual descent speeds, for more accurate fleet-wide benefits. Additionally, the overall approach, particularly the far-term anchor point concept, could be enhanced by addressing metered/non-metered arrival flight applicability, effect of ATM interruptions (possibly using higher fidelity IAT and/or AIM models), and more detailed analyses of actual aircraft-specific changes. Additionally, reduced flight time benefits and the extension of the trajectory optimization mechanisms to departure operations could be evaluated.

- **Upgrade Trajectory Prediction Accuracy Parameters and Models** – The assumptions made regarding trajectory prediction accuracy models and contributing errors should be continually updated with better trajectory geometry models (especially climbs), more routes/airports, and on-going field test results.

- **Analyze Other Traffic Scenarios** – The analyses in this report typically assumed a baseline 1996 traffic scenario for detailed per operation savings at a few airports and extrapolated these detailed results to 1996 annual/NAS-wide levels. Traffic scenarios from a day with higher operations could results in changes in per operation savings, reflecting changes in metering delays, as well as altering the number of applicable operations (e.g. increased arrival operations).

- **Sensitivity Analysis** - A sensitivity analyses of each of the results to key assumptions regarding DST technology improvements and trajectory accuracy parameters used in each of the studies could determine which parameters are most important to realizing the estimated EDA benefits and to set objectives in regard to EDA trajectory prediction accuracies.

- **Controller Benefits –**EDA controller benefits have not been quantitatively addressed. The assessment of controller benefits would require a high-fidelity simulation to show controller productivity gains and a human factors simulation to identify workload savings. Indeed, the most significant controller benefits may accrue when the system is able to achieve a threshold level of accuracy and controller

productivity, under EDA arrival accuracy and its shift to a more strategic trajectory orientation, that enables the relaxation of numerous airspace restrictions and facilitates the accommodation of user-preferred trajectories.

Acronyms

AATT	NASA's Advanced Air Transportation Technologies program
ACS	Acceptable Controller Spacing
ADL	FAA's Aeronautical Data Link Product Team
AFAST	CTAS Active Final Approach Spacing Tool
AOC	Airline Operational Control
ARR	Arrival Operation
ARTCC	Air Route Traffic Control Center
ARTS	Automated Radar Terminal System
ATL	Atlanta Hartsfield International Airport
ATM	Air Traffic Management
BADA	Eurocontrol Base of Aircraft Data
BDL	Bradley International Airport
BNA	Nashville International Airport
BOD	Bottom of Descent
BOS	Boston Logan International Airport
BWI	Baltimore-Washington International Airport
CA	Conflict Probe Correct Alert
CAS	Calibrated Airspeed
Center	Air Route Traffic Control Center (ARTCC)
cl	Climb flight mode
CLE	Cleveland Hopkins International Airport
CLT	Charlotte-Douglas International Airport
CPDLC	Controller-Pilot Data Link Communication
cr	Cruise flight mode
CTAS	Center/TRACON Automation System
CVG	Cincinnati/Northern Kentucky International Airport
d	Descent flight mode
D2	CTAS Direct-To Tool
DCA	Washington National Airport
DEN	Denver International Airport
DEP	Departure Operation
DFW	Dallas-Ft. Worth International Airport
DIR	Direct Routing
DST	Decision Support Tool

DTW	Detroit Metro Wayne County International Airport
EDA	CTAS En Route/Descent Advisor
EDX	En Route Data Exchange
ETMS	Enhanced Traffic Management System
EWR	Newark International Airport
FA	Conflict Probe False Alert
FAA	Federal Aviation Administration
FANG	FMS-ATM Next Generation
FAR	Federal Aviation Regulations
FLL	Ft. Lauderdale-Hollywood International Airport
FFP1	FAA's Free Flight Phase 1 Program
FMS	Flight Management System
FSF	Fuel Scale Factors
ft	feet
HSC	ARTCC Host System Computer
HOU	Houston Hobby International Airport
IAD	Washington Dulles International Airport
IAH	Houston–Intercontinental Airport
IAT	Integrated Air Traffic Model
IFR	Instrument Flight Rules
IMC	Instrument Meteorological Conditions
ITWS	Integrated Terminal Weather Service
JFK	N.Y. Kennedy International Airport
kt	knot, nautical mile per hour
LAS	Las Vegas McCarran International Airport
LAX	Los Angeles International Airport
LGA	N.Y. LaGuardia Airport
LNAV	Lateral Navigation
MA	Conflict Probe Missed Alert
MCO	Orlando International Airport
MDW	Chicago Midway Airport
MEM	Memphis International Airport
MF	Metering Fix
MIA	Miami International Airport
MSP	Minneapolis-St. Paul International Airport
NAS	National Airspace System

NASA	National Aeronautics and Space Administration
NOAA	National Oceanic and Atmospheric Administration
OAK	Oakland International Airport
OM	Outer Marker
ORD	Chicago O'Hare International Airport
OVR	Overflight Operation
PAZ	Protected Airspace Zone
PCA	Point of Closest Approach
PDX	Portland International Airport
pFAST	CTAS Passive-Final Approach Spacing Tool
PHL	Philadelphia International Airport
PHX	Phoenix Sky Harbor International Airport
PIT	Greater Pittsburgh International Airport
RTA	Required Time of Arrival
rss	Root-Sum-Squared
RUC	Rapid Update Cycle
SAN	San Diego International Airport
SEA	Seattle–Tacoma International Airport
SFO	San Francisco International Airport
SID	Standard Instrument Departure
SLC	Salt Lake City International Airport
SRC	System Resources Corporation
STA	Scheduled Time of Arrival
STAR	Standard Terminal Arrival
STL	St. Louis-Lambert International Airport
TH	Runway Threshold
TMA	CTAS Traffic Management Advisor
TOD	Top of Descent
TRACON	Terminal Radar Approach Control
TS	CTAS Trajectory Synthesizer
TW	ITWS Terminal Winds Program
URET CCLD	User-Request Evaluation Tool, Core Capabilities Limited Deployment
VFR	Visual Flight Rules
VMC	Visual Meteorological Conditions
VNAV	Vertical Navigation
Wx	Weather

ZAB	Albuquerque, NM ARTCC
ZAU	Chicago, IL ARTCC
ZBW	Nashau, NH ARTCC
ZDC	Leesburg, VA ARTCC
ZDV	Denver, CO ARTCC
ZFW	Ft.Worth, TX ARTCC
ZHU	Houston, TX ARTCC
ZID	Indianapolis, IN ARTCC
ZJX	Jacksonville, FL ARTCC
ZKC	Kansas City, KS ARTCC
ZLA	Los Angeles, CA ARTCC
ZLC	Salt Lake City, UT ARTCC
ZMA	Miami, FL ARTCC
ZME	Memphis, TN ARTCC
ZMP	Minneapolis, MN ARTCC
ZNY	New York, NY ARTCC
ZOA	Oakland, CA ARTCC
ZOB	Cleveland, OH ARTCC
ZSE	Seattle, WA ARTCC
ZTL	Atlanta, GA ARTCC

Appendix A Trajectory Prediction Accuracy

Trajectory Prediction Accuracy is defined as the accuracy of a flight trajectory predicted at a specific future location or set time horizon. This can be specified either in terms of (a) position uncertainty at a fixed future time point; or (b) timing uncertainty as to when the aircraft crosses a future range or altitude point.

In Chapter 1, the Airport Throughput Benefits used timing uncertainty of the arrival descent trajectory culminating at the arrival metering fix. This is used, in turn, to estimate downstream runway threshold separations. In Chapter 2, the Center/TRACON delay distribution benefits analysis also employs estimated arrival metering fix delivery timing accuracy to define the amount of delay that can be shifted and absorbed in upstream ARTCC airspace. In Chapter 4, the Separation Assurance ATM Interruptions benefits analysis incorporates 12-minute trajectory prediction accuracy of all flight modes (arrival, departure, over-flight), representing ATM conflict probe accuracy. Here, the assumption is that the conflict probe is looking ahead to where the aircraft will be 12 minutes into the future. In Chapter 4, the values of trajectory prediction accuracy are used to derive other ATM perception attributes, including acceptable controller spacing, perceived miss distance and probability of conflict.

This appendix derives the various trajectory prediction accuracy estimates used in these report chapters. Reference [12] includes more detail on the trajectory accuracy parameter assumptions and modeling.

Calculation of Timing Error at the End of Climb or Descent Flight Segments

We begin by defining the quantitative expression for the timing error ($\sigma_{t,M}$) for climb and descent flight segments. That is the uncertainty in timing of the trajectory crossing a certain point at the end of a climb or descent phase of flight. The variance of the climb/descent maneuver timing error was modeled using the following equation:

$$\sigma_{t,M} = \sqrt{\sum_{\forall i} A_i^2 \sigma_i^2} \qquad \text{(A.1)}$$

Where: $\sigma_{t,M}$ = Total time delay error uncertainty (e.g., metering fix crossing time error)
A_i = Sensitivity of timing error to the error in parameter *i* (e.g., surveillance error)
σ_i = Set of 10 parameters defining the progress, or characteristics, of a trajectory that are subject to error

Baseline estimates of the 10 A_i coefficients for the corresponding 10 contributing error parameters are summarized in Table A.1 for the climb and descent flight segments. Descent coefficients were based on high-fidelity aircraft simulation results, while climb coefficients reflect individual parameter sensitivities using a CTAS stand-alone system with field data. For several parameters, climb sensitivities were unknown or unmeasurable from the field data taken. In these cases (as noted in the table), the descent coefficient values were also used for climbs, as a first-cut approximation.

Table A.1 Climb and Descent Model Sensitivity Coefficients

Flight Phase Timing Error Sensitivity Coefficients			
Parameter	Units	Climb	Descent
Initial Weight	sec/%	24.2	0.88
(Thrust – Drag)	sec/%	4.08*	1.39
TOD Placement	sec/nm	N/A	4.08
Speed. Adherence	sec/kt	11.1*	1.46
X-Track Wander	sec/nm	1.77**	1.77
Aircraft Navigation Bias	sec/deg	1.94**	1.94
Turn Dynamics	sec/sec	1.11**	1.11
Wind Forecast	sec/kt	3.7*	0.95
Temperature Forecast	sec/^{o}C	8.7*	4.62
Surveillance	sec/kt	0.26**	0.26

* Path distance errors at TOC converted to time error based on speed of 415 kts at TOC
** Climb coefficients set equal to descent coefficients, due to lack of climb data.

Table A.2 presents the contributing error parameter values required to calculate ATM trajectory prediction timing accuracy using Equations (A.1). The error statistics in Table A.2 are presented in the form of a root-sum-square (rss) error. Reference [12] provides supporting detail on the component mean and standard deviation (σ) of the error used to derive the rss for each parameter and ATM DST technology case. Here, values are presented for the FFP1 Baseline and the EDA cases. These values draw extensively from the literature, current research, and supplemented by discussions with NASA conflict probe experts to quantitatively differentiate the various proposed technology cases by flight mode. In all cases, these error parameter values assume jet aircraft with an onboard FMS flight control (LNAV and VNAV) in the en route airspace.

A key Baseline limitation in predicting climb and descent timing is the lack of common ATM-aircraft knowledge of speed profile and top of climb/descent location. This leads to large errors in speed adherence and estimated TOD placement. These errors are reduced for metered descents with the EDA-calculated maneuver advisories, where the pilot is expected to be targeting the controller-cleared EDA descent advisory. The EDA improvement is reflected in the two shaded cells in Table A.2.

Table A.2 Assumed Trajectory Prediction Contributing Error Values

		Prediction Error (1-sigma, Jet with FMS)					
		FFP1 Baseline			EDA		
Parameter	Units	Cl	Cr	D	Cl	Cr	D
Initial Weight	%	9.2	N/A	7.8	9.2	N/A	7.8
(Thrust – Drag)	%	5.9	N/A	5.9	5.9	N/A	5.9
TOD Placement	nm	N/A	N/A	20	N/A	N/A	0.25
Speed Adherence(($\sigma_{V,FTE}$)	kt	15	15	15	15	15	4.0
X-Track Wander	nm	0.14	N/A	0.14	0.14	N/A	0.14
AC Navigation Bias	deg.	0.15	N/A	0.15	0.15	N/A	0.15
Turn Dynamics	Sec	2.3	N/A	2.3	2.3	N/A	2.3
Wind Forecast ($\sigma_{V,W}$)	kt	12.0	13.4	12.0	12.0	13.4	12.0
Temperature Forecast	°C	1.0	N/A	1.0	1.0	N/A	1.0
Surveillance-Speed ($\sigma_{V,S}$)	kt	13.1	12.5	13.1	13.1	12.5	13.1
Surveillance-Position	nm	N/A	0.87	N/A	N/A	0.87	N/A

Key Error Sources/References:

Initial Weight – Baseline root-sum-squar (rss) of airline fleet data [46].
Thrust - Drag – Baseline rss of NASA TSRV test results [47].
TOD Placement – Baseline CTAS-FMS mismatch, EDA FMS typical RNAV error rss of 0.25 nm.
Speed Adherence – Baseline CTAS-FMS mismatch & FTE, EDA improves arrival target [47].
X-Track Wander – Baseline rss [10].
AC Navigation Error – Baseline FMS GPS/INS Guidance system error of 0.15 degrees.
Turn Dynamics – Baseline FMS-guided rss error [48].
Wind Forecast – Baseline RUC 3-hour forecast [49].
Temperature Forecast – Baseline RUC 3-hour forecast [50].
Radar Surveillance – Baseline along-track position and ground speed error of Secondary Surveillance Radar [47].

Calculation of Position Error at the End of Climb, Cruise or Descent Flight Segments

We next define a quantitative expression for trajectory position prediction accuracy at the ends of climb, cruise and descent phases of flight. Here it is assumed that the climb phase ends with a cruise segment, the descent phase begins with a cruise segment, and the cruise phase is at a constant altitude. In each case, a fixed time horizon is used to define the end point of the particular phase.

A convenient mathematical model for determining the along-track position error of a single aircraft at a certain time point into the future can be described by the following equation:

$$\sigma_{P,Pred}(\tau) = \sqrt{\sigma_P^2 + \tau^2 \sigma_V^2} \qquad \text{(A.2)}$$

Where: $\sigma_{P,Pred}$ = Predicted trajectory position error
σ_P, σ_V = Position and velocity error terms
τ = Time period of flight cruise segment subject to velocity errors

The first variance term in Equation (A.2) represents either the initial or intermediate position error contribution of the trajectory. For a climb trajectory consisting of a climb segment followed by a cruise segment, it represents the position error at the end (top) of the climb segment. For a descent trajectory consisting of cruise and descent segments, it represents the contribution to position error due to the descent segment alone (i.e., at the end of the descent segment.) Thus, this position error term is directly related to the climb or descent timing error described previously by Equation (A.1) for those trajectories that have climb or descent segments. That is, if we use some average trajectory ground speed V_M, then:

$$\sigma_P = \sqrt{\sigma_{t,M}^2 V_M^2} \qquad \text{(A.3)}$$

Where: V_M = Average velocity during the climb or descent segment

In this study, an average climb or descent ground speed of 350 kts was used. This is the rough average of arrival/departure meter fix crossing speed of 280 kts and TOD/TOC speed of 415 kts.

For a cruise trajectory, the first term in Equation (A.2) represents the uncertainty in position of the aircraft at the beginning of that trajectory. This is simply the error in the surveillance system position measurement at that time.

In Equation (A.2), σ_V represents the velocity-related error contribution that accrues during the cruise segment of the trajectory with a particular time horizon. This term is expanded as:

$$\sigma_v = \sqrt{\sigma_{V,S}^2 + \sigma_{V,W}^2 + \sigma_{V,FTE}^2} \qquad \text{(A.4)}$$

Where: $\sigma_{V,S,}$ $\sigma_{V,W}$, $\sigma_{V,FTE}$ = Surveillance, wind, and speed adherence error terms from Table A.2.

Time Horizon and τ for Climb, Cruise, and Descent Trajectories

In Equation (A.2), for the climb trajectory, the parameter τ is set to the portion of the trajectory that is assumed to remain after the climb segment is complete. For the descent trajectory, τ is set to the time period of the cruise segment that precedes the descent segment. For the cruise trajectory, τ is set to the entire length of the trajectory time horizon being investigated.

In this study, advisories from the DSTs are assumed to be provided to controllers at 20 minutes before some predicted future conflict event. This is assumed to be followed by an 8-minute controller/pilot lag, resulting in a 12-minute time horizon. This 8-minute lag covers both the controller issuance and pilot initiation of the resolution maneuver. Although a DST technology-specific time horizon would likely be chosen to trade-off high false/missed alerts with the cost of conflict resolution, this simplifying 12-minute common time horizon was chosen to represent all cases.

For conflicts predicted to occur during cruise flight, only cruise trajectory prediction errors contribute. In this case, the value of τ in Equation (A.2) is set at 12 minutes. For conflicts identified to occur during either climb or descent flight, the conflict probe time horizon is assumed to nominally encompass half the climb or descent segment error, with the remaining time period accruing cruise accuracy errors. A 20-minute climb (10,000 ft to the TOC) and 15-minute descent (TOD to 10,000 ft) were assumed. Thus, for a climb trajectory, it is assumed that 10 minutes of the trajectory is from the climb segment, and τ is set at 2 minutes to cover the remaining cruise segment. For a descent trajectory, it is assumed that 7.5 minutes of the trajectory is from the descent segment, and τ is set to 4.5 minutes to cover the preceding cruise segment.

This approximate trajectory model is illustrated in Figure A.1 for arrivals. In Figure A.1, the prediction accuracy of a conflict predicted to involve a descending aircraft (at conflict PCA), but predicted while that aircraft was in cruise would include error contributions from both descent (half of 15-minute descent duration) and cruise (remaining 4.5 minutes) flight segments. Conversely, the prediction accuracy of a conflict predicted to involve a cruising arrival flight (PCA occurs prior to descent) would include only cruise error contributions. Parallel situations apply to trajectory accuracy of departure climb and cruise flight segments.

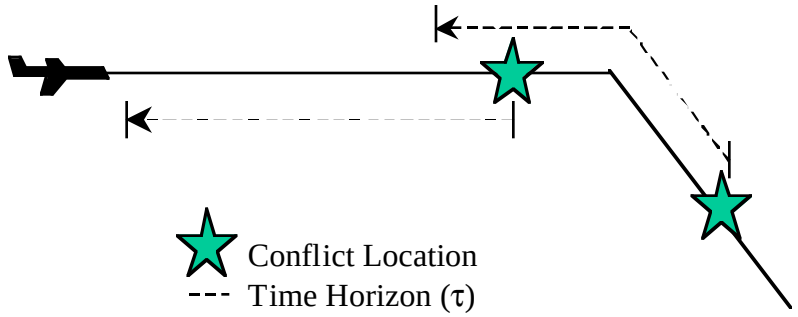

Figure A.1 Arrival Conflict Time Horizon

Estimated Trajectory Prediction Accuracy

Trajectory prediction accuracies in both timing and position are estimated using Table A.2 error parameter values in Equations (A.1) through (A.4), along with Table A.1 climb/descent timing sensitivity coefficients and the common 12-minute time horizon value. Table A.3 shows the error contributions and resulting 12-minute trajectory prediction error in climb, cruise and descent segments for arrival, overflight, and departure operations. The first row presents the timing error from Equation A.1 for Baseline and EDA cases. Note that EDA reduces the timing error at end of the descent segment from 86.1 sec to 17.9 sec. The second and third rows represent the position and velocity terms for Equation (A.2). For the climb and descent segments, the position error term is derived from the corresponding timing error term using Equation (A.3). The last row of Table A.3 shows composite predicted position error resulting from these calculations for the various flight phases. In the case of arrival-descent and departure-climb conflicts, the 12-minute trajectory prediction error includes a combination of climb or descent segment and cruise segment errors. Note that the FFP1 Baseline descent maneuver timing error was calibrated to approximate the 90 second arrival fix delivery accuracy observed in the 1997 DFW prototype TMA field tests [30]. The EDA case was similarly calibrated to the 15-20 second error observed in the 1992-1995 EDA prototype field tests [10]. Note that shading of a cell indicates improvement from the previous case.

Table A.3 Assumed ATM Trajectory Prediction Accuracy Parameters

	Units	FFP1 Baseline					EDA				
		DEP		OVR	ARR		DEP		OVR	ARR	
		CL	CR	CR	CR	D	CL	CR	CR	CR*	D
Error Components											
Maneuver σ_{t_M}	sec	283	NA	NA	NA	**86.1**	283	NA	NA	NA	**17.9**
Position σ_p	nm	13.7	0.87	0.87	0.87	4.18	13.7	0.87	0.87	0.87	0.87
Velocity σ_V	nm/min	0.39	0.39	0.39	0.39	0.39	0.39	0.39	0.39	0.30	0.30
12-minute Trajectory Prediction Accuracy											
Predicted Position Error $\sigma_{p,pred}(\tau)$	nm	13.8	4.7	4.7	4.7	4.5	13.8	4.7	4.7	3.74	4.0

Note: Bold values calibrated to approximate 90 and 15-20 second (1-sigma) metering fix delivery error of TMA [30] and EDA [10] prototype field tests.
* Applies to metered arrivals only.

Again, both Chapters 1 and 2 employ the arrival descent maneuver timing error (i.e., arrival metering fix delivery error) in the benefits calculations. Chapter 4 employs the 12-minute trajectory prediction accuracy of all flight phases, as part of ATM perception assumed in the estimation of separation assurance benefits.

Appendix B Annual/NAS Extrapolation Assumptions

Table B.1 CY1996 Domestic ARTCC Operations

	ARTCC Facility	ARTCC Departure Ops	ARTCC Overflight Ops	ARTCC Total Ops (1)
ZAB	Albuquerque, NM ARTCC	506,188	493,112	1,505,488
ZAU	Chicago, IL ARTCC	1,180,494	533,343	2,894,331
ZBW	Nashau, NH ARTCC (BOS)	697,875	331,101	1,726,851
ZDC	Leesburg, VA ARTCC (DC)	831,358	668,368	2,331,084
ZDV	Denver, CO ARTCC	434,387	658,530	1,527,304
ZFW	Ft.Worth, TX ARTCC	854,283	409,328	2,117,894
ZHU	Houston, TX ARTCC	825,674	201,509	1,852,857
ZID	Indianapolis, IN ARTCC	669,509	882,649	2,221,667
ZJX	Jacksonville, FL ARTCC	607,723	662,712	1,878,158
ZKC	Kansas City, KS ARTCC	691,746	602,863	1,986,355
ZLA	Los Angeles, CA ARTCC	927,509	125,726	1,980,744
ZLC	Salt Lake City, UT ARTCC	378,163	752,723	1,509,049
ZMA	Miami, FL ARTCC	725,485	90,866	1,541,836
ZME	Memphis, TN ARTCC	575,462	827,193	1,978,117
ZMP	Minneapolis, MN ARTCC	762,151	503,146	2,027,448
ZNY	New York, NY ARTCC	763,938	511,985	2,039,861
ZOA	Oakland, CA ARTCC	616,385	135,186	1,367,956
ZOB	Cleveland, OH ARTCC	967,543	935,158	2,870,244
ZSE	Seattle, WA ARTCC	647,722	97,069	1,392,513
ZTL	Atlanta, GA ARTCC	943,365	565,941	2,452,671
ZAN	Anchorage, A ARTCC	225,034	45,121	495,189
ZUA	Guam CERAP	32,112	8,560	72,784

(1) ARTCC Total Operations is calculated as: 2 x (ARTCC Departure ops) + (ARTCC Overflight Ops)

Source: Office of Aviation Policy and Plans, Washington, DC 20591, Air Traffic Activity query, APO Data System, FAA APO Home Page, Internet WWW Site (Nov 19,1998).

Table B.2 Airport Operations, Delays, and Rush Arrival Interruption Rates

Airport	CY1996 Airport Operations	CY1996 Delays >15 min per 1000 ops (1)	Delay Category No.	Rush Arrival Rate per 100 ops (2) Arr	Dep
EWR - Newark	443,431	65.25	1	39.46	47.45
SFO - San Francisco	442,281	56.57	1	39.46	47.45
LGA - N.Y. LaGuardia	342,618	46.22	1	39.46	47.45
ORD - Chicago O'Hare	909,186	34.46	2	34.91	41.97
STL - St. Louis	517,352	34.04	2	34.91	41.97
JFK - N.Y. Kennedy	360,511	29.53	2	34.91	41.97
BOS - Boston	462,507	26.37	2	34.91	41.97
LAX - Los Angeles	764,002	24.13	3	30.35	36.50
ATL - Atlanta	772,597	23.88	3	30.35	36.50
DFW - Dallas-Ft. Worth	869,831	19.59	3	30.35	36.50
PHL - Philadelphia	406,121	17.95	3	30.35	36.50
IAH - Houston International	391,939	11.45	4	24.28	29.20
CVG - Cincinnati	393,523	10.38	4	24.28	29.20
MSP - Minneapolis	483,570	9.29	4	24.28	29.20
DTW - Detroit	531,098	9.10	4	24.28	29.20
PHX - Phoenix	544,363	7.25	4	24.28	29.20
IAD - Washington Dulles	330,439	6.81	4	24.28	29.20
MIA - Miami	546,487	6.79	4	24.28	29.20
MDW - Chicago Midway	254,351	6.70	4	24.28	29.20
PIT - Pittsburgh	447,436	6.60	4	24.28	29.20
CLT - Charlotte	457,054	6.55	4	24.28	29.20
DCA - Washington National	309,754	6.53	4	24.28	29.20
SEA - Seattle	397,591	6.37	4	24.28	29.20
CLE - Cleveland	291,029	4.68	5	18.21	21.90
MCO - Orlando	341,942	4.59	5	18.21	21.90
LAS - Las Vegas	479,625	3.68	5	18.21	21.90
BWI - Baltimore-Washington	270,156	3.67	5	18.21	21.90
SLC - Salt Lake City	373,815	3.53	5	18.21	21.90
SAN - San Diego	243,595	3.31	5	18.21	21.90
HOU - Houston Hobby	252,254	2.57	5	18.21	21.90
PDX - Portland	305,964	2.41	5	18.21	21.90
DEN - Denver	454,234	1.90	5	18.21	21.90
FLL - Ft. Lauderdale	236,342	1.53	5	18.21	21.90
BDL - Bradley	160,752	1.36	5	18.21	21.90
BNA - Nashville	226,274	0.73	5	18.21	21.90
MEM - Memphis	363,945	Not Available	5	18.21	21.90
OAK - Oakland	516,498	Not Available	5	18.21	21.90

(1) Source: FAA "1997 Aviation Capacity Enhancement Plan," Office of System Capacity. (Dec 1997)

(2) Rush Arrival rates assumed to be 130%,115%, 100%, 80% and 60% of simulated DFW rush arrival rate [12], based on 1996 FAA delay data and category criteria shown in Table B.3

Table B.3 Rush Arrival Rate Criteria

Category No.	CY1996 (1) Delays > 15 minutes Per 1000 Airport Ops	Proportion of DFW (category 3) Rush Arrival Rate	Rush Arrival Rate (Rush Arrivals Per 100 Airport Ops)
1	>35	130%	39.46
2	25-35	115%	34.91
3	15-25	100%	30.35 (2)
4	5-15	80%	24.28
5	<5	60%	18.21

(1) FAA CY1996 Delay Data [31], as shown in Table B.2.
(2) DFW Rush Arrival Rate per ATM Interruptions Model analysis of Chapters 3 and 4.

Appendix C Airport Throughput Analysis Assumptions

Table C.1 Assumed Airport Runway Configurations

	Configuration	Arrival Runways	Departure Runways
Atlanta (ATL)	IFR & VFR	08L, 09R	08R, 09L
Nashville (BNA)	IFR & VFR	02C, 02R	02L, 02R, 31
Boston (BOS)	IFR	04R	04R, 04L, 09
	VFR	04R, 04L	04R, 04L, 09
Baltimore (BWI)	IFR	15R, 15L, 10	15R, 15L
	VFR	33L, 33R, 28 22	33R, 28, 22
Charlotte (CLT)	IFR & VFR	36L, 36R	36L, 36R
Cincinnati (CVG)	IFR & VFR	18L, 18R	18L, 18R, 27
Washington National (DCA)	IFR	36	36, 33, 03
	VFR	36, 33, 03	36, 33, 03
Denver (DEN)	IFR & VFR	34, 35L, 35R	34, 35L, 35R
Dallas-Ft. Worth (DFW)*	IFR	36L, 35C, **35R**	35L, 36R
	VFR	36L, 35C, **35R**, 31R	35L, 36R, 31L
Detroit (DTW)	IFR & VFR	03L, 03R	03C, 03L
N.Y. Newark (EWR)	IFR	04R	04L
	VFR	04R, 11	04L, 11
Washington Dulles (IAD)	IFR	01R	01L, 30
	VFR	01R, 01L	01L, 30
Houston Intercontinental (IAH)	IFR	26, 27	14L, 14R
	VFR	08, 09	14L, 14R
N.Y. Kennedy (JFK)	IFR & VFR	13L, 13R	13L, 13R
Las Vegas (LAS)	IFR	25R, 25L	25R, 25L
	VFR	19L, 25R, 25L	19L, 25R, 25L
Los Angeles (LAX)	IFR	25L, 24R	25R, 24L
	VFR	25L, 24R	25R, 24L
N.Y. LaGuardia (LGA)	IFR	04	13
	VFR	22	13
Orlando (MCO)	IFR	18L, 17	18R, 17
	VFR	18R, 18L, 17	18R, 18L, 17
Memphis (MEM)	IFR	**18L**, 18R	18C, 18R
	VFR	**18L**, 18R, 27	18C, 18R
Miami (MIA)	IFR	09L, 09R	09L, 09R, 12
	VFR	09L, 09R, 12	09L, 09R, 12
Minneapolis (MSP)	IFR & VFR	29L, 29R	29L, 29R
Chicago O'Hare (ORD)	IFR	14R, 14L	09R, 09L
	VFR	14R, 22R, 22L	27L, 22R
Philadelphia (PHL)	IFR & VFR	27R, 17	27L, 17
Phoenix (PHX)	IFR	08R	08L
	VFR	08L, 08R	08L, 08R
Pittsburgh (PIT)	IFR & VFR	10L, 10R	10C, 14
Seattle (SEA)	IFR	16R	16L
	VFR	16L, 16R	16L, 16R
San Francisco (SFO)	IFR	28R	28L, 28R
	VFR	28R, 28L	01L, 01R
Salt Lake City (SLC)*	IFR	**34L**, 34R	34R, 35
	VFR	**34L**, 34R	**34L**, 34R, 35
St. Louis (STL)	IFR	30L, 30R	30L, 30R
	VFR	30L, 30R, 24	30L, 30R

* New airport runways indicated in bold type.

Table C.2 FAA-Based 1998 Time and Fuel Cost Rates by Aircraft Class

Engine Type	Engine Num	A/C Size	A/C Class	FAA-Based Cost Rates ($/hr) Time Cost Crew	Maint.	Subtotal	Fuel & Oil Cost *Airborne*	*Ground* **	Fuelburn* (lbs/min) Gd Hold (1)
J	4	H	4JH	2,488	1,699	4,187	2,703	901	150
J	4	L	4JL	582	990	1,572	829	276	46
J	3	H	3JH	1,981	1,459	3,440	1,827	609	102
J	3	L	3JL	1,188	712	1,900	1,025	342	57
J	3	S+	3JS+	280	596	876	626	209	35
J	2	H	2JH	1,489	780	2,269	1,152	384	64
J	2	LH	2JLH	1,164	493	1,657	754	251	42
J	2	L	2JL	851	531	1,382	651	217	36
J	0	L	JL	701	527	1,228	593	198	33
J	2	LS	2JLS	551	523	1,074	535	178	30
J	2	S+	2JS+	251	515	766	420	140	23
J	0	S+	JS+	238	438	676	335	112	19
J	2	S	2JS	225	361	586	249	83	14
J	1	L	1JL	240	400	640	300	110	18
J	1	S+	1JS+	175	250	425	210	80	13
J	1	S	1JS	110	180	290	130	50	8
T	4	L	4TL	672	998	1,670	571	190	32
T	3	L	3TL	439	671	1,110	421	140	23
T	2	L	2TL	205	344	549	270	90	15
T	0	L	TL	203	324	527	226	75	13
T	2	S+	2TS+	201	303	504	181	60	10
T	0	S+	TS+	197	280	477	164	55	9
T	2	S	2TS	193	257	450	147	49	8
T	0	S	TS	155	199	354	128	43	7
T	1	S+	1TS+	117	140	257	109	36	6
T	1	S	1TS	114	110	224	103	34	6
P	4	L	4PL	250	275	525	500	167	28
P	3	S	3PS	220	245	465	445	148	25
P	2	L	2PL	190	215	405	390	130	22
P	2	S+	2PS+	200	204	404	193	64	11
P	0	S+	PS+	136	149	285	131	44	7
P	2	S	2PS	72	93	165	68	23	4
P	0	S	PS	72	77	149	57	19	3
P	1	S+	1PS+	72	60	132	45	15	3
P	1	S	1PS	72	27	99	22	7	1
(Rockwell	0	0	SST	2,488	1,699	4,187	7,363	2,454	409
J	8	L	8JH	2,488	1,699	4,187	2,703	901	150

Consumer Price index (CPI)		Oil & Gas Deflater	
1982-84 base	100.0	1992 base	100
1996	153.0	1996	104.2

Escalation Factor		Crew	Maint	Subtotal	Airbourne	Ground
1996	1.000	1.000	1.000	1.000	1.000	1.000

Note: Shaded aircraft classes are interpolated/extrapolated from non-shaded values of FAA source.

* Assumes Fuelcost of $0.10/lb

** Ground Fuel and oil cost is assumed to be 1/3 of airbourne per advice of airline personnel.

Sources: FAA, "Economic Values for Evaluation of Federal Administration Investment and Regulatory Programs," Final Report FAA-APO-98-8, Office of Aviation Policy and Plans. (June 1998)

FAA, "FAA Aviation Forecasts Fiscal Years 1998-2009," Final Report FAA-APO-98-1, Office of Avaiation Policy and Plans. (March 1998)

Table C.3 Airport Characteristics

Airport		Historical Share (%)	1996 Airport Cost Rates ($/min) **	
		IMC*	Departure	Arrival
ATL	Atlanta	14.2%	27.76	35.60
BDL	Bradley	14.6%	16.92	21.72
BNA	Nashville	9.5%	14.54	18.44
BOS	Boston	15.6%	19.74	25.11
BWI	Baltimore	12.4%	19.37	24.65
CLE	Cleveland	15.6%	21.54	27.44
CLT	Charlotte	12.5%	18.50	23.48
CVG	Cincinnati	15.0%	19.52	24.99
DCA	Washington National	10.7%	20.99	26.62
DEN	Denver	6.0%	23.71	30.25
DFW	Dallas/Ft. Worth	8.4%	23.53	30.08
DTW	Detroit	16.6%	24.54	31.27
EWR	Newark	16.6%	24.99	32.09
FLL	Ft. Lauderdale	3.0%	18.14	23.17
HOU	Houston Hobby	13.5%	18.64	23.94
IAD	Washington Dulles	11.7%	16.90	21.53
IAH	Houston Intercontinental	12.7%	22.15	28.34
JFK	N.Y. Kennedy	15.0%	34.19	44.75
LAS	Las Vegas	0.3%	20.33	25.83
LAX	Los Angeles Int'l	22.2%	26.45	33.96
LGA	N.Y. LaGuardia	16.4%	23.30	29.72
MCO	Orlando	5.9%	21.19	27.05
MDW	Chicago Midway	15.1%	20.31	26.02
MEM	Memphis	9.2%	23.52	30.23
MIA	Miami	2.3%	23.60	30.32
MSP	Minneapolis	11.6%	22.23	28.30
OAK	Oakland	14.4%	14.14	18.18
ORD	Chicago O'Hare	16.1%	26.91	34.53
PDX	Portland	10.2%	18.40	23.50
PHL	Philadelphia	15.0%	20.37	25.91
PHX	Phoenix	0.5%	20.84	26.44
PIT	Pittsburgh	24.6%	19.14	24.23
SAN	San Diego	12.6%	25.76	32.96
SEA	Seattle	14.9%	23.33	29.84
SFO	San Francisco	12.5%	27.46	35.26
SLC	Salt Lake City	5.6%	20.96	26.84
STL	St. Louis	11.5%	22.33	28.46

* Annual Occurrence of IMC (percent) during hours of 7AM to 10PM [54].

* Average value, weighted by aircraft class distribution. Departure rates assume ground hold rates, arrival rates assume airborne rates.

Appendix D Metering Conformance Analysis Assumptions

Table D.1 B737 Fuelburn Rates from High-Fidelity Model Simulations

	B737 Fuelburn (lbs/min)																
Cruise	CAS Cruise Speed (kts)																
Altitude (ft)	100	200	205	210	215	220	225	230	235	240	245	250	255	260	265	270	275
10000	81.6	81.6	82.6	83.6	84.9	86.2	87.7	89.3	90.9	92.8	94.8	96.9	99.0	101.4	103.9	106.4	109.0
11000	81.6	81.6	82.6	83.6	84.9	86.2	87.7	89.3	90.9	92.8	94.8	96.9	99.0	101.4	103.9	106.4	109.0
13000	80.7	80.7	81.6	82.7	84.0	85.3	86.7	88.4	90.0	91.8	93.9	95.9	98.1	100.3	102.8	105.4	108.0
15000	79.8	79.8	80.8	81.8	83.1	84.4	85.8	87.4	89.1	90.9	92.9	94.9	97.1	99.4	101.9	104.5	107.1
17000	79.2	79.2	80.1	81.1	82.4	83.6	85.0	86.6	88.3	90.1	92.1	94.2	96.3	98.6	101.1	103.6	106.3
19000	78.5	78.5	79.5	80.5	81.6	82.9	84.2	85.9	87.6	89.4	91.4	93.5	95.6	97.8	100.2	102.7	105.3
21000	78.0	78.0	79.0	80.0	81.1	82.4	83.8	85.4	87.1	88.8	90.8	92.9	95.0	97.1	99.6	102.1	104.6
23000	77.7	77.7	78.6	79.6	80.7	82.0	83.4	85.1	86.7	88.4	90.4	92.5	94.7	96.9	99.2	101.7	104.3
25000	77.4	77.4	78.2	79.2	80.4	81.7	83.1	84.7	86.5	88.2	90.2	92.3	94.3	96.4	98.8	101.4	104.1
27000	77.3	77.3	78.2	79.1	80.2	81.5	82.8	84.3	86.0	87.7	89.5	91.6	93.8	96.0	98.4	101.1	103.8
29000	77.2	77.2	77.9	78.8	79.9	81.2	82.4	83.8	85.5	87.3	89.2	91.4	93.6	96.0	98.4	101.2	104.1
31000	77.3	77.3	77.9	78.9	79.9	81.1	82.4	83.8	85.6	87.5	89.4	91.6	93.9	96.4	98.9	101.8	105.1
33000	77.7	77.7	78.2	79.1	80.1	81.4	82.7	84.2	86.0	87.8	89.8	92.2	94.8	97.5	100.8	104.4	110.2
35000	78.5	78.5	78.8	79.8	80.8	82.1	83.5	85.0	86.9	89.0	91.1	93.9	98.1	102.8	109.4	112.6	112.7
37000	80.4	80.4	80.7	81.6	82.5	83.8	85.4	87.1	89.1	92.8	97.2	102.7	102.1	102.1	102.2	102.2	102.2
39000	84.3	84.3	84.3	84.8	86.0	87.2	89.4	91.8	90.2	90.3	90.4	90.4	90.5	90.5	90.5	90.6	90.6
Cruise																	
Altitude (ft)	280	285	290	295	300	305	310	315	320	325	330	335	340	345	350	400	
10000	111.7	114.6	117.6	120.8	123.9	127.2	130.6	134.1	137.8	141.6	145.4	149.3	153.3	157.6	162.0	162.0	
11000	111.7	114.6	117.6	120.8	123.9	127.2	130.6	134.1	137.8	141.6	145.4	149.3	153.3	157.6	162.0	162.0	
13000	110.7	113.6	116.7	119.8	123.0	126.3	129.6	133.1	136.7	140.4	144.3	148.4	152.6	156.9	161.2	161.2	
15000	109.8	112.7	115.7	118.9	122.1	125.4	128.6	132.0	135.7	139.6	143.6	147.7	151.8	156.1	160.4	160.4	
17000	108.9	111.7	114.7	117.8	120.9	124.2	127.7	131.2	134.9	138.8	142.8	146.9	151.0	155.5	160.1	160.1	
19000	107.9	110.6	113.6	116.8	120.1	123.5	127.0	130.5	134.2	138.1	142.1	146.4	150.9	155.5	160.4	160.4	
21000	107.3	110.1	113.1	116.4	119.6	123.0	126.5	130.1	133.8	137.8	142.1	146.7	151.5	156.3	162.0	162.0	
23000	107.0	109.8	112.8	116.1	119.3	122.8	126.4	130.1	134.1	138.5	142.9	147.8	153.9	161.9	169.2	169.2	
25000	106.7	109.5	112.5	115.8	119.4	123.0	126.9	130.9	134.9	140.0	147.1	155.6	158.6	158.6	158.6	158.6	
27000	106.6	109.7	112.9	116.4	120.1	124.0	128.5	134.3	142.5	150.1	149.5	149.5	149.5	149.6	149.6	149.6	
29000	107.2	110.3	113.9	117.9	123.0	130.5	139.3	140.3	140.4	140.4	140.4	140.4	140.4	140.4	140.5	140.5	
31000	108.8	113.0	119.0	128.2	131.1	131.1	131.2	131.2	131.2	131.2	131.2	131.3	131.3	131.3	131.3	131.3	
33000	118.7	121.6	121.7	121.7	121.7	121.7	121.8	121.8	121.8	121.8	121.8	121.8	121.8	121.9	121.9	121.9	
35000	112.7	112.7	112.7	112.8	112.8	112.8	112.8	112.8	112.9	112.9	112.9	112.9	112.9	112.9	112.9	112.9	
37000	102.3	102.3	102.3	102.3	102.4	102.4	102.4	102.4	102.4	102.5	102.5	102.5	102.5	102.5	102.5	102.5	
39000	90.6	90.7	90.7	90.7	90.7	90.7	90.8	90.8	90.8	90.8	90.8	90.8	90.9	90.9	90.9	90.9	

Table D.2 BADA "Low" Cruise Speeds by Altitude and Aircraft Class [37]

FL	Aircraft Class	4J/H	4J/L	3J/H	3J/L	3J/S+	2J/H	2J/LH	2J/L	J/L	2J/LS	2J/S+	J/S+	2J/S	1J/L	1J/S+	1J/S	4T/L
	Aliased Class:									2J/L			2J/S+	2J/S+	2J/S+	2J/S+	2J/S+	
		Cruise CAS (kt)																
		250	250	250	250	250	250	250	250	250	250	237	237	237	237	237	237	220
		Cruise TAS (kt)																
0		na	na	na	na	na	na	na	na	na	na	na	na	na	na	na	na	na
5		na	na	na	na	na	na	na	na	na	na	na	na	na	na	na	na	na
10		na	na	na	na	na	na	na	na	na	na	na	na	na	na	na	na	na
15		na	na	na	na	na	na	na	na	na	na	na	na	na	na	na	na	na
20		na	na	na	na	na	na	na	na	na	na	na	na	na	na	na	na	na
30		261	261	261	261	261	261	261	261	261	261	247	247	247	247	247	247	230
40		265	265	265	265	265	265	265	265	265	265	251	251	251	251	251	251	233
60		272	272	272	272	272	272	272	272	272	272	258	258	258	258	258	258	240
80		280	280	280	280	280	280	280	280	280	280	266	266	266	266	266	266	247
100		289	289	289	289	289	289	289	289	289	289	273	273	273	273	273	273	254
120		297	297	297	297	297	297	297	297	297	297	282	282	282	282	282	282	262
140		306	306	306	306	306	306	306	306	306	306	290	290	290	290	290	290	270
160		316	316	316	316	316	316	316	316	316	316	299	299	299	299	299	299	279
180		326	326	326	326	326	326	326	326	326	326	309	309	309	309	309	309	288
200		336	336	336	336	336	336	336	336	336	336	319	319	319	319	319	319	297
220		346	346	346	346	346	346	346	346	346	346	329	329	329	329	329	329	306
240		358	358	358	358	358	358	358	358	358	358	339	339	339	339	339	339	316
260		369	369	369	369	369	369	369	369	369	369	350	350	350	350	350	350	327
280		381	381	381	381	381	381	381	381	381	381	362	362	362	362	362	362	338
300		394	394	394	394	394	394	394	394	394	394	374	374	374	374	374	374	349
320		407	407	407	407	407	407	407	407	407	407	386	386	386	386	386	386	361
340		420	420	420	420	420	420	420	420	420	420	399	399	399	399	399	399	373
360		434	434	434	434	434	434	434	434	434	434	413	413	413	413	413	413	386
380		452	452	452	452	452	452	452	452	452	452	431	431	431	431	431	431	403
400		472	472	472	472	472	472	472	472	472	472	449	449	449	449	449	449	420

FL	Aircraft Class	2T/L	T/L	2T/S+	T/S+	2T/S	T/S	1T/S+	1T/S	4P/L	3P/S	2P/L	2P/S+	P/S+	2P/S	P/S	1P/S+	1P/S
	Aliased Class:		2T/L		2T/S+		2T/S	2T/S	2T/S	2P/S	2P/S	2P/S	2P/S	2P/S		2P/S	1P/S	
		Cruise CAS (kt)																
		250	209	210	210	226	226	226	226	154	154	154	154	154	154	154	130	130
		Cruise TAS (kt)																
0		na	na	na	na	na	na	na	na	na	na	na	na	na	na	na	na	na
5		na	na	na	na	na	na	na	na	na	na	na	na	na	na	na	na	na
10		na	na	na	na	na	na	na	na	na	na	na	na	na	na	na	na	na
15		na	na	na	na	na	na	na	na	na	na	na	na	na	na	na	na	na
20		na	na	na	na	na	na	na	na	na	na	na	na	na	na	na	na	na
30		218	218	219	219	236	236	236	236	161	161	161	161	161	161	161	136	136
40		221	221	222	222	240	240	240	240	163	163	163	163	163	163	163	138	138
60		228	228	229	229	247	247	247	247	168	168	168	168	168	168	168	142	142
80		235	235	236	236	254	254	254	254	173	173	173	173	173	173	173	146	146
100		242	242	243	243	262	262	262	262	178	178	178	178	178	178	178	151	151
120		249	249	250	250	270	270	270	270	184	184	184	184	184	184	184	156	156
140		257	257	258	258	278	278	278	278	190	190	190	190	190	190	190	161	161
160		265	265	266	266	287	287	287	287	196	196	196	196	196	196	196	166	166
180		274	274	275	275	296	296	296	296	202	202	202	202	202	202	202	171	171
200		282	282	284	284	305	305	305	305	209	209	209	209	209	209	209	177	177
220		291	291	293	293	315	315	315	315	216	216	216	216	216	216	216	183	183
240		301	301	302	302	325	325	325	325	223	223	223	223	223	223	223	189	189
260		311	311	312	312	336	336	336	336	231	231	231	231	231	231	231	196	196
280		321	321	323	323	347	347	347	347	239	239	239	239	239	239	239	203	203
300		332	332	334	334	359	359	359	359	247	247	247	247	247	247	247	210	210
320		344	344	345	345	371	371	371	371	256	256	256	256	256	256	256	218	218
340		356	356	357	357	383	383	383	383	266	266	266	266	266	266	266	226	226
360		368	368	370	370	396	396	396	396	275	275	275	275	275	275	275	234	234
380		384	384	386	386	414	414	414	414	288	288	288	288	288	288	288	245	245
400		401	401	403	403	431	431	431	431	301	301	301	301	301	301	301	257	257

Appendix E Separation Assurance Analysis Assumptions

Table E.1 Climb Fuelburn by Altitude and Aircraft Class [37]

FL	Aircraft Class:	4J/H	4J/L	3J/H	3J/L	3J/S+	2J/H	2J/LH	2J/L	J/L	2J/LS	2J/S+	J/S+	2J/S	1J/L	1J/S+	1J/S	4T/L	3T/L
	Aliased Class:									2J/L			2J/S+		2J/S+	2J/S	2J/S		2T/L
		Fuel Burn Rate (kg/min)																	
0		481.5	117.6	254.1	109.3	41.0	319.6	177.5	89.9	89.9	101.5	27.4	27.4	10.3	27.4	10.3	10.3	58.6	18.0
5		477.2	116.6	252.0	108.5	40.6	316.2	175.8	89.0	89.0	100.0	27.1	27.1	10.2	27.1	10.2	10.2	59.9	17.9
10		473.0	115.6	249.9	107.7	40.2	312.8	174.1	88.2	88.2	98.4	26.8	26.8	10.2	26.8	10.2	10.2	59.5	17.8
15		468.9	115.8	250.7	108.2	39.7	310.1	172.9	87.7	87.7	97.1	26.7	26.7	10.5	26.7	10.5	10.5	59.2	17.7
20		464.7	114.8	248.6	107.4	39.3	306.8	171.2	86.8	86.8	95.6	26.5	26.5	10.5	26.5	10.5	10.5	58.9	17.5
30		456.9	117.6	255.7	111.3	38.5	302.7	169.9	86.8	86.8	93.5	26.6	26.6	11.7	26.6	11.7	11.7	58.2	17.2
40		449.2	122.7	268.2	117.9	37.7	299.9	169.7	87.6	87.6	91.9	27.2	27.2	13.6	27.2	13.6	13.6	57.6	16.9
60		436.9	130.3	270.0	125.1	36.1	291.7	166.3	87.9	87.9	88.9	28.4	28.4	16.2	28.4	16.2	16.2	56.4	16.4
80		420.2	125.7	261.1	121.3	34.5	279.1	159.6	84.4	84.4	83.3	27.2	27.2	16.1	27.2	16.1	16.1	55.1	15.8
100		403.6	121.2	252.1	117.4	33.0	266.8	152.9	81.0	81.0	77.9	26.0	26.0	15.9	26.0	15.9	15.9	53.9	15.2
120		384.2	125.5	275.8	125.9	31.5	260.1	150.3	80.5	80.5	73.6	24.9	24.9	15.7	24.9	15.7	15.7	52.8	14.6
140		367.8	120.9	266.1	121.7	30.1	248.3	143.7	77.1	77.1	68.7	23.9	23.9	15.4	23.9	15.4	15.4	51.7	14.0
160		351.5	116.3	256.5	117.5	28.7	236.8	137.2	73.7	73.7	64.1	22.8	22.8	15.2	22.8	15.2	15.2	50.6	13.5
180		335.3	111.9	246.9	113.3	27.4	225.6	130.8	70.5	70.5	59.8	21.8	21.8	15.0	21.8	15.0	15.0	49.5	13.0
200		319.2	107.1	237.3	109.0	26.1	214.7	124.5	67.3	67.3	55.7	20.9	20.9	14.7	20.9	14.7	14.7	48.5	12.5
220		303.2	102.1	227.9	104.7	24.9	204.1	118.3	64.1	64.1	51.9	19.9	19.9	14.4	19.9	14.4	14.4	47.6	12.0
240		287.2	97.3	218.6	100.3	23.7	193.7	112.2	61.1	61.1	48.5	18.9	18.9	14.1	18.9	14.1	14.1	46.6	11.5
260		271.4	92.5	209.3	95.9	22.6	183.7	106.1	58.0	58.0	45.1	17.9	17.9	13.7	17.9	13.7	13.7	45.8	11.0
280		255.6	88.0	199.5	91.5	21.5	173.9	100.1	54.7	54.7	42.0	17.0	17.0	13.3	17.0	13.3	13.3	45.0	9.8
300		240.8	83.1	188.2	86.6	20.4	164.4	94.3	51.4	51.4	39.1	16.2	16.2	12.9	16.2	12.9	12.9	44.2	9.4
320		225.5	77.7	175.4	80.6	19.5	154.5	87.9	48.1	48.1	36.6	15.4	15.4	12.5	15.4	12.5	12.5	43.5	7.3
340		210.0	72.6	162.7	74.0	18.5	144.6	81.4	44.9	44.9	34.5	14.6	14.6	11.8	14.6	11.8	11.8	42.9	7.0
360		194.7	67.8	150.6	67.5	17.6	135.1	75.1	41.7	41.7	32.6	13.7	13.7	10.8	13.7	10.8	10.8	42.4	6.0
380		179.4	63.4	139.9	61.7	16.8	126.2	69.1	38.8	38.8	31.1	13.0	13.0	10.0	13.0	10.0	10.0	42.2	4.1
400		164.3	59.3	129.6	56.1	16.0	117.6	63.2	36.0	36.0	29.9	12.3	12.3	9.2	12.3	9.2	9.2	42.2	3.9

FL	Aircraft Class:	2T/L	T/L	2T/S+	T/S+	2T/S	T/S	1T/S+	1T/S	4P/L	3P/S	2P/L	2P/S+	P/S+	2P/S	P/S	1P/S+	1P/S	SST	8J/H
	Aliased Class:		2T/L		2T/S+		2T/S	2T/S	2T/S	2P/S	2P/S	2P/S	2P/S	2P/S		2P/S	1P/S		4J/H	4J/H
		Fuel Burn Rate (kg/min)																		
0		18.0	18.0	10.1	10.1	5.6	5.6	5.6	5.6	2.5	2.5	2.5	2.5	2.5	2.5	2.5	0.5	0.5	481.5	481.5
5		17.9	17.9	10.2	10.2	5.6	5.6	5.6	5.6	2.5	2.5	2.5	2.5	2.5	2.5	2.5	0.5	0.5	477.2	477.2
10		17.8	17.8	10.2	10.2	5.6	5.6	5.6	5.6	2.5	2.5	2.5	2.5	2.5	2.5	2.5	0.5	0.5	473.0	473.0
15		17.7	17.7	10.2	10.2	5.7	5.7	5.7	5.7	2.5	2.5	2.5	2.5	2.5	2.5	2.5	0.5	0.5	468.9	468.9
20		17.5	17.5	10.1	10.1	5.6	5.6	5.6	5.6	2.5	2.5	2.5	2.5	2.5	2.5	2.5	0.5	0.5	464.7	464.7
30		17.2	17.2	10.0	10.0	5.5	5.5	5.5	5.5	2.5	2.5	2.5	2.5	2.5	2.5	2.5	0.5	0.5	456.9	456.9
40		16.9	16.9	9.8	9.8	5.4	5.4	5.4	5.4	2.5	2.5	2.5	2.5	2.5	2.5	2.5	0.5	0.5	449.2	449.2
60		16.4	16.4	9.5	9.5	5.2	5.2	5.2	5.2	2.5	2.5	2.5	2.5	2.5	2.5	2.5	0.5	0.5	436.9	436.9
80		15.8	15.8	9.2	9.2	5.1	5.1	5.1	5.1	2.5	2.5	2.5	2.5	2.5	2.5	2.5	0.5	0.5	420.2	420.2
100		15.2	15.2	8.9	8.9	4.9	4.9	4.9	4.9	2.5	2.5	2.5	2.5	2.5	2.5	2.5	0.5	0.5	403.6	403.6
120		14.6	14.6	8.7	8.7	4.7	4.7	4.7	4.7	2.5	2.5	2.5	2.5	2.5	2.5	2.5	0.5	0.5	384.2	384.2
140		14.0	14.0	8.3	8.3	4.6	4.6	4.6	4.6	2.5	2.5	2.5	2.5	2.5	2.5	2.5	0.5	0.5	367.8	367.8
160		13.5	13.5	8.1	8.1	4.4	4.4	4.4	4.4	2.5	2.5	2.5	2.5	2.5	2.5	2.5	0.5	0.5	351.5	351.5
180		13.0	13.0	7.7	7.7	4.2	4.2	4.2	4.2	2.5	2.5	2.5	2.5	2.5	2.5	2.5	na	na	335.3	335.3
200		12.5	12.5	7.4	7.4	4.1	4.1	4.1	4.1	1.8	1.8	1.8	1.8	1.8	1.8	1.8	na	na	319.2	319.2
220		12.0	12.0	7.0	7.0	4.0	4.0	4.0	4.0	1.8	1.8	1.8	1.8	1.8	1.8	1.8	na	na	303.2	303.2
240		11.5	11.5	6.7	6.7	3.8	3.8	3.8	3.8	1.8	1.8	1.8	1.8	1.8	1.8	1.8	na	na	287.2	287.2
260		11.0	11.0	6.3	6.3	3.7	3.7	3.7	3.7	1.4	1.4	1.4	1.4	1.4	1.4	1.4	na	na	271.4	271.4
280		9.8	9.8	5.9	5.9	3.5	3.5	3.5	3.5	1.4	1.4	1.4	1.4	1.4	1.4	1.4	na	na	255.6	255.6
300		9.4	9.4	5.5	5.5	3.4	3.4	3.4	3.4	1.4	1.4	1.4	1.4	1.4	1.4	1.4	na	na	240.8	240.8
320		7.3	7.3	4.4	4.4	3.3	3.3	3.3	3.3	0.7	0.7	0.7	0.7	0.7	0.7	0.7	na	na	225.5	225.5
340		7.0	7.0	2.4	2.4	3.1	3.1	3.1	3.1	0.7	0.7	0.7	0.7	0.7	0.7	0.7	na	na	210.0	210.0
360		6.0	6.0	2.3	2.3	3.0	3.0	3.0	3.0	0.7	0.7	0.7	0.7	0.7	0.7	0.7	na	na	194.7	194.7
380		4.1	4.1	2.2	2.2	2.9	2.9	2.9	2.9	na	na	na	na	na	na	na	na	na	179.4	179.4
400		3.9	3.9	2.1	2.1	2.5	2.5	2.5	2.5	na	na	na	na	na	na	na	na	na	164.3	164.3

Table E.2 Cruise Fuelburn by Altitude and Aircraft Class [37]

FL	Aircraft Class: / Aliased Class:	4J/H	4J/L	3J/H	3J/L	3J/S+	2J/H	2J/LH	2J/L	J/L 2J/L	2J/LS	2J/S+	J/S+ 2J/S+	2J/S	1J/L 2J/S+	1J/S+ 2J/S	1J/S 2J/S	4T/L	3T/L 2T/L
		Fuel Burn Rate (kg/min)																	
0		na	na	na	na	na	na	na	na	na	na	na	na	na	na	na	na	na	na
5		na	na	na	na	na	na	na	na	na	na	na	na	na	na	na	na	na	na
10		na	na	na	na	na	na	na	na	na	na	na	na	na	na	na	na	na	na
15		na	na	na	na	na	na	na	na	na	na	na	na	na	na	na	na	na	na
20		na	na	na	na	na	na	na	na	na	na	na	na	na	na	na	na	na	na
30		145.5	45.8	80.3	37.1	16.1	86.0	53.1	30.3	30.3	26.0	11.7	11.7	7.1	11.7	7.1	7.1	40.4	10.7
40		145.5	45.3	80.9	37.4	16.1	86.2	53.2	30.4	30.4	26.0	11.6	11.6	7.2	11.6	7.2	7.2	41.0	10.8
60		145.4	44.2	82.1	38.0	16.0	86.4	53.5	30.6	30.6	26.0	11.5	11.5	7.4	11.5	7.4	7.4	42.3	10.9
80		145.4	43.2	83.3	38.6	16.0	86.6	53.7	30.8	30.8	26.1	11.3	11.3	7.6	11.3	7.6	7.6	43.6	11.1
100		145.3	42.2	84.6	39.2	16.0	86.8	53.9	31.0	31.0	26.1	11.2	11.2	7.8	11.2	7.8	7.8	44.9	11.3
120		166.2	53.8	115.0	56.4	21.0	100.3	59.8	37.6	37.6	31.2	13.9	13.9	7.9	13.9	7.9	7.9	46.4	11.4
140		165.7	54.4	116.6	57.1	20.9	100.4	60.0	37.8	37.8	31.1	14.0	14.0	8.2	14.0	8.2	8.2	47.8	11.6
160		165.2	55.1	118.2	57.9	20.8	100.5	60.3	38.0	38.0	31.1	14.1	14.1	8.4	14.1	8.4	8.4	49.4	11.5
180		164.6	55.7	119.8	58.8	20.6	100.6	60.5	38.1	38.1	31.1	14.2	14.2	8.6	14.2	8.6	8.6	51.0	11.5
200		164.0	56.4	121.4	59.6	20.5	100.8	60.7	38.4	38.4	31.1	14.3	14.3	8.8	14.3	8.8	8.8	52.6	11.2
220		163.4	57.0	123.1	60.5	20.4	100.8	60.9	38.6	38.6	31.1	14.4	14.4	9.0	14.4	9.0	9.0	54.4	10.8
240		162.7	57.7	124.8	61.3	20.2	100.9	61.1	38.8	38.8	30.9	14.4	14.4	9.3	14.4	9.3	9.3	56.2	10.4
260		161.9	57.1	126.3	60.7	20.1	100.9	61.4	38.6	38.6	30.0	14.4	14.4	9.5	14.4	9.5	9.5	56.4	10.0
280		159.3	56.3	124.8	59.8	19.4	101.0	61.6	38.0	38.0	28.9	14.1	14.1	9.8	14.1	9.8	9.8	56.1	9.0
300		157.0	55.5	122.1	59.1	18.1	100.7	61.8	37.0	37.0	27.5	13.6	13.6	10.1	13.6	10.1	10.1	55.8	8.7
320		154.1	53.1	119.9	57.4	16.9	98.4	60.9	35.9	35.9	26.4	13.1	13.1	10.3	13.1	10.3	10.3	54.8	6.9
340		151.3	50.4	116.3	55.0	15.8	96.0	59.5	34.8	34.8	25.4	12.5	12.5	10.1	12.5	10.1	10.1	52.2	6.6
360		148.0	48.1	113.8	53.0	14.8	93.6	58.6	33.8	33.8	24.7	11.9	11.9	9.7	11.9	9.7	9.7	49.7	5.9
380		144.8	46.5	112.9	50.3	14.0	92.0	58.4	33.2	33.2	24.2	11.5	11.5	9.4	11.5	9.4	9.4	47.6	4.1
400		139.1	45.3	111.8	47.8	13.3	91.2	58.8	32.0	32.0	23.9	11.1	11.1	8.7	11.1	8.7	8.7	45.6	4.0

FL	Aircraft Class: / Aliased Class:	2T/L	T/L 2T/L	2T/S+	T/S+ 2T/S+	2T/S	T/S 2T/S	1T/S+ 2T/S	1T/S 2T/S	4P/L 2P/S	3P/S 2P/S	2P/L 2P/S	2P/S+ 2P/S	P/S+ 2P/S	2P/S	P/S 2P/S	1P/S+ 1P/S	1P/S	SST 4J/H	8J/H 4J/H
		Fuel Burn Rate (kg/min)																		
0		na	na	na	na	na	na	na	na	na	na	na	na	na	na	na	na	na	na	na
5		na	na	na	na	na	na	na	na	na	na	na	na	na	na	na	na	na	na	na
10		na	na	na	na	na	na	na	na	na	na	na	na	na	na	na	na	na	na	na
15		na	na	na	na	na	na	na	na	na	na	na	na	na	na	na	na	na	na	na
20		na	na	na	na	na	na	na	na	na	na	na	na	na	na	na	na	na	na	na
30		10.7	10.7	6.0	6.0	4.3	4.3	4.3	4.3	2.5	2.5	2.5	2.5	2.5	2.5	2.5	0.5	0.5	145.5	145.5
40		10.8	10.8	6.1	6.1	4.3	4.3	4.3	4.3	2.5	2.5	2.5	2.5	2.5	2.5	2.5	0.5	0.5	145.5	145.5
60		10.9	10.9	6.3	6.3	4.4	4.4	4.4	4.4	2.5	2.5	2.5	2.5	2.5	2.5	2.5	0.5	0.5	145.4	145.4
80		11.1	11.1	6.5	6.5	4.4	4.4	4.4	4.4	2.5	2.5	2.5	2.5	2.5	2.5	2.5	0.5	0.5	145.4	145.4
100		11.3	11.3	6.7	6.7	4.4	4.4	4.4	4.4	2.5	2.5	2.5	2.5	2.5	2.5	2.5	0.5	0.5	145.3	145.3
120		11.4	11.4	6.6	6.6	3.9	3.9	3.9	3.9	2.5	2.5	2.5	2.5	2.5	2.5	2.5	0.5	0.5	166.2	166.2
140		11.6	11.6	6.5	6.5	3.9	3.9	3.9	3.9	2.5	2.5	2.5	2.5	2.5	2.5	2.5	0.5	0.5	165.7	165.7
160		11.5	11.5	6.5	6.5	3.9	3.9	3.9	3.9	2.5	2.5	2.5	2.5	2.5	2.5	2.5	0.5	0.5	165.2	165.2
180		11.5	11.5	6.3	6.3	3.8	3.8	3.8	3.8	2.5	2.5	2.5	2.5	2.5	2.5	2.5	na	na	164.6	164.6
200		11.2	11.2	6.0	6.0	3.6	3.6	3.6	3.6	1.8	1.8	1.8	1.8	1.8	1.8	1.8	na	na	164.0	164.0
220		10.8	10.8	5.8	5.8	3.5	3.5	3.5	3.5	1.8	1.8	1.8	1.8	1.8	1.8	1.8	na	na	163.4	163.4
240		10.4	10.4	5.6	5.6	3.3	3.3	3.3	3.3	1.8	1.8	1.8	1.8	1.8	1.8	1.8	na	na	162.7	162.7
260		10.0	10.0	5.4	5.4	3.2	3.2	3.2	3.2	1.4	1.4	1.4	1.4	1.4	1.4	1.4	na	na	161.9	161.9
280		9.0	9.0	5.2	5.2	3.1	3.1	3.1	3.1	1.4	1.4	1.4	1.4	1.4	1.4	1.4	na	na	159.3	159.3
300		8.7	8.7	5.0	5.0	3.0	3.0	3.0	3.0	1.4	1.4	1.4	1.4	1.4	1.4	1.4	na	na	157.0	157.0
320		6.9	6.9	4.0	4.0	2.9	2.9	2.9	2.9	0.7	0.7	0.7	0.7	0.7	0.7	0.7	na	na	154.1	154.1
340		6.6	6.6	1.8	1.8	2.8	2.8	2.8	2.8	0.7	0.7	0.7	0.7	0.7	0.7	0.7	na	na	151.3	151.3
360		5.9	5.9	1.7	1.7	2.7	2.7	2.7	2.7	0.7	0.7	0.7	0.7	0.7	0.7	0.7	na	na	148.0	148.0
380		4.1	4.1	1.7	1.7	2.6	2.6	2.6	2.6	na	na	na	na	na	na	na	na	na	144.8	144.8
400		4.0	4.0	1.7	1.7	2.2	2.2	2.2	2.2	na	na	na	na	na	na	na	na	na	139.1	139.1

Table E.3 Descent Fuelburn by Altitude and Aircraft Class [37]

FL	Aircraft Class: / Aliased Class:	4J/H	4J/L	3J/H	3J/L	3J/S+	2J/H	2J/LH	2J/L	J/L 2J/L	2J/LS	2J/S+	J/S+ 2J/S+	2J/S	1J/L 2J/S+	1J/S+ 2J/S	1J/S 2J/S	4T/L	3T/L 2T/L
		Fuel Burn Rate (kg/min)																	
0		40.2	43.5	37.6	22.7	13.9	25.0	18.4	11.9	11.9	15.1	9.8	9.8	4.2	9.8	4.2	4.2	18.1	6.6
5		39.9	43.2	37.3	22.7	13.7	24.9	18.3	11.9	11.9	15.1	9.7	9.7	4.2	9.7	4.2	4.2	18.0	6.5
10		39.5	42.9	37.1	22.6	13.5	24.7	18.3	11.9	11.9	15.1	9.6	9.6	4.2	9.6	4.2	4.2	17.8	6.5
15		39.2	42.6	36.8	22.6	13.3	24.6	18.3	11.9	11.9	15.1	9.5	9.5	4.2	9.5	4.2	4.2	17.7	6.5
20		38.9	42.2	36.5	22.5	13.1	24.4	18.2	11.9	11.9	15.1	9.4	9.4	4.2	9.4	4.2	4.2	17.6	6.5
30		38.3	41.5	35.9	22.4	12.7	24.1	18.2	11.8	11.8	15.0	9.2	9.2	4.2	9.2	4.2	4.2	17.3	6.4
40		37.6	40.9	35.3	22.3	12.3	23.8	18.1	11.8	11.8	15.0	9.1	9.1	4.2	9.1	4.2	4.2	17.1	6.4
60		36.2	39.6	34.2	22.1	11.5	23.3	18.0	11.8	11.8	14.9	8.7	8.7	4.1	8.7	4.1	4.1	16.6	6.3
80		34.9	38.2	33.0	21.9	10.7	22.7	17.9	11.7	11.7	14.9	8.3	8.3	4.1	8.3	4.1	4.1	16.1	6.2
100		33.5	36.9	31.9	21.7	10.0	22.1	17.7	11.7	11.7	14.8	8.0	8.0	4.1	8.0	4.1	4.1	15.6	6.1
120		32.2	35.6	30.8	21.5	9.2	21.5	17.6	11.7	11.7	14.7	7.6	7.6	4.0	7.6	4.0	4.0	15.1	6.0
140		30.8	34.3	29.6	21.3	8.4	20.9	17.5	11.6	11.6	14.7	7.2	7.2	4.0	7.2	4.0	4.0	14.6	5.9
160		29.5	33.0	28.5	21.1	7.6	20.4	17.4	11.6	11.6	14.6	6.8	6.8	4.0	6.8	4.0	4.0	14.1	6.0
180		28.1	31.7	27.3	20.9	6.9	19.8	17.2	11.5	11.5	14.5	6.5	6.5	4.0	6.5	4.0	4.0	13.6	6.0
200		25.8	30.4	26.2	20.7	6.5	19.2	17.1	11.5	11.5	14.4	6.1	6.1	3.9	6.1	3.9	3.9	13.1	5.9
220		24.4	29.0	25.0	20.5	6.2	18.6	17.0	11.5	11.5	14.4	5.9	5.9	3.9	5.9	3.9	3.9	12.6	5.8
240		23.1	27.7	23.9	20.3	5.9	18.0	16.9	11.4	11.4	14.3	5.6	5.6	3.9	5.6	3.9	3.9	12.1	5.7
260		21.7	26.4	22.7	20.1	5.6	17.5	16.7	13.1	13.1	14.2	5.3	5.3	5.4	5.3	5.4	5.4	11.6	5.6
280		20.4	25.1	21.6	19.9	5.4	16.8	16.6	12.9	12.9	14.2	6.6	6.6	5.2	6.6	5.2	5.2	11.1	5.0
300		40.4	23.7	20.4	19.7	5.1	16.3	16.5	16.4	16.4	14.1	7.9	7.9	4.9	7.9	4.9	4.9	10.6	5.0
320		37.7	22.4	19.3	19.5	4.9	15.7	16.3	15.8	15.8	17.2	7.7	7.7	4.5	7.7	4.5	4.5	10.1	4.0
340		35.0	21.1	18.2	19.3	4.6	15.1	16.2	15.2	15.2	16.8	7.3	7.3	4.2	7.3	4.2	4.2	9.6	4.0
360		52.8	19.8	17.0	19.1	4.4	15.1	16.1	14.6	14.6	16.4	6.9	6.9	3.9	6.9	3.9	3.9	9.1	3.6
380		48.8	18.5	15.9	18.9	4.2	14.3	16.0	14.1	14.1	16.0	6.6	6.6	3.6	6.6	3.6	3.6	8.6	2.7
400		44.7	17.1	14.7	18.7	4.0	13.6	15.8	13.6	13.6	15.7	6.4	6.4	3.6	6.4	3.6	3.6	8.1	2.7

FL	Aircraft Class: / Aliased Class:	2T/L	T/L 2T/L	2T/S+	T/S+ 2T/S+	2T/S	T/S 2T/S	1T/S+ 2T/S	1T/S 2T/S	4P/L 2P/S	3P/S 2P/S	2P/L 2P/S	2P/S+ 2P/S	P/S+ 2P/S	2P/S	P/S 2P/S	1P/S+ 1P/S	1P/S	SST 4J/H	8J/H 4J/H
		Fuel Burn Rate (kg/min)																		
0		6.6	6.6	4.5	4.5	3.2	3.2	3.2	3.2	1.0	1.0	1.0	1.0	1.0	1.0	1.0	0.3	0.3	40.2	40.2
5		6.5	6.5	4.5	4.5	3.2	3.2	3.2	3.2	1.0	1.0	1.0	1.0	1.0	1.0	1.0	0.3	0.3	39.9	39.9
10		6.5	6.5	4.5	4.5	3.2	3.2	3.2	3.2	1.0	1.0	1.0	1.0	1.0	1.0	1.0	0.3	0.3	39.5	39.5
15		6.5	6.5	4.5	4.5	3.2	3.2	3.2	3.2	1.0	1.0	1.0	1.0	1.0	1.0	1.0	0.3	0.3	39.2	39.2
20		6.5	6.5	4.4	4.4	3.1	3.1	3.1	3.1	1.0	1.0	1.0	1.0	1.0	1.0	1.0	0.3	0.3	38.9	38.9
30		6.4	6.4	4.4	4.4	3.1	3.1	3.1	3.1	1.0	1.0	1.0	1.0	1.0	1.0	1.0	0.3	0.3	38.3	38.3
40		6.4	6.4	4.4	4.4	3.0	3.0	3.0	3.0	1.0	1.0	1.0	1.0	1.0	1.0	1.0	0.3	0.3	37.6	37.6
60		6.3	6.3	4.3	4.3	2.9	2.9	2.9	2.9	1.0	1.0	1.0	1.0	1.0	1.0	1.0	0.3	0.3	36.2	36.2
80		6.2	6.2	4.2	4.2	2.8	2.8	2.8	2.8	1.0	1.0	1.0	1.0	1.0	1.0	1.0	0.3	0.3	34.9	34.9
100		6.1	6.1	4.1	4.1	2.7	2.7	2.7	2.7	1.0	1.0	1.0	1.0	1.0	1.0	1.0	0.3	0.3	33.5	33.5
120		6.0	6.0	4.1	4.1	2.6	2.6	2.6	2.6	1.0	1.0	1.0	1.0	1.0	1.0	1.0	0.3	0.3	32.2	32.2
140		5.9	5.9	4.0	4.0	2.5	2.5	2.5	2.5	1.0	1.0	1.0	1.0	1.0	1.0	1.0	0.3	0.3	30.8	30.8
160		6.0	6.0	3.9	3.9	2.4	2.4	2.4	2.4	1.0	1.0	1.0	1.0	1.0	1.0	1.0	0.3	0.3	29.5	29.5
180		6.0	6.0	3.9	3.9	2.3	2.3	2.3	2.3	1.0	1.0	1.0	1.0	1.0	1.0	1.0	na	na	28.1	28.1
200		5.9	5.9	3.8	3.8	2.2	2.2	2.2	2.2	0.7	0.7	0.7	0.7	0.7	0.7	0.7	na	na	25.8	25.8
220		5.8	5.8	3.7	3.7	2.1	2.1	2.1	2.1	0.7	0.7	0.7	0.7	0.7	0.7	0.7	na	na	24.4	24.4
240		5.7	5.7	3.6	3.6	1.9	1.9	1.9	1.9	0.7	0.7	0.7	0.7	0.7	0.7	0.7	na	na	23.1	23.1
260		5.6	5.6	3.6	3.6	1.8	1.8	1.8	1.8	0.5	0.5	0.5	0.5	0.5	0.5	0.5	na	na	21.7	21.7
280		5.0	5.0	3.5	3.5	1.7	1.7	1.7	1.7	0.5	0.5	0.5	0.5	0.5	0.5	0.5	na	na	20.4	20.4
300		5.0	5.0	3.4	3.4	1.6	1.6	1.6	1.6	0.5	0.5	0.5	0.5	0.5	0.5	0.5	na	na	40.4	40.4
320		4.0	4.0	2.7	2.7	1.5	1.5	1.5	1.5	0.3	0.3	0.3	0.3	0.3	0.3	0.3	na	na	37.7	37.7
340		4.0	4.0	1.3	1.3	1.3	1.3	1.3	1.3	0.3	0.3	0.3	0.3	0.3	0.3	0.3	na	na	35.0	35.0
360		3.6	3.6	1.3	1.3	1.2	1.2	1.2	1.2	0.3	0.3	0.3	0.3	0.3	0.3	0.3	na	na	52.8	52.8
380		2.7	2.7	1.3	1.3	1.1	1.1	1.1	1.1	na	na	na	na	na	na	na	na	na	48.8	48.8
400		2.7	2.7	1.3	1.3	0.9	0.9	0.9	0.9	na	na	na	na	na	na	na	na	na	44.7	44.7

Appendix F Trajectory Optimization Analysis Assumptions

Table F.1 Trajectory Optimization Aircraft Assumptions

Aircraft Type	FAA Weight Class	Initial Weight (lb)	Altitude (Cruise) (ft)	Altitude (MF) (ft)	CAS (Cruise) (kt)	CAS (MF) (kt)	CAS (Ave. Descent) (kt)	Fuel Scale Factor w.r.t B727
AT42	S	33069	25000	7000	184.30	180	182.15	0.37
BA31	S	13669	25000	7000	167.50	200	183.75	0.18
BE20	S	11010	32000	7000	176.20	205	190.6	0.30
AT72	LNJ	44092	23000	10000	192.20	195	193.6	0.25
BATP	LNJ	44092	23000	10000	161.70	180	170.85	0.15
B727	LJ	163140	33000	10000	292.70	250	271.35	1.00
B737	LJ	101412	37000	10000	231.60	250	240.8	1.08
B73S	LJ	119048	37000	10000	238.60	250	244.3	1.21
BA46	LJ	79366	31000	10000	257.40	250	253.7	0.63
DC9	LJ	100089	35000	10000	272.30	250	261.15	1.23
EA32	LJ	136685	39000	10000	241.40	250	245.7	1.44
FK10	LJ	83775	35000	10000	235.20	250	242.6	1.04
FK28	LJ	52910	35000	10000	235.20	250	242.6	0.79
MD80	LJ	134922	37000	10000	245.70	250	247.85	1.04
B747	H	617288	36000	10000	273.50	250	261.75	3.63
B74F	H	661380	39000	10000	265.80	250	257.9	5.75
B757	H	209437	41000	10000	237.10	250	243.55	1.42
B767	H	330690	39000	10000	248.30	250	249.15	1.76
DC10	H	374782	39000	10000	255.30	250	252.65	2.04
EA30	H	275575	38000	10000	247.10	250	248.55	1.63
EA31	H	264552	41000	10000	237.10	250	243.55	1.26
L101	H	340611	40000	10000	249.40	250	249.7	0.80
MD11	H	501106	37000	10000	271.00	250	260.5	1.36

Note: Weight, altitudes, and speeds assumptions are from Reference [37].

References

[1] NASA, "AATT Program Products Descriptions," Draft Manuscript, Advanced Air Transportation Technologies (AATT) Program Office, NASA Ames Research Center. (June 1998), website http://www.asc.nasa.gov/aatt/

[2] RTCA Task Force 3, "Final Report of RTCA Task Force 3: Free Flight Implementation," RTCA, Inc. (October 1995)

[3] Swenson, H., et al, "Design & Operational Evaluation of the Traffic Management Advisor at the Fort Worth ARTCC," 1st USA/Europe ATM R&D Seminar, France. (June 1997)

[4] Celio, J., Bowen, K., Winokur, D., Lindsay, K., Newberger, E., Sicenavage, D., "Free Flight Phase 1 Conflict Probe Operational Description," MITRE Technical Report MTR 0W00000100. (March 2000)

[5] Davis, T., Krzeczowski, K., Bergh, C., "The Final Approach Spacing Tool," 13th IFAC Symposium on Automation Control in Aerospace. (September 1994)

[6] Green, S.M., and Vivona, R., "En route Descent Advisor (EDA) Concept," Advanced Air Transportation Technologies (AATT) Project Milestone 5.10 Report, NASA Ames Research Center. (September 1999)

[7] Leiden, K., Green, S., "Trajectory Orientation: A Technology-Enabled Concept Requiring a Shift in Controller Roles and Responsibilities, " 3rd USA/Europe Air Traffic Management R&D Seminar, forthcoming. (June 2000).

[8] Weidner, T., Mueller, T., "Benefits Assessment Compilation for En Route Data Exchange (EDX)," Seagull Technology TR00188.27-01f. (December 2000)

[9] Green, S., Goka, T., Williams, D., "Enabling User Preferences through Data Exchange," AIAA GNC Conference. (August 1997)

[10] Green, S., Vivona, R., and Grace, M., "Field Evaluation of Descent Advisor Trajectory Prediction Accuracy for En route Clearance Advisories," AIAA98-4479, AIAA GNC Conference. (August 1998)

[11] Davidson, T.G., Weidner, T., Birtcil, L., "En Route Descent Advisor Potential Benefits Assessment," TR98175.6-01, Seagull Technology. (December 1998)

[12] Weidner, T., et al, "EDA and EDX ATM Interruption Benefits," TR98188.26-01f, Seagull Technology. (December 2000)

[13] Hunter, G., Weidner, T., Couluris, G., Sorensen, J., Bortins, R., " CTAS Error Sensitivity, Fuel Efficiency, and Throughput Benefits Analysis," Seagull Technology TR96150-02. (July 1996)

[14] Weidner, T., "Capacity-Related Benefits of Proposed CNS/ATM Technologies," 2nd USA/Europe Air Traffic Management R&D Seminar (ATM98). (December 1998)

[15] Hunter, C.G., Weidner, T., "Performance and Benefits Modeling of Center Airspace ATM Improvements," AIAA GNC Conference. (August 1997)

[16] Weidner, T., Green, S., "Modeling ATM Automation Metering Conformance Benefits," 3rd USA/Europe Air Traffic Management R&D Seminar, forthcoming. (June 2000).

[17] Systems Resources Corporation, CSSI, Inc., "Potential Benefits of En Route Decision Support Tools, Task 4 Report: Preliminary Benefits Assessment and Economic Conversion Report for EDA," NASA AATT TO-11. (December 1998)

[18] Sorensen, J., Shen, M., "Study of Alternate Fuel Burn Models for ATC automation, Seagull Technology TR93120-02. (January 1993)

[19] Davidson, T.G., Hunter, G., "Preliminary Investigation of Sector Tools Descent Advisory Benefits," Seagull Technology TR97159-01. (August 1997)

[20] Davidson, T.G., Birtcil, L., "Sector Tools Potential Benefits Analysis," Seagull TR98154-01D. (draft April 1998)

[21] Green, S., "En Route Spacing Tool: Efficient Conflict free Spacing to Flow-Restricted Airspace," 3rd USA/Europe Air Traffic Management R&D Seminar, forthcoming. (June 2000).

[22] Brinton, C., Berry, J., "Assessment/Analysis of En-Route Descent Advisor (EDA) Spacing Tool Capability," Metron, NASA AATT TO-49. (November 2000)

[23] den Braven, W., "Design and Evaluation of an Advanced Air-Ground Data-Link System for Air Traffic Control," NASA TM 103899. (January 1992)

[24] den Braven, W., "Fully Automated Simulation of Air Traffic Control Concepts," Joint FAA/NASA CTAS/Datalink Workshop. (November 1994)

[25] Vivona, R.A., Ballin, M.G., Green, S.M., Bach, R.E., and McNally, B.D., "A System Concept for Facilitating User Preferences in En Route Airspace, " NASA TM4763, November 1996.

[26] Davidson, T.G., Birtcil, L., "Comparison of Fuel Optimal, CTAS and FMS Time-of-Arrival Control Strategies for MD-80 Aircraft Trajectories," Seagull TR178-02. (September 98)

[27] Davidson, T.G., Birtcil, L., "Comparison of Fuel Optimal, CTAS and FMS Time-of-Arrival Control Strategies for B-747 Aircraft Trajectories," Seagull TR178-03 (September 98)

[28] Davidson, T.G., Birtcil, L., Green, S., "Comparison of CAS/EDA and FMS Time-of-Arrival Control Strategies," AIAA99-4230, Guidance, Navigation, and Control Conference. (August 1999)

[29] Weidner, T., et al, "Potential Benefits of User-Preferred Descent Speed Profile," TR98188.26-01, Seagull Technology. (July 2000)

[30] Crown Communications, Inc., "Center TRACON Automation Traffic Management Advisor Build 2 (TMA) Assessment - Final Report," Doc. No. CTASDS-BAPRPT-003, FAA. (December 1996)

[31] Federal Aviation Administration (FAA), "1997 Aviation Capacity Enhancement Plan," Office of System Capacity. (December 1997)

[32] Crown Communications, Inc., "Center TRACON Automation Passive Final Approach Spacing Tool (P-FAST) Assessment - Final Report," Doc. No. CTASDS-BAPRPT-002, FAA. (December 1996)

[33] Couluris, G., Weidner, T., "Terminal Airspace Decision Support Tool Functions, Preliminary Potential Benefits Analysis," Seagull Technology, TR99185.02-01. (December 1999)

[34] Visits and consultations with Atlanta, Fort Worth, Los Angeles, and New York ARTCCs and Atlanta, Dallas-Fort Worth, Southern California, and New York TRACONs (July 1999).

[35] CSSI Inc. , "Traffic Demand Scenarios" computer data files. (September 1998)

[36] FAA, "1997 Terminal Area Forecast (TAF) System," Office of Aviation Policy and Plans, FAA APO Home Page, Internet WWW Site. (October 1998)

[37] Eurocontrol Experimental Centre, "User Manual for the Base of Aircraft Data (BADA) Revision 3.1," EED Note No. 23/97, Eurocontrol. (October 1998)

[38] Personal communication with Harry Swenson, NASA Ames Research Center, Moffett Field, CA. (April 2000)

[39] Mukai, C., "Design and Analysis of Aircraft Dynamics Models for the ATC Simulation at NASA Ames Research Center," Seagull TR92119-02. (March 1992)

[40] Personal communication with Danny Vincent, Traffic Management Supervisor, Ft. Worth ARTCC (ZFW). (September 2000)

[41] Communication with McNally, B.D., and Bilimoria, K., NASA Ames Research Center. (1999)

[42] FAA, "Air Traffic Rules and Procedures Service, Air Traffic Control FAA Order 7110.65, USDOT. (1998)

[43] Brudnicki, D., McFarland, A., "User Request Evaluation Tool (URET) Conflict Probe Performance and Benefits Assessment," MITRE CAASD, MP 9720000112. (June 1997)

[44] Slattery, R.A., and S.M. Green, "Conflict-Free Trajectory Planning for Air Traffic Control Automation, NASA Technical Memorandum 108790. (1994)

[45] Weidner, T., Davidson, G., Coppenbarger, R. Green, S., "Modeling ATM Interruption Benefits," AIAA99-4296, AIAA GNC Conference. (June 1999)

[46] Weidner, T., Davidson, T.G., "Preliminary En Route Data Exchange Potential Benefits Assessment," Seagull Technology, TR98175.9-01. (December 1998)

[47] Williams, D., Green, S., "Flight Evaluation of Center-TRACON Automation System Trajectory Prediction Process," NASA/TP-1998-208439. (July 1998)

[48] Green, S., and Vivona, R., "Field Evaluation of Descent Advisor Trajectory Prediction Accuracy," AIAA 96-3764. (July 1996)

[49] Kayton, M., and Fried, W.R., "Avionics Navigation Systems," Second Edition, John Wiley & Sons. (1997)

[50] Benjamin, Stanley G., et al, "Aviation Forecasts From the RUC-2," 8th Conference on Aviation, Range, and Aerospace Meteorology, Dallas. (January 1999)

[51] FAA Office of Aviation Policy & Plans, Air Traffic Activity Query, APO Data System, FAA APO Home Page, Internet website. (November 19, 1998)

[52] FAA, "Economic Values for Evaluation of FAA Investment and Regulatory Programs," FAA-APO-98-8, Office of Aviation Policy and Plans. (June 1998)

[53] FAA, "FAA Aviation Forecasts Fiscal Years 1998-2009," Final Report FAA-APO-98-1, Office of Aviation Policy & Plans. (March 1998)

[54] Federal Aviation Administration, "Ceiling and Climatological Study and System Enhancement Factors," Final Report FAA Office of Aviation System Plans. (June 1975)